Spring 2020

Diels-Alder Functionalized Particles for Mechanical Improvements in Additive Manufacturing

Elizabeth Hailey Sylvester
University of New Hampshire, Durham

DIELS-ALDER FUNCTIONALIZED PARTICLES FOR MECHANICAL IMPROVEMENTS IN ADDITIVE MANUFACTURING

BY

ELIZABETH H. SYLVESTER

Materials Science and Engineering (B.S.), Virginia Polytechnic Institute and State University

THESIS

Submitted to the University of New Hampshire

In Partial Fulfillment of

the Requirements for the Degree of

Master of Science

In Chemistry

May 2020

This thesis has been examined and approved in partial fulfillment of the requirements for the degree of Master of Science (M.S.) in Chemistry by:

Thesis Director, Erik Berda, Professor of Chemistry

Arthur Greenberg, Professor of Chemistry

Margaret Greenslade, Associate Professor of Chemistry

On April 23, 2020

Original approval signatures are on file with the University of New Hampshire Graduate School

Table of Contents

Dedication

This thesis is dedicated to my husband, family, and friends for their consistent support and encouragement throughout my time at the University of New Hampshire. Furthermore, I would like to dedicate this thesis to my professors and mentors at the University of New Hampshire for their time and guidance in my career as a graduate student in chemistry.

Acknowledgements

I would like to acknowledge my advisor, Professor Erik Berda, for his advice, support, and guidance during my time at the University of New Hampshire. In addition, I would like to recognize my lab members for their assistance on this research as well as their continued words of encouragement and support throughout my graduate career.

LIST OF SCHEMES

LIST OF TABLES

LIST OF FIGURES

ABSTRACT

DIELS-ALDER FUNCTIONALIZED PARTICLES FOR MECHANICAL IMPROVEMENTS IN ADDITIVE MANUFACTURING

By

Hailey Sylvester

University of New Hampshire, May 2020

This thesis explores the use of Diels-Alder functionalized particles to aide in the mechanical enhancement of additively manufactured objects. To date, materials generated via additive manufacturing lack isotropic properties due to the nature in which they are created – in a layer by layer fashion. This methodology often leads to poor interfacial adhesion at the junction between printed layers, lowering the stability of the part and thereby limiting its use in many applications. Dynamic covalent chemistry, such as the reversible Diels-Alder reaction, has the ability to alleviate this anisotropy to print stronger, more uniform objects. To do so, this work investigates crosslinked, Diels-Alder functionalized particles generated by two separate methods: polymerization via reversible addition fragmentation chain transfer (RAFT) followed by atom transfer radical coupling (ATRC) and free radical emulsion polymerization. These particles can be blended with a polymeric filament for 3D printing, where upon heating during the extrusion process of additive manufacturing, the retro-Diels-Alder reaction is initiated and releases the crosslinked particles exposing reactive diene and dienophile pairs. In subsequent

cooling after the printing process, these moieties undergo the forward Diels-Alder reaction and form chemical linkages between printed layers of the substrate to improve the mechanical integrity and uniformity of objects produced by means of additive manufacturing.

Chapter 1: Introduction

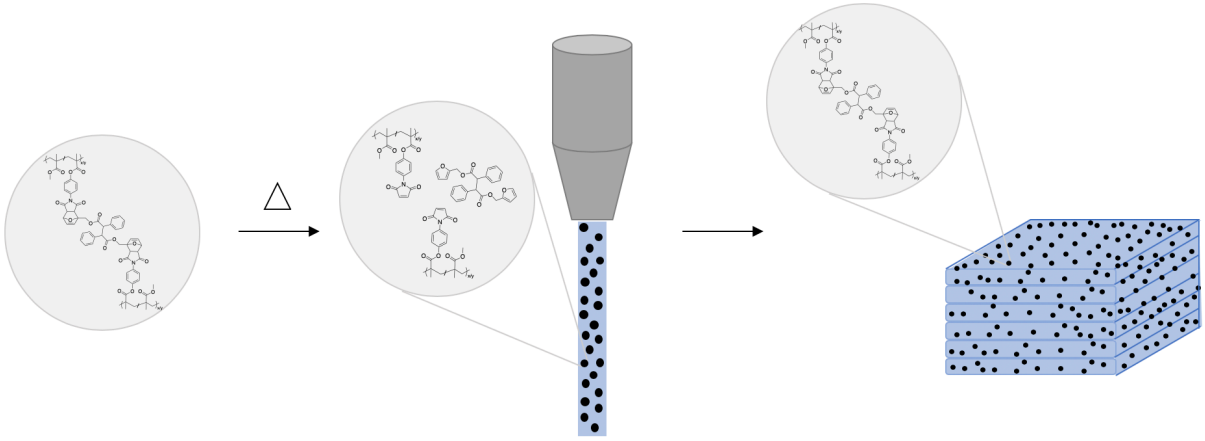

Figure 1: Process overview for the implementation of thermally responsive particles into the additive manufacturing process for the improvement of mechanical properties.

Additive Manufacturing

Additive manufacturing, or more commonly known as 3D printing, has been a rapidly growing field for its promise to achieve the production of previously unachievable complex architectures generated from seemingly limitless material sources. Its foundation began in 1986 when Charles Hull developed stereolithography,[1] a category of additive manufacturing for polymeric materials, which sparked interest in other researchers to explore this novel area of technology. This exploration generated many new techniques that are still in use today such as deposition modeling,[2] selective laser sintering, selective laser melting,[3] inkjet printing,[4] direct energy deposition,[5] and many more. Over the years, processes have been developed for printing metallic, ceramic, polymeric and composite substrates as a result of the exciting ability to enhance the precision with which products can be generated, reduce the amount of waste produced during that process, and simplify the production of customized items. Research in this field continues to be driven by refinement of the resolution and mechanical properties of

printed materials as the degree of their structural complexity continues to increase while this technique becomes more popular across both industry and research.[6]

Of the methods for additive manufacturing that have been developed, the majority have been for the production of polymeric materials. This is due to their already well-known ease of processability as well as facile tuning of chemical composition and mechanical properties. The most popular of these methods fall in the category of material extrusion, powder bed fusion or vat photopolymerization. Material extrusion is the most recognized technique and is accomplished by extruding filament(s) through a nozzle to generate 3D objects in a layer by layer fashion as seen in Figure 2. Depending on composition and physical properties, these materials can be heated or melted prior to deposition or alternatively, they can be extruded at room temperature. Powder bed fusion entails the binding of polymeric powders in targeted arrangements. These powders are spread in a thin layer across a flat surface and exposed to a targeted heat source, such as a laser, to generate a single layer. This process is repeated by covering the sintered material in another layer of powder and exposing to heat to generate successive layers and form the desired object. Finally, vat photopolymerization, which includes stereolithography, is a process that involves the polymerization of a monomer solution/resin layer using photolithography (light) and successively building on those layers to generate a solid object. This process often involves the

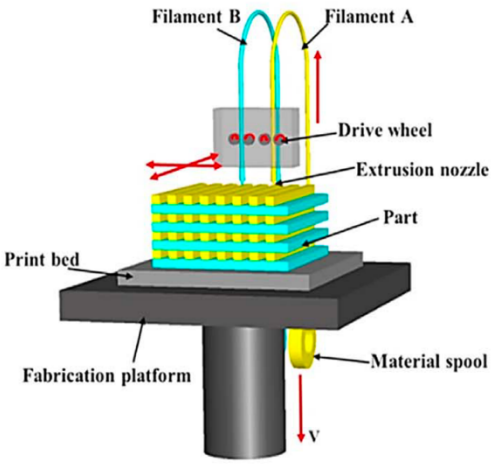

Figure 2: Representation of the Fused Deposition Modeling process.

incorporation of photo-initiators and catalysts to allow these polymerizations to take place at a rate fast enough for printing.[7]

This work focuses on the production of polymeric particles to aid in the stability of articles generated by the material extrusion process. To date, a major challenge of this method is achieving isotropic material properties across the printed object stemming from poor inter-layer adhesion caused by the layer by layer fashion in which these objects are created.[8] The anisotropic nature of these printed items limits their ability to be used on the large-scale and warrants investigation of new materials to enhance their mechanical properties[6]. Efforts have been made to alleviate these behaviors and include the investigation of dynamic covalent chemistry,[9,10,11] adhesion in 3D printed nanocomposites,[12] and process parameters such as layer thickness, printing speed, and build orientation.[2] However, these approaches are not applicable across a variety of materials or printing methods, thereby limiting their ability to be used on the industrial scale. Therefore, development of processes for the improvement of interfacial adhesion between 3D printed layers is still needed.

Diels-Alder

The Diels-Alder reaction is a thermoreversible, self-contained [4+2] cycloaddition reaction that has recently been investigated for its use in dynamic covalent chemistry applications such as self-healing and shape memory

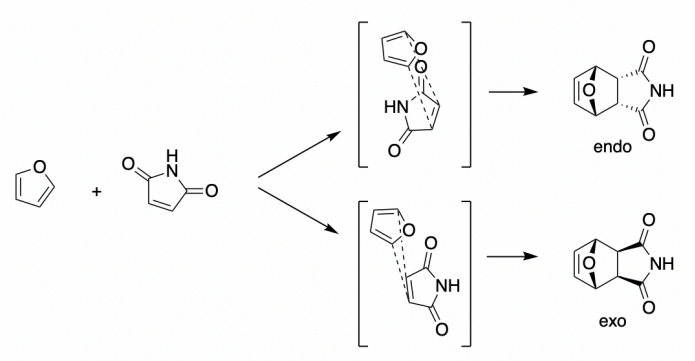

Figure 3: Representation of the transition state and resulting *endo* and *exo* diastereomers of the Diels-Alder reaction.

materials.[13,14,15,16] This chemistry was first explored by Otto Diels and Kurt Alder in 1928 between cyclopentadiene and quinone and its impact earned them the Nobel Prize in 1950 for their discovery and development of the synthetic process.[17,18] This reaction proceeds by the addition of a diene and dienophile to generate two new sigma bonds and one pi bond in the form of a six membered ring (Figure 3). Until recently, the Diels-Alder reaction had not yet been explored for its dynamic covalent capabilities even though it was shown over 50 years prior that this reaction was reversible. The dynamic covalent character of this chemistry stems from systems with low activation barriers of ring formation producing slightly exergonic products. In most cases, this allows for the reverse reaction to easily occur and an equilibrium to be formed between products and reactants. The position of this equilibrium can be controlled through external stimuli such as temperature, solvent and concentration. The reversibility, however, is tailored by altering the substituents of both the diene and dienophile to control their electron density and therefore their propensity to undergo both the forward and reverse reactions.[19,20]

The most common example of this which has been exploited in the field of dynamic covalent chemistry is the reaction between furan and maleimide derivatives which, like other Diels-Alder systems, produces both a kinetic *endo* product and a thermodynamic *exo* product (Figure 3). The formation of this Diels-Alder adduct can occur at or near room temperature while the retro-cyclization requires elevated temperatures dependent on the stability of the synthesized cycloaddition adduct (~100°C).[21] According to the Diels-Alder *endo* rule, the kinetic *endo* adduct is favored by the reaction and will be produced in excess to the *exo* adduct due to pi orbital overlap in its transition state configuration, lowering the transition state energy

barrier, which is not present in the transition state for the *exo* adduct.[22] However, as temperature or reaction time of the system increases, the ratio of the thermodynamic *exo* adduct is increased. Additionally, in terms of the retro-Diels-Alder reaction, the *endo* adduct is the first to undergo the unblocking reaction (at a lower temperature) as compared to the more stable *exo* adduct. This again is due to the lower transition state energy for the retro-cyclization reaction in addition to the higher energy state of the *endo* product resulting in a smaller energy barrier.

Froidevaux, et al. utilized the information above to target the *endo* adduct and investigate the retro-Diels-Alder reaction of furan – maleimide systems as a function of Diels-Alder partner substituents and reaction condition effects. It is well known that the nature of the substituents of the furan/maleimide pairs influence the ratio of *endo* to *exo* isomers as well as the stability of the cycloaddition adduct and therefore its propensity to undergo the retro-Diels-Alder reaction. It was observed that more electron donating substituents of the diene and electron withdrawing substituents of the dienophile increase the rate of formation of the Diels-Alder adduct. However, in terms of the retro-cyclization reaction, electron withdrawing groups were found to facilitate the reformation of diene and dienophile pairs and decreased the temperature required to do so. Additionally, substituents favoring the formation of a more stable *endo* adduct and thereby increasing its ratio as compared to the *exo* adduct, corresponded to slower kinetics in the unblocking reaction. Therefore, in order to obtain a system for efficient retro-Diels-Alder reactions, a balance needs to be achieved in terms of the stability of the *endo* adduct to be stable enough to favor its formation over the *exo* conformation while not being too stable hindering the retro-cyclization.[21]

The reversibility of this system was also investigated by Boutelle and Northrop as a function of diene and dienophile substitution both computationally and experimentally. They discovered that the furan-maleimide Diels-Alder reaction could be tailored as a function of the electronic properties of chosen substituents to form reactions ranging from significantly exergonic to endergonic. In the extreme cases of the former or latter, irreversible or inability to undergo the cycloadditon reaction respectively occurred. Firstly, it was seen that substitution of the furan had greater influence over Diels-Alder reactivity than substitution of the maleimide dienophile. Additionally, the position of the substituent and the electronic effects it imposed upon the furan was significant: more electron donating substituents resulted in reactions of greater exergonicity as well as lower transition state free energy barriers. Although promising for adduct formation, high exergonicity decreases the favorability of these compounds in dynamic covalent chemistry because it creates high energy barriers for the retro-Diels-Alder reaction. Slightly donating substituents such as alkyl groups, results in lower exergonicity in a range suitable for the desired reversibility. Alternatively, electron withdrawing moieties were observed to produce both exergonic as well as endergonic products depending on the regiochemistry of their substituents and whether the *endo* or *exo* adduct was being formed. Substitution of the 2nd position on the furan ring produced an endergonic reaction for both isomers while substitution of the 3rd position resulted in an endergonic reaction for reactions favoring the *endo* adduct and exergonic for ones favoring the *exo* adduct. This coincided with the evidence that reactions involving furan substituted in the 3rd position were more exergonic and had lower transition state barriers in the Diels-Alder reaction.[19]

The information provided above in addition to fundamental literature is invaluable in the synthesis of Diels-Alder adducts for dynamic covalent chemistry. These adducts must be tailored to attain both the forward and reverse cycloaddition reactions under temperature conditions determined by intended applications of the system. Knowledge of the variables influencing the stability of the Diels-Alder adduct allows one to produce and examine such adducts and was utilized in this study in the preparation of thermally responsive particles for 3D printing applications.

RDRP

Reversible deactivation radical polymerization (RDRP) is a technique that expanded the realm of radical polymerization by allowing the formation of functional polymers with defined molecular weights, narrow polydispersities and complex/controlled molecular architectures. This form of polymerization includes three major categories of techniques: nitroxide mediated polymerization (NMP), atom transfer radical polymerization (ATRP) and reversible addition fragmentation chain transfer polymerization (RAFT) and functions by partitioning the propagating radicals between active propagating and dormant polymer chains in an equilibrium reaction. To do so, both NMP and ATRP function through reversible termination using either a nitroxide species or metal halides, respectively. The dormant species is favored throughout the process in order to maintain a low concentration of radicals and mitigate undesired side reactions (Figure 4). RAFT on the other hand, forms an equilibrium between the propagating and dormant species in order to keep

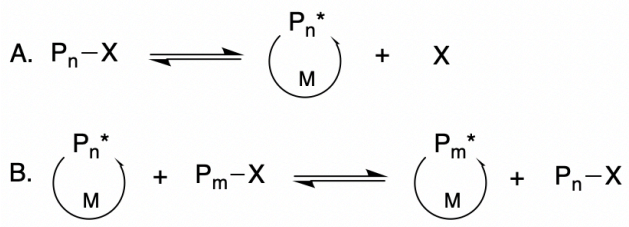

Figure 4: General mechanism of the RDRP process.

radical concentration low which is controlled by the introduction of an external radical initiator[23] (Figure 5). RAFT and ATRC (a coupling process founded upon ATRP) will be evaluated in this research.

Reversible Addition Fragmentation Chain Transfer

Reversible addition fragmentation chain transfer (RAFT) is a form of polymerization that was discovered in 1998 by Chiefari et al. and has developed into one of the most useful and versatile techniques for the polymerization and generation of complex polymeric architectures.[24] This form of polymerization follows a reversible deactivation radical polymerization (RDRP) process which allows for the attainment of targeted polymer molecular weights with low polydispersity indices while maintaining high chain end fidelity and therefore the ability to carry on chain growth. The RAFT process is founded upon an equilibrium between active propagating and dormant chains attainable via degenerative chain transfer. This is achieved by utilizing a chain transfer agent that can reversibly attach to polymeric chain ends, temporarily halting propagation until it is removed through reaction with an active radical. The mechanism of this process is shown in Figure 5 and follows: after initiation of the radical source, the generated high energy center reacts with a monomer unit to generate an active propagating chain. That species can then enter into a pre-equilibrium stage between an active and dormant chain by adding to a chain transfer agent (CTA). The

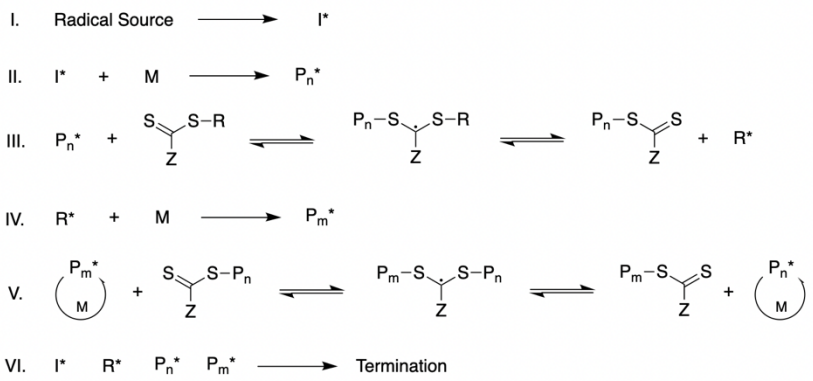

Figure 5: General mechanism for the RAFT polymerization process.

intermediate formed in this process can fragment into a macro-CTA (dormant chain) and a new radical source that can then move on to activate another monomer unit and generate a new active chain. Preferably, this pre-equilibrium stage is completed relatively quickly to attain an efficient RAFT process with minimal molecular weight dispersion. The active chain then enters the main RAFT equilibrium where polymer chains alternate between active and dormant states via reversible transfer of the functional component of the chain transfer agent. Throughout, the active species can undergo termination via disproportionation or coupling reactions to stop growth.[23]

In this form of polymerization, the overall number of radicals throughout is unchanging and are therefore required from an external source such as a radical initiator as seen in the above mechanism. The ability to incorporate a known amount of external radical source allows the user to have control over both the rate of polymerization as well as the fraction of active, propagating chains throughout the process. However, the number of radicals generated from this source also directly affects the extent of bimolecular termination events that occur throughout the polymerization (which can be calculated from the amount of initiator decomposition) although this termination process does not affect the number of living chain ends present in the system. Because of the direct relationship between radical concentration and termination, it is pertinent to minimize the amount of initiator required in order to obtain an efficient RAFT polymerization system with optimal living character.[25] RAFT accomplishes this through the formation of many shorter chains as compared to conventional radical polymerization.[23]

Most commonly, the initiator utilized in RAFT polymerization as a radical source is one that is degraded thermally. Commonly, these initiators are either diazo or peroxide compounds and there are a variety of these compounds available across a range of degradation temperatures allowing modulation of polymerization temperature conditions. For example, one of the most commonly used initiators, 2,2'azobisisobutyronitrile (AIBN), has a half life of 10h at 65°C while 2,2'-azobiz(4-methoxy-2,4-dimethylvaleronitrile) (V-70) has a half life of 10h at 30°C. Although most commonly conducted using thermal initiation, radical sources for RAFT polymerization can extend to any radical source similar to conventional radical polymerization. It has been seen that initiation through redox reactions and light initiation have also produced successful polymers with control over molecular weight and polydispersity.[25]

Although different, the rate of a RAFT polymerization is similar to that of a conventional free radical polymerization and follows equation 1 below.

$$R_p = k_p[M]\sqrt{\frac{fk_d[I_0]e^{-k_d t}}{k_t}} \quad (1)$$

The polymerization rate (R_p) is therefore dependent on the propagation rate coefficient (k_p), monomer concentration [M], the initiator efficiency (*f*), the initiator decomposition rate coefficient (k_d), the initial initiator concentration ($[I]_0$), the termination rate coefficient (k_t) and time (t). However, unlike a conventional free radical polymerization, the livingness of a RAFT system can also be quantified as seen by equation 2 where $[CTA]_0$ is the initial chain transfer agent concentration and f_c is the coupling factor for radical-radical bimolecular termination events.

$$L = \frac{[CTA]_0}{[CTA]_0 + 2f[I]_0\left(1-e^{-k_d t}\right)\left(1-{}^{f_c}/_{2}\right)} \quad (2)$$

Additionally, due to the fact that the livingness of these polymerizations depends on the number of generated radicals from the selected initiator (which controls the number of dead polymer chains as seen above), the conversion of these chains does not need to be stopped before reaching 100% like other RDRP systems, if chain extension is desired to form block copolymers or the like.

As previously stated, RAFT has become an attractive method of polymerization for its control over molecular weight while maintaining end group fidelity and a low polydispersity. The ability to attain targeted molecular weights results from the use of chain transfer agent which regulates the number of chains generated during the polymerization. This, in conjunction with the initial concentration of monomer, allows a user to determine the number average molecular weight ($M_{n,th}$) that will be achieved by the propagating polymeric chains which can be calculated following equation 3 where $[M]_0$, $[CTA]_0$, and $[I]_0$ are the initial monomer, chain transfer agent and initiator concentrations, and p, M_M, and M_{CTA} are the conversion, monomer molar mass and chain transfer agent molar mass, respectively.

$$M_{n,th} = \frac{[M]_0 p M_M}{[CTA]_0 + 2f[I]_0(1-e^{k_d t})\left(1-{}^{f_c}/_{2}\right)} + M_{CTA} \quad (3)$$

Because an efficient RAFT polymerization is achieved by using minimal amounts of initiator to decrease the number of radicals during the polymerization, the second term in the denominator is typically removed which simplifies the calculation to equation 4.[25]

$$M_{n,th} = \frac{[M]_0 p M_M}{[CTA]_0} + M_{CTA} \quad (4)$$

The control over polydispersity of these systems stems from the rapid equilibrium between active and dormant chains generated by the exchange of the chain transfer agent.

Because the rate at which this occurs is faster than the propagation rate of the growing chains, each chain is essentially growing at the same time resulting in chains of approximately the same number of repeating units.[23]

ATRC

Atom transfer radical polymerization (ATRP) was first published by Wang and Matyjaszewski in 1995 and has since grown into one of the most popular forms of controlled radical polymerization to date. This form of polymerization was developed based on transition metal catalyzed atom transfer radical addition (ATRA) (Figure 6) for carbon-carbon bond formation and was found to behave as a living system, producing polymers of small molecular weight dispersities with negligible termination events. Figure 7 represents their initial proposed mechanism for the polymerization process based upon ATRA where the Cu^{I} and Cu^{II} species exist in a redox equilibrium and a halogen atom is abstracted by Cu^{I} to generate an active radical species and a Cu^{II} species in both the initiation and propagation processes.

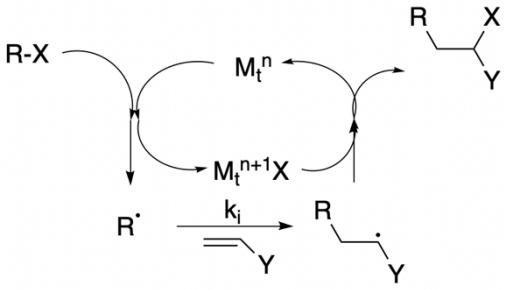

Figure 6: Mechanism for the ATRA process.

Like other controlled radical polymerizations, this system operates based upon an equilibrium between an acitve and dormant species, which in this case is mediated by the two forms of the copper catalyst. To achieve control over the polymerization, a low concentration of radicals needs to be maintained throughout the reaction. These

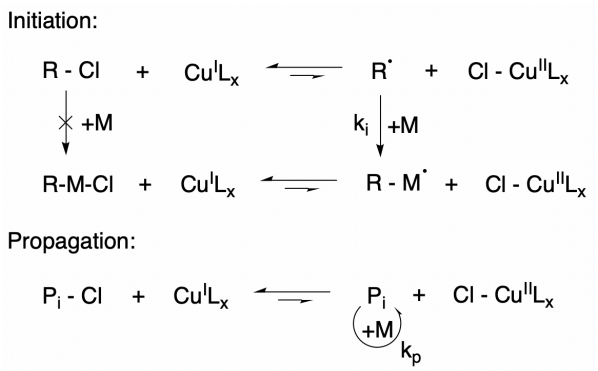

Figure 7: First proposed mechanism for ATRP by Matyjaszewski et al.

moieties do so by creating an equilibrium where the dormant polymer chain and Cu^{I} species is favored and the redox reaction is fast relative to bimolecular termination events.[26,27,28,29]

While one of the main goals of an ATRP system is to minimize radical concentration to achieve optimal control over polymerization and minimize termination, aleviating this minimization of radical concentration can afford an efficient atom transfer radical coupling (ATRC) reaction. In 1997, Matyjaszewski et al. investigated the optimization of the ATRP process by decreasing the amount of deactivator (Cu^{II} species), which was present in excess in the system, slowing the polymerization. Anadvertently, this developed a method for increasing radical concentration and thereby influencing the formation of ATRC. They observed that by using a zerovalent metal (Cu^{0}) along with a suitable ligand, the Cu^{II} species was reduced to generate the activating species, Cu^{I} while at the same time reducing the amount metal catalyst required for a controlled ATRP process and increasing polymerization rate[30] (Figure 8).

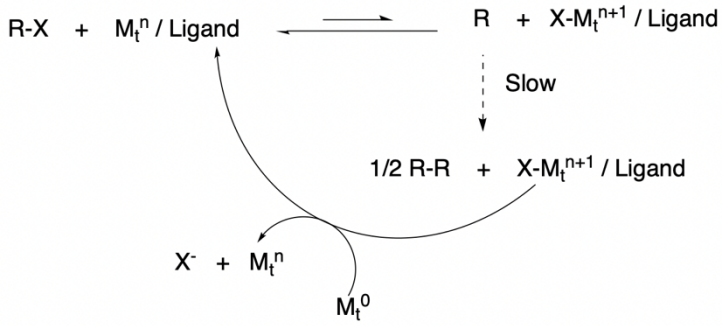

Figure 8: Resulting mechanism for the introduction of Cu^0 to the ATRP reaction system resulting in the reduction of Cu^{II} to the activator, Cu^{I}.

Building upon this discovery, Debuigne et al. found that by introducing the optimal ratios of Cu^{I}, Cu^{0},

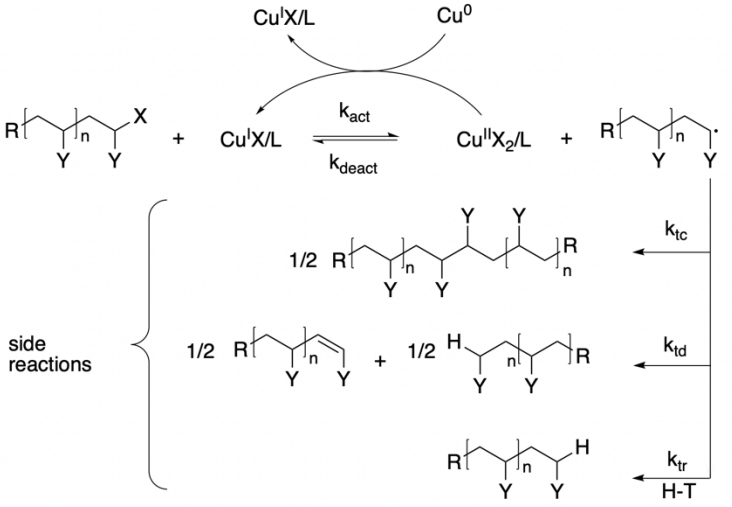

Figure 9: Figure shows the termination reactions competing with the desired ATRC process (k_{tc}) including disproportionation (k_{td}) and chain transfer (k_{tr}) .

and amino ligands to an ATRP system, Cu^0 can act to supress the formation of Cu^{II} enough to cause termination rate to increase and thereby induce a greater amount of coupling reactions. However, it was observed that this process competes with other forms of termination as seen in Figure 9 such as disproportionation and chain transfer, the extent of which is dependent on chain functionality[31].

Fukuda et al. were the first to report the use of ATRC to couple polymer chains while investigating termination and chain transfer events in living radical polymerization by looking at monomer free systems. Both ω-bromopolystyrene and α,ω-dibromopolystyrene were evaluated, attaining a coupling efficiencty of up to 0.91 and at minimum, doubling the molecular weight of the polymer chains with each reaction. The extent of coupling was enhanced by increasing the concentration of active polymer chains which could be controlled by both concentration of bromo-functionalized species as well as ligand selection. Additionally, they observed that the extent of the various termination mechanisms followed literature reported termination constants where combination was the predominant pathway lending ATRC to be a viable tool for coupling reactions.[32] Since then, ATRC has been used to synthesize a plethora of functional materials including but not limited to telechelic polymers,[33,34] block copolymers,[35] and macrocycles.[36,37]

This work hopes to take advantage of the efficient ATRC reaction to generate Diels-Alder functionalized particles for additive manufacturing applications. It is the intention to utilize this coupling strategy in the crosslinking of polymer chains generated via RAFT polymerization, containing Diels-Alder moieties to enable the formation of nano- to micro-scale particles for evaluation of their thermally responsive properties.

Chapter 2: Results and Discussion

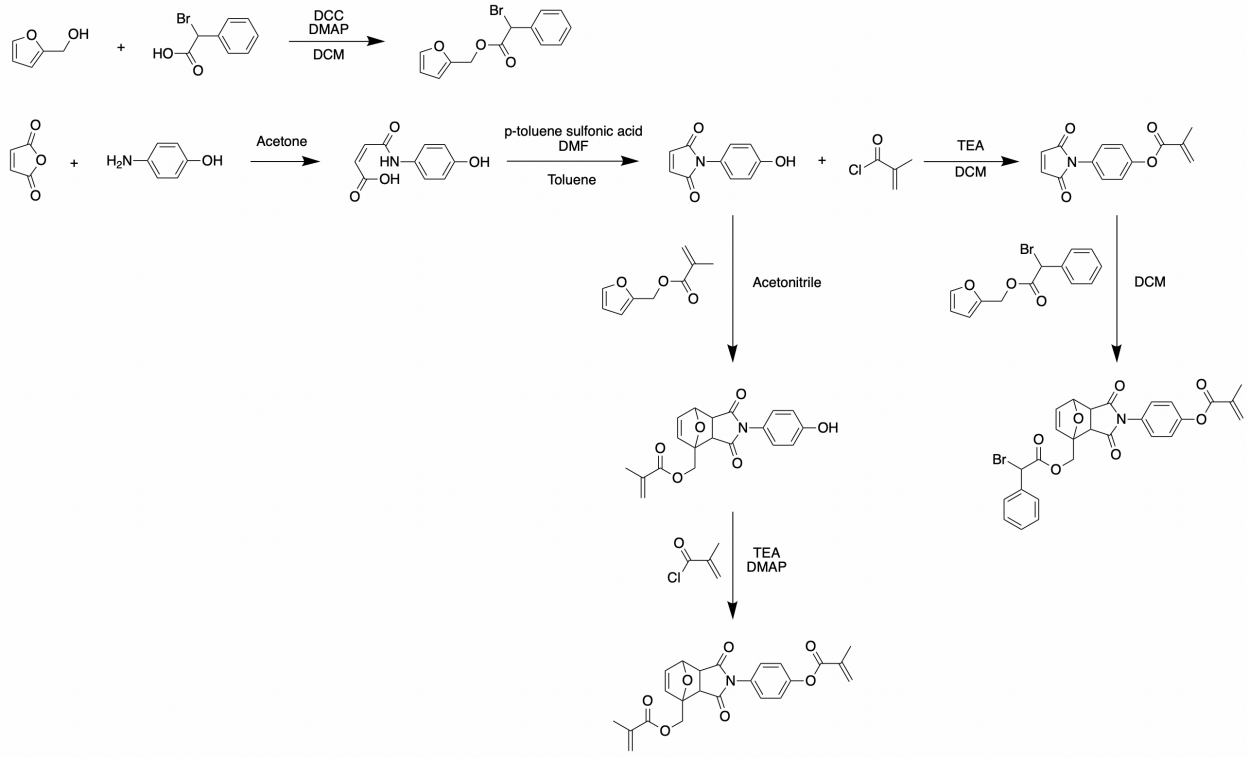

Figure 10: Synthetic Scheme for the production of Diels-Alder functionalized monomers to be utilized in the synthesis of thermally responsive particles for improvements in the mechanical properties of objects generated by 3D printing.

An overview of the synthetic scheme for the preparation of Diels-Alder functionalized monomers can be seen in Figure 10. In brief, the diene was either commercially obtained (furfuryl methacrylate) or prepared via a Steglich esterification between furfuryl alcohol and α-bromophenyl acetic acid employing dicyclohexylcarbodiimide and 4-dimethylaminopyradine in dichloromethane at room temperature (Figure A1 and A2). The preparation of the dienophile was evaluated using several different methods reported in literature. In the first attempt, an amic acid precursor was prepared via an amination reaction between 4-aminophenol and

maleic anhydride in acetone at room temperature (Figures A3 and A4). To drive the cyclization reaction for the formation of the maleimide, the resulting compound was treated with dicyclohexylcarbodiimide and refluxed in dichloromethane,[38,39] the mechanism for which can be seen in Scheme 1. Although success was reported in the literature, the desired material was not achieved in this case as evidenced by ^{1}H NMR as seen in Figure A5 in the Appendix. It is proposed that a macrocyclic dimer was formed instead, due to an intermolecular reaction between two amic acid precursors.

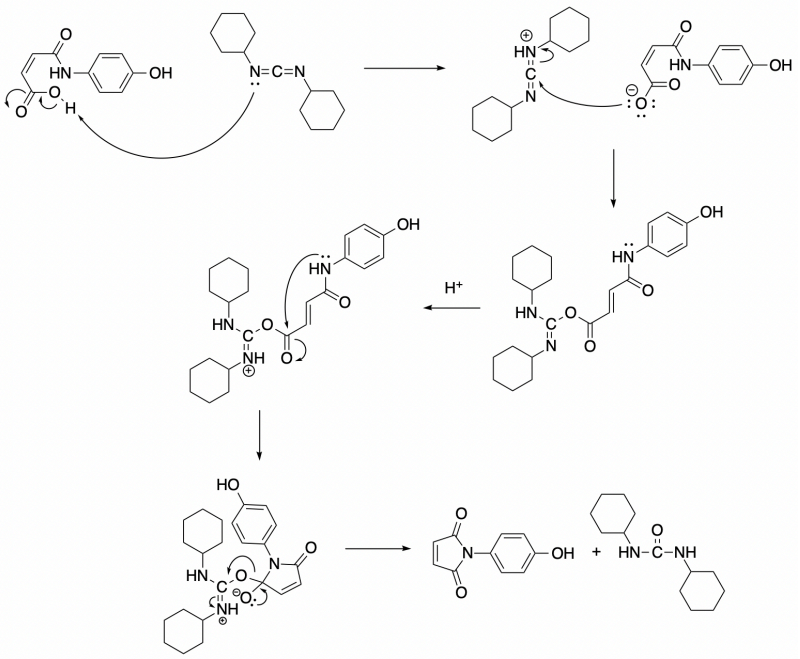

Scheme 1: Mechanism for the synthesis of the desired phenolic maleimide dienophile employing dicyclohexylcarbodiimide.

An alternative method reported in the literature is the implementation of anhydrous sodium acetate and acetic anhydride to obtain the desired product as can be seen in Scheme 2.[40] This again, did not yield successful formation of the desired maleimide, but resulted in the

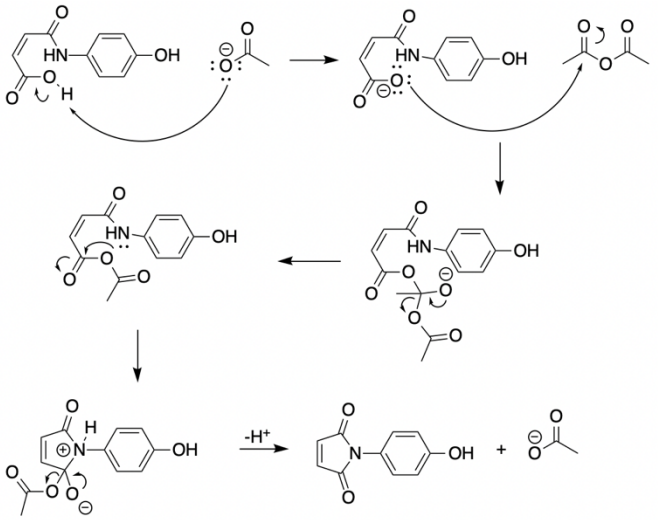

Scheme 2: Mechanism for the synthesis of the phenolic maleimide dienophile employing anhydrous sodium acetate and acetic anhydride.

esterification of the phenol in addition to the ring closure evidenced by ^{1}H NMR (Figures A6 and A7).

The selected method for the successful production of the maleimide was conducted utilizing the prepared amic acid precursor in a ring closure reaction promoted by an acidic environment formed by the addition of p-toluenesulfonic acid in a mixture of toluene and N,N-dimethylformamide (DMF).[41,42] Isolation of resulting product however, proved to be challenging due to the formation of a biphasic system where a high viscosity oil was suspended in the resulting toluene/DMF solution. Isolation of the product became more challenging with increasing scale due to inability to obtain efficient precipitation. To alleviate this issue, a study was conducted on the amount of DMF (utilized to aid in solubility of the oil) necessary for optimal reaction conditions as theoretical yields were increased. As can be seen in Table 1, an increase in the amount of incorporated DMF did not aid or hinder yields of product obtained; however, it did significantly impact the precipitation process and resulted in a more straightforward purification route. Any remaining impurities after the cyclization reaction were then removed via hot filtration in dichloromethane to afford the phenolic maleimide as a yellow-orange powder verified by ^{1}H NMR (Figures A8 and A9)

Table 1: Volumetric ratios and resulting prevent yields in the study of DMF incorporation for efficient synthesis of the phenolic maleimide dienophile.

Theoretical Yield (g)	DMF/Toluene (v/v)	Amic Acid/DMF (v/v)	Percent Yield (%)
1	0.11	2.14	37
1	0.14	1.64	30
1.5	0.11	2.14	47
1.5	0.14	1.64	48
2	0.11	2.14	54
2	0.16	1.46	51
2.5	0.11	2.14	33
2.5	0.17	1.37	39

Functionalization of the phenolic maleimide was then attempted to introduce the ATRC capable moiety, α-bromophenylacetic acid. To do so, a Steglich esterification was employed utilizing reaction conditions as seen in the synthesis of the diene, stated above. However, the resulting ^{1}H NMR spectra unfortunately revealed the reaction was unsuccessful as seen in Figure A10. This was attributed to base induced coupling reactions between maleimide functionalities producing oligomeric compounds rather than the desired esterification proposed in Scheme 3. To alleviate reaction at the maleimide, the synthesis was conducted utilizing a furan protecting group, which could then be removed post-functionalization via heating to induce a retro-Diels-Alder reaction. To do so, 4-aminophenol was treated with 7-oxabicyclo[2.2.1.]-hept-5-ene-2,3-dicarboxylic anhydride by refluxing in glacial acetic acid at 118°C.[43] Unfortunately, this resulted in little product and a significant amount of the unprotected amic acid precursor due to the high reaction temperatures initiating the retro-Diels-Alder reaction observed by ^{1}H NMR in Figure A11 in the Appendix. To remedy this issue, the reaction was conducted in methanol at

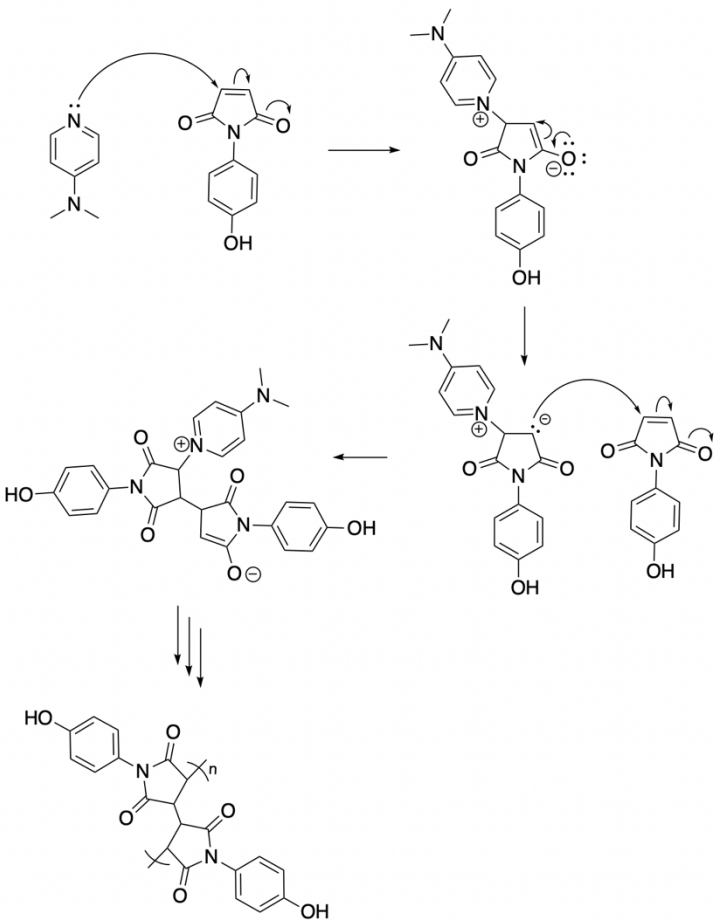

Scheme 3: Mechanism for the proposed side reaction resulting from the utilization of DMAP in the functionalization of N-(4-hydroxyphenyl) maleimide.

70°C to afford the protected maleimide as seen in Figure A12. The desired Steglich esterification could then be performed on the protected phenolic maleimide to yield the desired ester purified by column chromatography and characterized by ^{1}H NMR (Figure A13). Although successful, a more efficient synthetic route was identified by conducting the Diels-Alder cycloaddition with the desired diene previous to functionalization of the phenol to eliminate the deprotection step. Therefore, this was the route taken moving forward (Figures A14-A15).

To then generate Diels-Alder functionalized monomers, several studies were conducted to evaluate optimal reaction conditions for the cycloaddition reaction. The first monomer evaluated was the ATRC capable Diels-Alder adduct. The synthesis of this functionalized adduct was first attempted naively via reaction of the phenolic maleimide with an excess of α-bromo-2-furanylmethylester benzeneacetic acid (BP) in dichloromethane at 60°C for 24h. The elevated temperature utilized was in an effort to drive the equilibrium towards the products in hopes for higher yields.[3,21,44,11,14] However, this resulted in loss of solvent before adequate formation of the Diels-Alder adduct could be obtained for further modification due to the relatively low boiling point of dichloromethane. Therefore, in subsequent experiments, temperature was reduced to 40°C and reaction time was extended. Additionally, after later variable temperature ^{1}H NMR experiments of the synthesized adduct, it was also revealed that the retro-Diels-Alder reaction of this

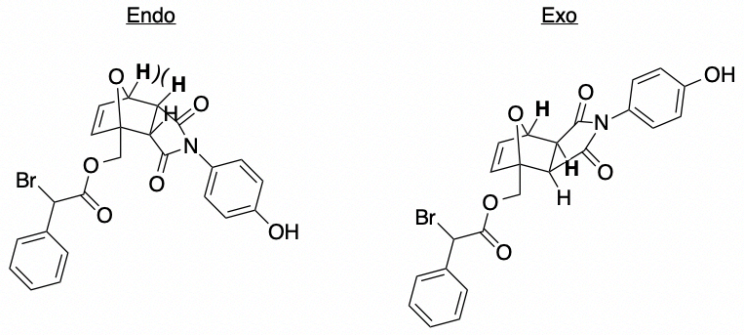

Figure 11: *Endo* and *exo* diastereomers of the ATRC-functionalized Diels-Alder Adduct.

system initiates at temperatures below 60°C providing further reason to avoid the cycloaddition reaction under these reaction conditions.

Reaction at 40°C gave successful formation of the desired product in sufficient yields (approximately 60% yield) where upon purification via column chromatography, it was found that *endo* and *exo* isomers could conveniently be isolated after evaluation by ^{1}H and ^{13}C NMR (Figures A16-A19). It is hypothesized that this is the case due to the large moieties bonded to the diene and dienophile counterparts as seen in Figure 11, resulting in a significant difference in polarity of the two diastereomers allowing them to be separated by this method.

Due to this observation, studies were conducted on the diastereomeric ratio produced over various reaction time intervals at 40°C in dichloromethane, the results of which can be

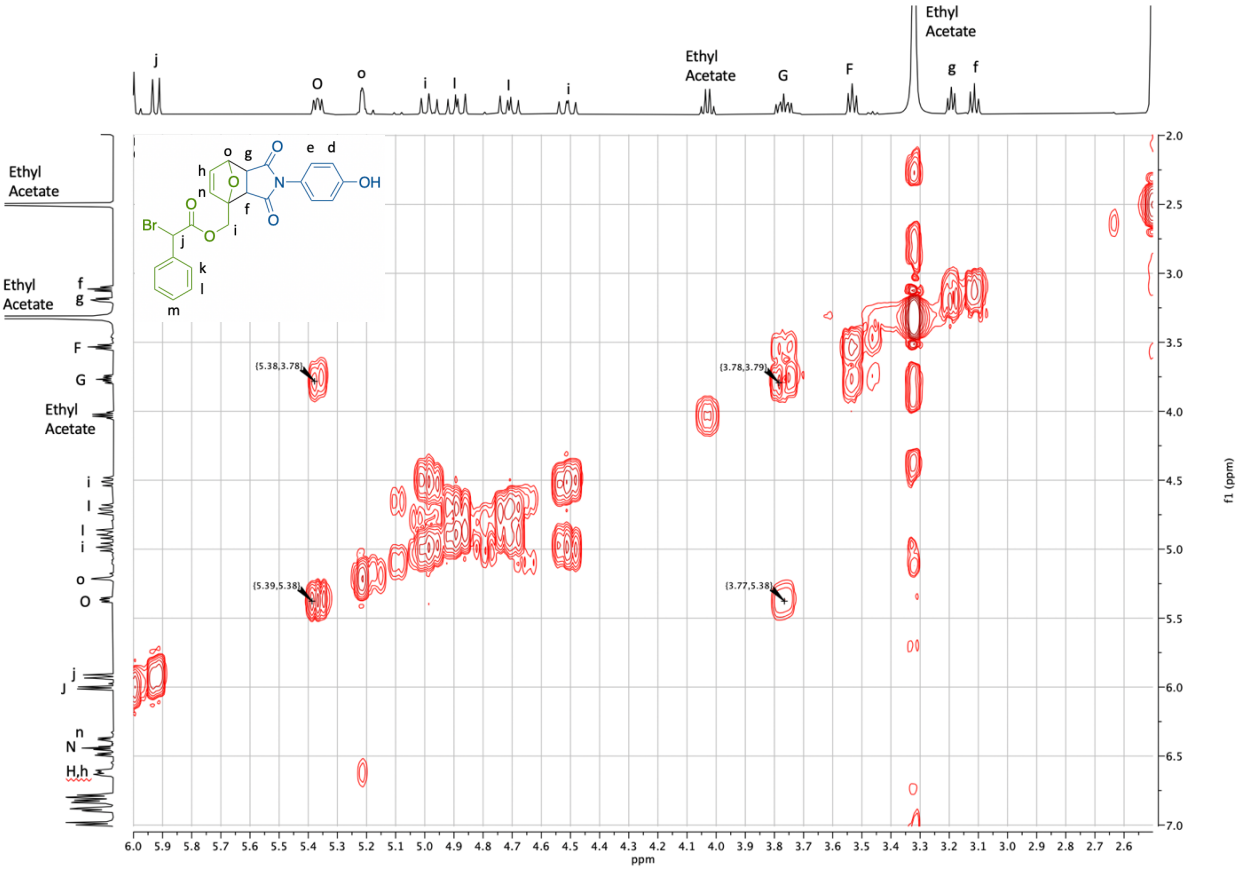

Figure 12: Example of COSY ^{1}H NMR data showing the interaction (or lack thereof) of protons o, O, g, and G for the ATRC-capable Diels-Alder adduct where the *endo* diastereomer displays such an interaction and the *exo* does not. (*Endo* is represented by the uppercase alphabet; *exo* is represented by the lowercase alphabet.)

seen in Table 2. Each trial was conducted using an excess of diene and were purified by column chromatography, combining the *exo* and *endo* diastereomer fractions for accurate ratio evaluation by NMR. To identify the respective isomers ^{1}H-^{1}H correlation spectroscopy (COSY) experiments were utilized to detect the interaction (or lack thereof) between relevant protons of the adduct (identified in bold in Figure 11). In analysis of COSY data, the *endo* diastereomer would be expected to show an interaction between the highlighted protons due to their proximity resulting from their location on the top face of the Diels-Alder adduct, while the same protons of the *exo* diastereomer would lie on opposite faces of the adduct, as seen in Figure 11, and therefore would not be expected to show an interaction. This behavior was observed in the current system as can be seen in Figure 12; where protons O and G display an interaction while o and g do not, thus identifying these peaks as belonging to the *endo* and *exo* diastereomers, respectively. This process was conducted for each of the trials of different reaction times to identify the peaks corresponding to the diastereomers present (Figures A20-A31).

Once identified, ratios were taken of the benzylic proton integrations belonging to each respective adduct to determine the diastereomeric ratio resulting from the progressing reaction times. The increasing trend in diastereomeric ratio observed in Table 2 and Figure 13 shows that with increasing time, the ratio of the thermodynamic *exo* adduct to kinetic *endo* adduct increases, as expected.[22] Because this is a system in equilibrium, the forward and reverse reactions are constantly

Table 2: Investigation of the diastereomeric ratio of the ATRC-capable Diels-Alder adduct over time.

Isomer Study of Diels-Alder Adduct Formation		
Theoretical Yield: 0.5g		
Reaction Time (days)	% *Endo*	% *Exo*
1	70	30
3	55	45
4	54	46
5	56	44
6	52	48

occurring at any point in time, enabling reconfigurations of the Diels-Alder adduct isomers and therefore shifts in the diastereomeric ratio. As previously mentioned in the Introduction, the *endo* conformation requires less energy to undergo the retro-Diels-Alder reaction due to its lower transition state energy and less stable adduct conformation.[19] Over time, the *endo* adduct reverts back to its diene and dienophile counterparts more readily than the *exo* adduct and does so to a greater extent. These regenerated starting materials can then undergo the forward Diels-Alder reaction to generate the more stable *exo* isomer, increasing its concentration relative to the *endo* isomer. Intuitively, this also means the *exo* isomer can undergo cyclo-reversion to its starting materials; however, due to the higher transition state energy of the retro-cyclization and stability of the product, this occurs to a lesser extent than reversion of the *endo* adduct. This process enables the ratio between *exo* and *endo* diastereomers to increase with reaction time.

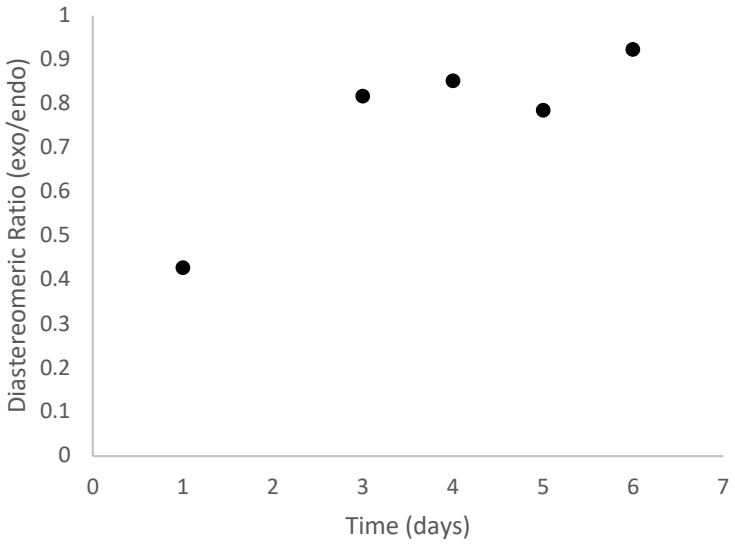

Figure 13: Trend in the (*exo/endo*) diastereomeric ratio with time of the ATRC-capable Diels-Alder adduct.

To then generate the desired ATRC-capable monomer, it was attempted to functionalize the successfully synthesized Diels-Alder adduct with a methacrylate moiety at the phenolic position via an esterification reaction following several different synthetic routes. The first attempt was a modified procedure from Wilborn et al. where the separate diastereomers were treated with triethylamine, 4-dimethylaminopyradine, and methacryloyl chloride in tetrahydrofuran.[45] DMAP was utilized to act as both a catalyst and base in the esterification of methacryloyl chloride as can be seen in Scheme 4. The resulting reaction mixture was washed with 1M hydrochloric acid, saturated sodium bicarbonate and brine and the organic layer was isolated and characterized. Unfortunately, ^{1}H NMR (Figure A32) revealed the targeted product was not obtained which was attributed to undesired side reactions hypothesized to be instigated by attack of dimethylaminopyradine on the carbonyl moieties of the Diels-Alder functionalized compound rather than aiding in the esterification of the phenolic functional group as it is a good nucleophile and leaving group. To alleviate this issue, DMAP was removed from the system and the reaction was run utilizing simply methacryloyl chloride (2eq.), triethylamine (1.1eq.) and the Diels-Alder functionalized compound (1eq.). ^{1}H NMR revealed the desired esterification product was obtained; although,

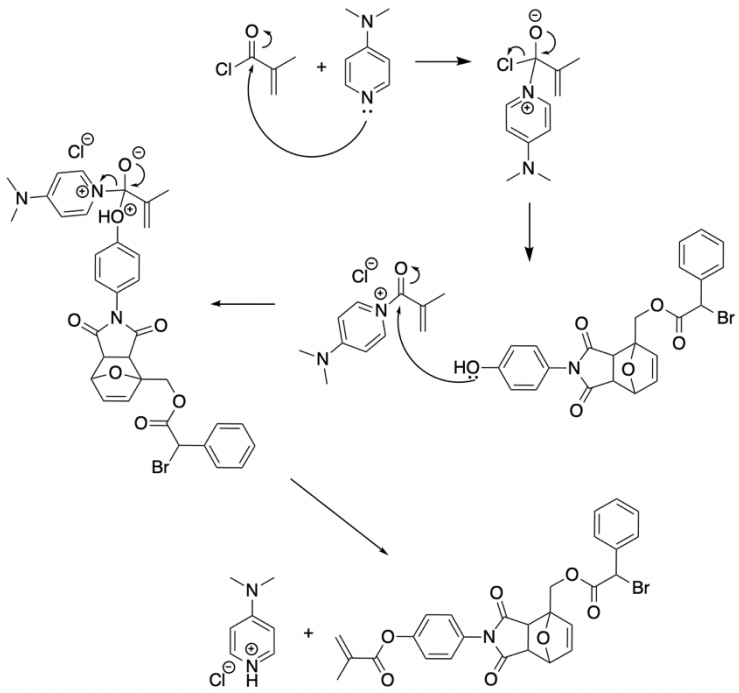

Scheme 4: Mechanism for the steglich esterification of the ATRC-capable Diels-Alder adduct with methacryloyl chloride.

along with a significant production of impurities initially thought to be due to the excess of methacryloyl chloride used in the reaction (Figure A33). However, when the incorporation of methacryloyl chloride was decreased to one equivalent, the impurities continued to persist (Figure A34) and therefore alternate functionalization routes were explored.

To avoid these issues moving forward, a new approach was taken to produce the desired ATRC-capable monomer by conducting the esterification of the phenolic moiety of the dienophile before the Diels-Alder cycloaddition reaction. This was done by exposing the phenolic maleimide to triethylamine and methacryloyl chloride that had been purified by vacuum distillation. This resulted in a pure product verified by ^{1}H NMR (Figure A14-A15) after purification by washing three times with dilute hydrochloric acid (0.1M) to avoid reaction at the

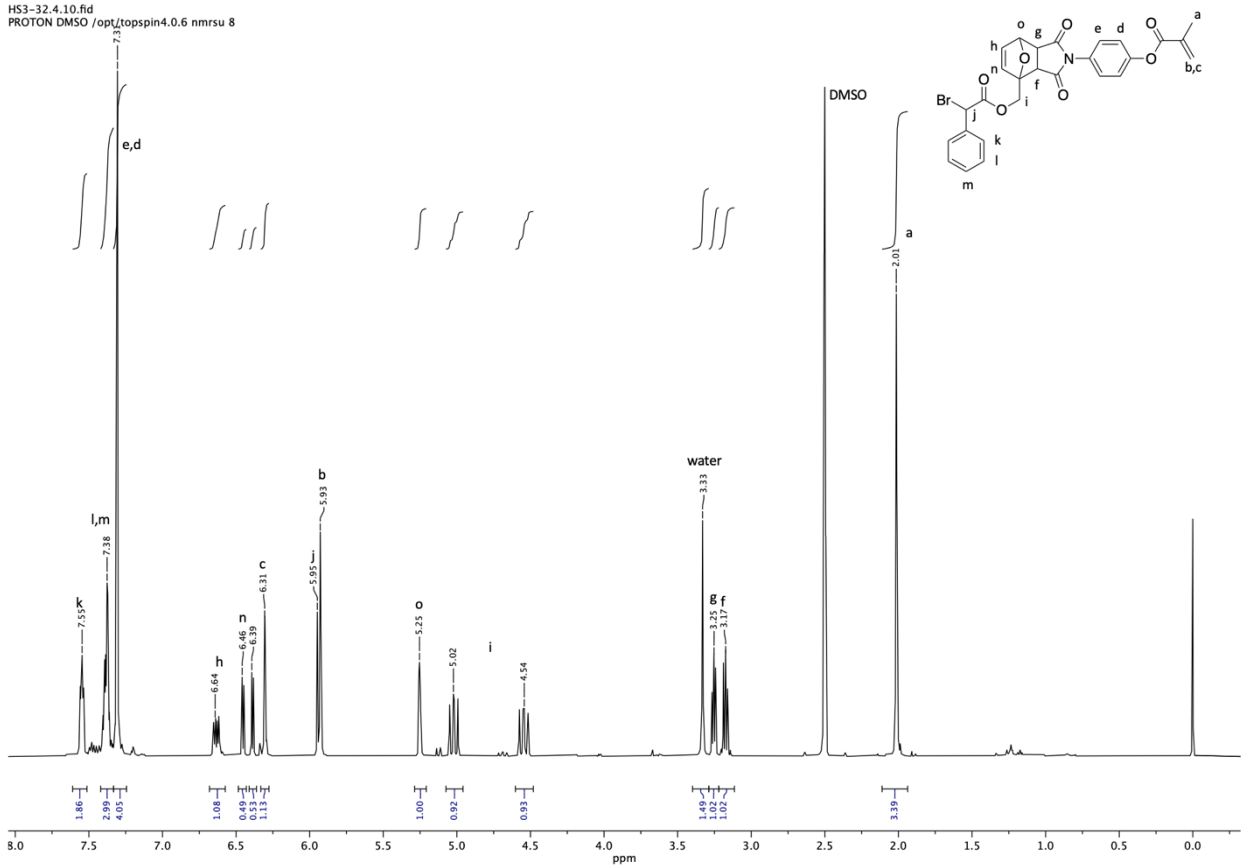

Figure 14: ^{1}H NMR of the isolated and purified ATRC-capable Diels-Alder Adduct (*exo* diastereomer).

maleimide, saturated sodium bicarobonate and brine and isolating the product from the organic layer after drying with anhydrous magnesium sulfate. This reaction proved to be easily scalable for further use in Diels-Alder cycloaddition reactions to synthesize a pure, ATRC-capable monomer.

Initially, the solvent utilized for the synthesis of this adduct was re-evaluated in an attempt to achieve precipitation of the cycloaddition product from the reaction solution to drive the Diels-Alder equilibrium towards the left while simplifying the purification process as has been reported in literature.[45,46,47] Both tetrahydrofuran and acetonitrile were assessed and were introduced to the reaction system at 45°C in minimal amounts to form a saturated solution and aid in precipitation of the product with time. Unfortunately, precipitation was not observed over the course of 48h for either solvent therefore purification was conducted via column chromatography to isolate the Diels-Alder adduct seen in Figure 14.

The diastereomeric ratio behavior previously described for this Diels-Alder adduct pre-esterification over an increasing reaction time should also hold true under increasing temperature conditions. This was observed under variable temperature NMR for the successfully synthesized ATRC-capable

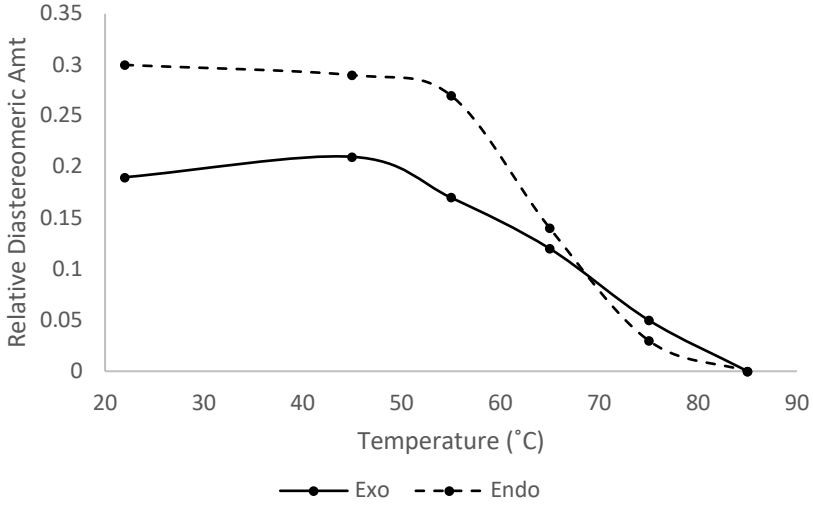

Figure 15: Plot represents trends in *exo* and *endo* diastereomers of the ATRC-capable Diels-Alder adduct with increasing temperature. (Lines are included as a representation of trends in diastereomeric amount)

monomer utilizing a Varian 400MHz mercury solution state NMR. Experiments were conducted in 10°C intervals starting from room temperature and increasing to 85°C where solutions were allowed to equilibrate for 10 minutes after each temperature was reached and stabilized by the instrument before the spectra was taken. To track the relative quantities of *endo* and *exo* diastereomers, the relative diastereomeric amount as seen Figure 15 was determined. Its value was found by calculating the ratio between the respective integrations for *exo* or *endo* peaks corresponding to the tertiary protons of the adduct (f and F, respectively) and the deuterated dimethylsulfoxide peak used as the NMR solvent which maintained a constant concentration throughout the study. Results, which can be seen in Figure 15 and Figures A36-A41, verify that with increasing temperature, the diastereomeric ratio between *exo* and *endo* configurations increases, consistent with reported literature[19,21]. Similar to the explanation above, because the transition energy barrier for the retro-Diels-Alder reaction of the *endo* diastereomer is lower than that of the *exo* analogue, this isomer will undergo cyclo-reversion at a lower temperature. Once reverted to its diene and dienophile precursors, it can reform the cyclo-addition adduct but now in the more thermodynamically favorable *exo*-conformation. The conversion from the less thermodynamically stable *endo* diastereomer to the *exo* diastereomer therefore does not occur as a normal isomerization but must undergo the retro-Diels-Alder reaction first as has been previously reported in the literature[21] and is observed here.

Furthermore, it is observed that with increasing temperature the diastereomeric ratio becomes inverted at 75°C where the concentration of the *exo* diastereomer surpasses that of the *endo* diastereomer. Although both the *endo* and *exo* configurations are undergoing the

retro-cyclization reaction at this relatively high temperature, the *endo* diastereomer does so to a greater extent as previously explained resulting in the inversion and the observed trend.

Additionally, this data is informative to the temperature at which the retro-Diels-Alder reaction begins for this system and the extent to which it occurs which is valuable for its application in additive manufacturing. Figure 15 shows a slight decrease in the *endo* adduct beginning at approximately 45°C where the retro-Diels-Alder reaction begins and after which, the slope significantly decreases with temperature as the rate of this retro-cyclization increases with increasing temperature[21]. The *exo* adduct shows a small increase in concentration at this temperature (45°C) then begins to decline on a more gradual slope as enough energy is applied to the system to initiate its cyclo-reversion. Several proton peaks can be followed to determine this trend in diastereomeric ratio; in this case, peaks "f/F" were selected from each diastereomer corresponding to the proton attached to the tertiary carbon formed by the Diels-Alder adduct as it is easily and consistently isolated from other peaks to avoid peak overlap and inaccurate data. It can also be seen that both adducts have completely undergone the retro-Diels-Alder reaction at 85°C as the ^{1}H NMR peaks at 3.17, 3.23, 3.57 and 3.81ppm corresponding to the tertiary protons of the cycloaddition adduct for the *endo* and *exo* isomers respectively, have disappeared.

It can be seen in Figure 16 and Figures A38-A41 that new peaks begin to appear at 65°C that do not correspond to either the *endo* or *exo* diastereomers and therefore it is believed that a new Diels-Alder product is formed as a result of side reactions occurring throughout the variable temperature ^{1}H NMR experiment. It is possible that such reactions can occur before or

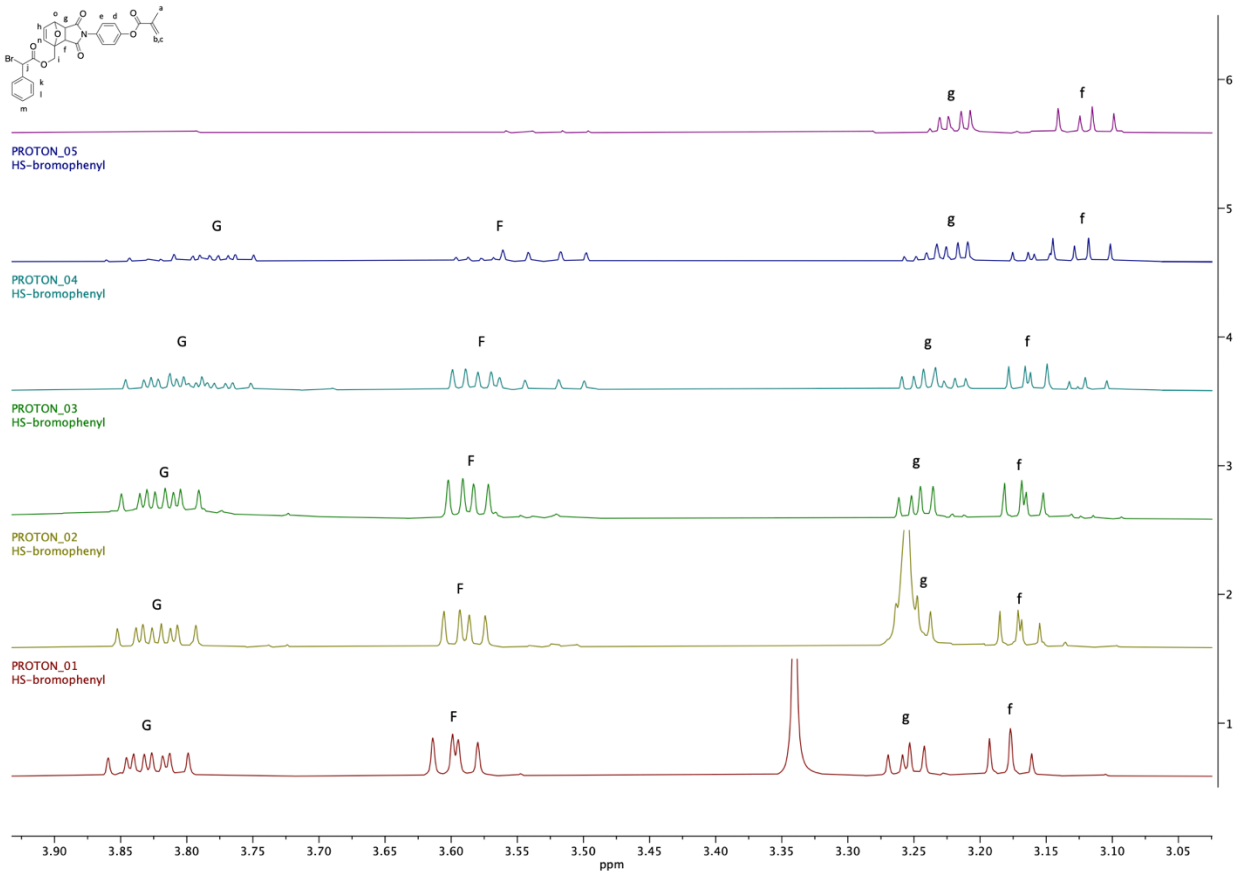

Figure 16: Variable temperature ^{1}H NMR experiment of the ATRC-capable monomer - tertiary protons generated by the Diels-Alder reaction are emphasized (Uppercase alphabet represents the *exo* diastereomer, lowercase alphabet represents the *endo* diastereomer)

after the retro-Diels-Alder reaction has ensued giving rise to several different products. For example, water, present in the reaction vessel from the d-DMSO (proton peak at 3.33ppm seen in Figure 16) used to prepare the NMR sample, is capable of acting as a nucleophile in an S_N1 reaction at the alpha position of the ester carbonyl to substitute the bromine for a hydroxy group. Alternatively, once the maleimide functionality has been exposed after a cyclo-reversion reaction at elevated temperatures, it can be hydrolyzed by the water present, making it incapable of undergoing the forward-Diels-Alder reaction. Therefore, in future steps it is pertinent to thoroughly remove water from the system to avoid these side reactions and obtain our desired polymeric product. Additionally, further investigation should be conducted to

evaluate and confirm the reactions occurring and identity of the byproducts produced under these conditions.

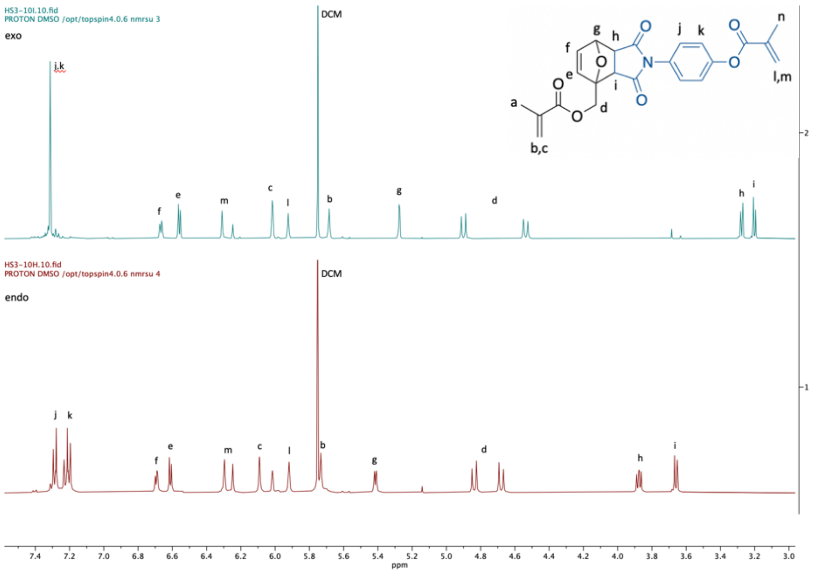

Figure 17: Stacked ^{1}H NMR of the isolated and purified diastereomers of the Diels-Alder functionalized crosslinker. (*Exo* diastereomer = top; *endo* diastereomer = bottom)

The second adduct evaluated was that of furfuryl methacrylate and N-(4-hydroxyphenyl maleimide), further identified as the Diels-Alder functionalized crosslinker, synthesized using a modified procedure from Wilborn et al[45]. An initial solvent study was conducted between two commonly utilized solvents reported in literature for the Diels-Alder reaction, dichloromethane and acetonitrile, to determine optimal reaction conditions for the greatest yield[21]. For each trial, the dienophile was added to an excess of furfuryl methacrylate and allowed to run for 4 days at 40°C or 45°C in dichloromethane or acetonitrile, respectively. While yields of the Diels-Alder adduct were not significantly different after purification by column chromatography (57% yield for acetonitrile vs. 50% yield in dichloromethane), the enhanced solubility of both the reactants and products in acetonitrile facilitated the reaction procedure and was therefore used moving forward. Additionally, it was observed by ^{1}H NMR that the *endo* and *exo* Diels-Alder adducts could also be separated via column chromatography (Figure 17). It is hypothesized this is due to their significant difference

in polarity owing to the large moieties bonded to both the diene and dienophile similar to that of the previous Diels-Alder adduct examined.

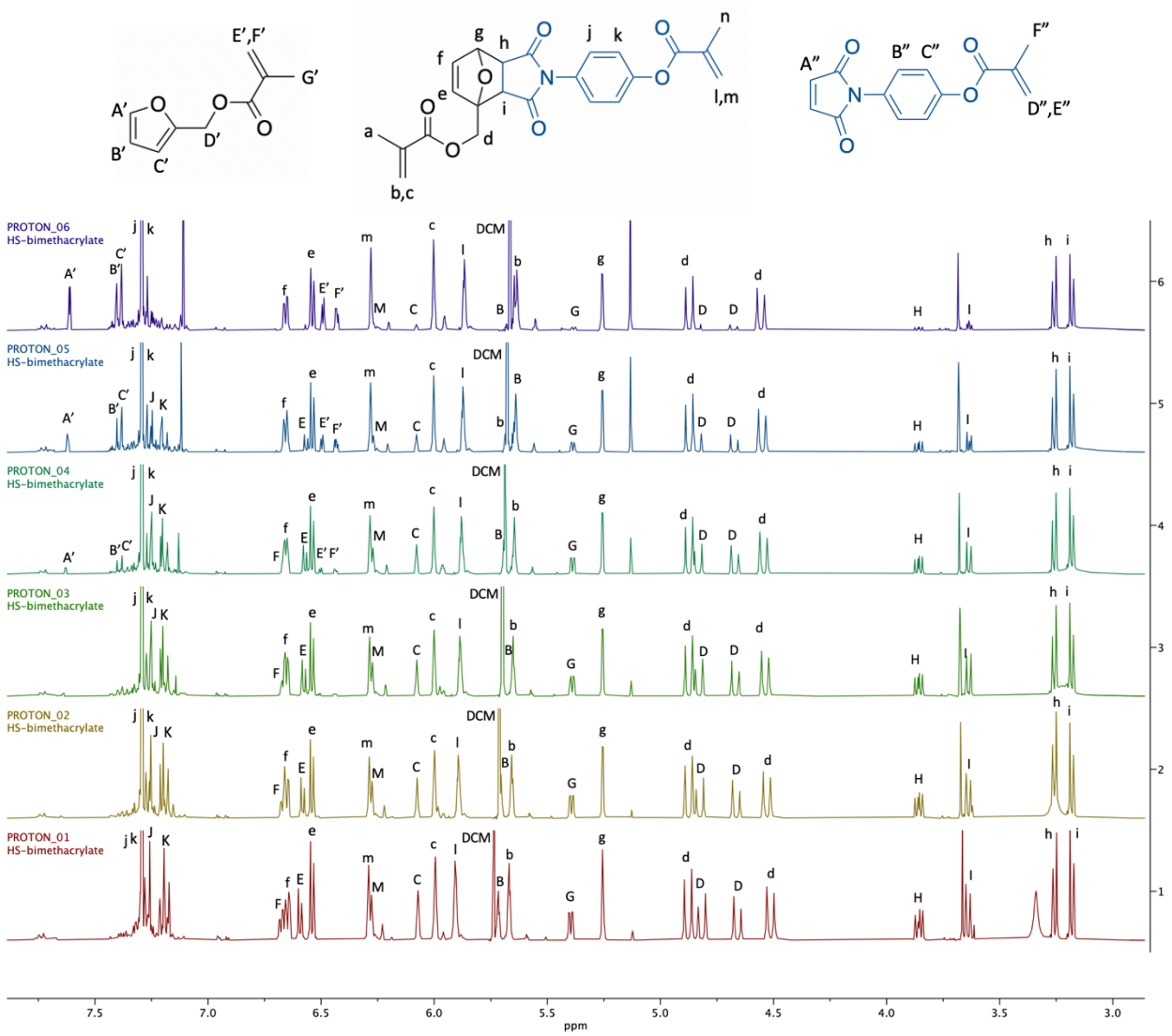

Figure 18: Variable temperature NMR experiment of Diels-Alder functionalized crosslinker – Uppercase alphabet = *endo* diastereomer, lower case alphabet = *exo* diastereomer

The same process utilized in the evaluation of the diastereomeric ratio with temperature for the ATRC-capable monomer was employed here. Several proton peaks from the variable temperature NMR experiment shown in Figure 18 can be followed to determine this trend in diastereomeric ratio; in this case, peaks "g/G" were selected from each diastereomer corresponding to the proton attached to the tertiary carbon included in the Diels-

Alder adduct as it is easily and consistently isolated from other peaks to avoid peak overlap and inaccurate data. The same calculation utilized for the ATRC-capable monomer was employed here to determine the relative diastereomeric amount and observe trends in *endo* and *exo* diastereomers with increasing temperature. Figure 19 shows that with increasing temperature, both the *endo* and *exo* diastereomers show a decreasing trend at approximately 55°C revealing initiation of the retro-Diels-Alder reaction at this temperature. However, although both decrease, there is a significant difference in the extent and rate at which the two diastereomers do so. The steeper slope of the *endo* diastereomer shows its greater propensity to undergo retro-cyclization which is attributed to its smaller transition state energy barrier and therefore lower amount of heat required to initiate the reaction. Additionally, this diastereomer reaches a relative diastereomeric amount of 0.03 at 85°C where the more thermodynamically stable *exo* diastereomer only decreases to a value of 0.29 showing the greater extent to which the *endo* isomer undergoes the retro-Diels-Alder reaction at elevated temperatures.

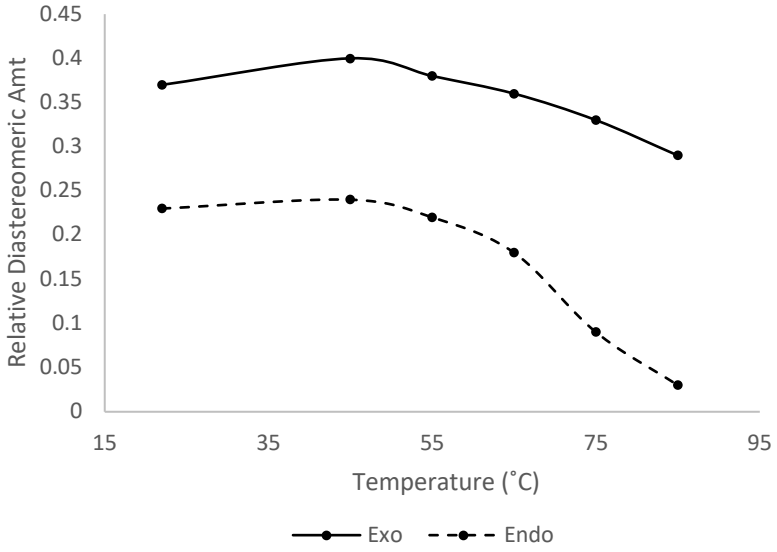

Figure 19: Plot represents trends in the *endo* and *exo* diastereomers of the Diels-Alder functionalized crosslinker with increasing temperature. (Lines are included as a representation of trends in diastereomeric amount)

The difference in behavior under elevated temperatures between the Diels-Alder crosslinker and ATRC-capable monomer should be noted. It can be seen that the latter

undergoes retro-cyclization to a greater extent than that of the crosslinker as both the *endo* and *exo* diastereomers underwent full conversion to their diene and dienophile starting materials. Additionally, the ratio of *endo* to *exo* configurations of the ATRC-capable monomer experienced an inversion resulting in an excess of *exo* isomer at 75°C where no such inversion was evident for the crosslinker examined. These behaviors can be attributed to the difference in stability of the two adducts leading to discrepancies in retro-Diels-Alder temperatures/extent of the retro-Diels-Alder reaction. There has been little literature precedent for exact substituent effects on the rate of the retro-Diels-Alder reaction for various systems; however, it can be concluded that a less stable adduct requires less energy to undergo the retro-cyclization reaction and will therefore revert to its starting materials at a lower temperature. Both adducts examined have identical dienophile components and differ in their diene. However, both dienes investigated are substituted with an alkyl substituent in the 2-position of the furan ring leading to similar amounts of electron density being donated to the diene. Therefore, it is hypothesized the difference in retro-Diels-Alder reactivity is attributed to steric effects. The retro-cyclization is favored for the ATRC capable monomer containing the relatively bulky bromophenyl functionality to relieve strain on the system. However, further investigation of this behavior is necessary to confirm this effect.

Finally, copolymerization of the ATRC-capable monomer with methyl methacrylate was attempted under reduced temperatures to avoid cyclo-reversion of the Diels-Alder adduct. To do so, 2,2'-azobis(2,4-dimethylvaleronitrile) (V-70) was employed as an initiator which has a half-life of 10h at 30°C. Number average molecular weights of 20 and 25kDa were targeted with ATRC-capable monomer incorporations of 5, 10, and 15mol%. Polymerizations were conducted

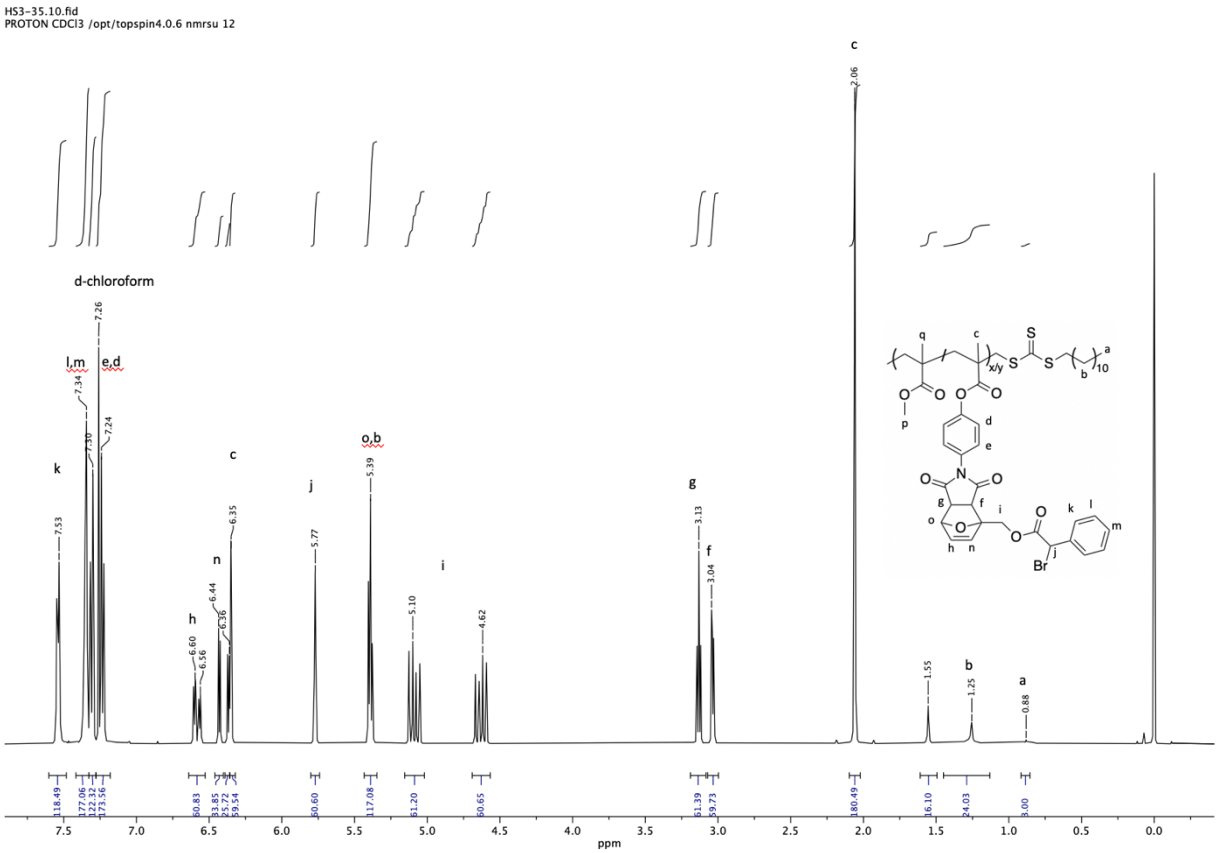

Figure 20: Resulting ^{1}H NMR of the attempted copolymerization of methyl methacrylate and ATRC-capable monomer via RAFT (25kDa, 15mol% incorporation ATRC-capable monomer) after purification by precipitation in small amounts of cold methanol.

under inert atmosphere at 35°C and were run for either 24 or 48h. Unfortunately, each of these systems failed to produce the desired Diels-Alder functionalized copolymer. This was first evident by difficulties in the precipitation process which was conducted in methanol in a dry ice/isopropanol bath (-78°C) where it was found the reaction mixture would only precipitate in small quantities of solvent (~5mL) and remain in solution on the larger scale. Isolation of a precipitate was achieved for characterization via addition of approximately 5 mL of cold methanol to the condensed reaction mixture, allowing the generated solid to settle followed by extraction of the resulting solution with a pipette. Analysis of the resulting material revealed

oligomeric materials of pure ATRC-capable monomer with no incorporation of methyl methacrylate (Figure 20).

Therefore, investigation into the reactivity of methyl methacrylate versus the ATRC-capable monomer under these conditions was conducted via homopolymerizations of each at 35°C (25kDa). Analysis by ^{1}H NMR revealed failure of methyl methacrylate to polymerize under these reaction conditions (Figure A57) as only monomer was observed in the spectra. The ATRC-capable monomer formed an insoluble solid and therefore, analysis by solution state NMR could not be conducted. However, it was shown under the initial copolymerization conditions that this monomer is reactive and propagates through the vinyl group of the methacrylate unit. To increase the rate of radical production and aid in the initiation of the homopolymerization of methyl methacrylate, the reaction was run again at the maximum temperature to avoid initiation of the retro-Diels-Alder reaction, 50°C. Although minimal, this did result in polymerization observed by peaks corresponding to the backbone of poly(methyl methacrylate) in ^{1}H NMR (Figure A58). Unfortunately, increasing temperature conditions further to induce methyl methacrylate polymerization is not an option if the retro-Diels-Alder reaction is to be avoided. Therefore, further investigation of alternate monomers of greater reactivity under low-temperature conditions for the copolymerization of the ATRC-capable monomer is necessary in addition to more thorough characterization of the given polymerization system.

Chapter 3: Conclusions

In conclusion, to aid in the enhancement of the mechanical stability of 3D printed objects, the synthesis of two systems of Diels-Alder functionalized monomers to implement in thermally responsive particles was investigated. Both systems took advantage of the dynamic covalent character of the cycloaddition reaction between furan and maleimide diene and dienophile counterparts, respectively and were decorated with moieties dependent upon the method in which their intended adduct was to be used for particle formation. The first monomer considered was formulated for particle crosslinking via ATRC chemistry and therefore a bromophenyl functionality was incorporated into the diene via a simple Steglich esterification. The synthesized dienophile was intended for use in both monomers explored and therefore incorporated a versatile phenolic moiety allowing for functionalization with a plethora of chemistries. To generate the maleimide, a variety of synthetic routes were evaluated to determine the most facile process resulting in an optimized approach. The second monomer investigated implements bifunctionality to achieve particle formation by incorporation of methacrylate functionalities in both the diene and dienophile.

The synthesis of these monomers was evaluated in terms of reaction conditions and resulting diastereomeric ratios as a result. Consistent with reported literature, it was found that increasing reaction time or temperature favored the formation of the more thermodynamically stable *exo* adduct. Additionally, when exposed to increasing temperature conditions, the kinetic *endo* configuration was observed to be the first to undergo the retro-Diels-Alder reaction and does so at a greater rate than the more stable *exo* configuration. This data is directly applicable to the intended use of these adducts in 3D printing purposes. The objective of this work is to

investigate the production of thermally responsive particles to be blended with filaments for additive manufacturing. The retro-Diels-Alder reaction is instigated during the heated extrusion process which, along with an expected reduction in viscosity of the filament, is an integral mechanism for mechanical property enhancement of the resulting 3D printed objects. Therefore, the difference in temperature for the initiation of the retro-Diels-Alder reaction and the rate at which it occurs influences the materials and conditions that can be utilized. Additionally, in many cases it is desirable to target lower processing temperatures to avoid degradation of materials utilized in the additive manufacturing process as well as energy consumption and therefore, knowledge of the systems that present the lowest retro-Diels-Alder temperatures is desirable.

Finally, copolymerization of the ATRC capable monomer with methyl methacrylate via RAFT was investigated. Although successful copolymerization was not observed, valuable information pertaining to the reactivity of the monomers was gathered under the reaction conditions employed to avoid the retro-cyclization reaction of the Diels-Alder moieties incorporated.

Chapter 4: Future Work

To progress the research discussed here, several steps should be taken for the formation of thermally responsive particles to aide in the enhancement of additively manufactured objects. Firstly, investigation into the polymerization of these systems should be conducted utilizing both RAFT as well as heterogeneous polymerization systems for the ATRC-capable monomer and Diels-Alder functionalized crosslinker, respectively; covering various molecular weights and Diels-Alder functionalized monomer incorporations. These reactions should be investigated under relatively mild conditions so as to not reverse the Diels-Alder linkages present in the synthesized functional monomers. Proper characterization via NMR and gel permeation chromatography should be utilized to verify production of these polymers and their functional incorporations. Subsequently, ATRC chemistry should be employed to induce particle formation of the polymers generated via RAFT polymerization.

After formation of the desired particles, characterization of their thermally responsive behavior should be conducted utilizing methods such as differential scanning calorimetry, variable temperature NMR, and gel permeation chromatography. Once successful formation and characterization of these systems is obtained, implementation into filaments for additive manufacturing can be realized and evaluation of their impact on 3D printed objects can be performed.

Chapter 5: Experimental

I. Reagents and Solutions

All reagents and solvents utilized were purchased from Sigma-Aldrich, Acros Organics, Alfa Aesar, FUJIFILM Wako Chemicals, TCI America, Oakwood Products, Inc., Fluka or Fisher Scientific unless otherwise noted. All chemicals were used as received unless specifically stated. The removal of solvent under reduced pressure refers to utilizing a rotary evaporator. Solutions of saturated sodium bicarbonate and hydrochloric acid refer to aqueous solutions and brine is used to reference a saturated aqueous solution of sodium chloride.

II. Instrumentation

Nuclear magnetic resonance (NMR) spectra were obtained utilizing Varian Mercury 400 and 500 MHz spectrometers. Chemical shifts are reported in parts per million (ppm) relative to an internal standard of tetramethylsilane and are reported using an s for singlet, d for doublet, t for triplet or m for multiplet. Deuterated solvents used were dependent on the compound being investigated and are referenced in each case. Additional NMR investigations were made utilizing homonuclear correlation spectroscopy (g-COSY) and hereonuclear single quantum coherence spectroscopy (gHSQC).

III. Experimental Procedures and Data

α-Bromo-2-furanylmethylester-benzeneacetic acid

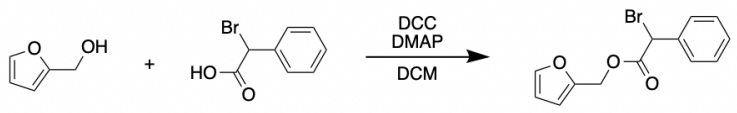

A 250mL round bottom flask was placed in an ice bath and charged with α-bromophenylacetic acid (2.905g, 13.51mmol), 4-dimethylaminopyridine (0.0825g, 0.675mmol), N,N'-

dicyclohexylcarbodiimide (3.064g, 14.85mmol), dichloromethane (60mL), and furfuryl alcohol (3.973g, 40.50mmol). The resulting solution was brought to 25°C and stirred for 24h. After the reaction, the product was isolated by rotary evaporation and purified by column chromatography (SiO_2, dichloromethane) to yield the compound as a white solid. (2.82g, 71% yield): ^{1}H NMR (500MHz, $(CD_3)_2SO$) δ 5.18 (m, 2H), 5.98(s, 1H), 5.46 (s, 1H), 6.55 (s, 1H), 7.37 (m, 3H), 7.52-7.53 (m, 2H), 7.69 (s, 1H); ^{13}C NMR (500MHz, $(CD_3)_2SO$) δ 47.03 (s), 59.91 (s), 111.26 (s), 112.02 (s), 129.11 (s), 129.24 (s), 129.66 (s), 136.60 (s), 144.54 (s), 148.92 (s), 168.12 (s).

Amic Acid

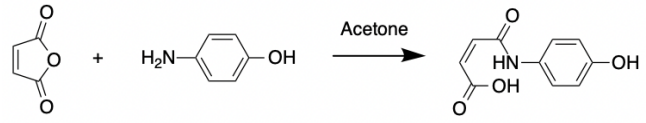

In a 250mL round bottom flask, 4-aminophenol (6.42g, 58.83mmol) was dispersed in acetone (60mL) at room temperature. Maleic anhydride pellets (5.64g, 57.52mmol) were added in portions to the stirring solution to form a yellow precipitate and the reaction mixture was stirred overnight. The product was isolated by vacuum filtration and purified by washing with cold acetone. (11.42g, 96% yield): ^{1}H NMR (500MHz, $(CD_3)_2SO$) δ 6.30 (d, 1H), 6.45 (d, 1H), 6.74 (d, 2H), 7.43 (d, 2H), 9.34 (s, 1H), 10.40 (s, 1H) 13.66 (s, 1H); ^{13}C NMR (500MHz, $(CD_3)_2SO$) δ 115.70 (s), 121.96 (s), 130.25 (s), 131.76 (s), 132.22 (s), 154.53 (s), 163.20 (s), 166.95 (s).

N-(4-hydroxyphenyl maleimide): Dicyclohexylcarbodiimide Method

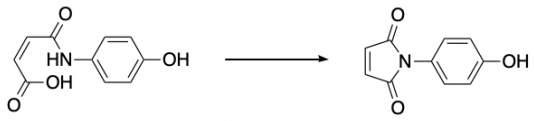

A 25mL round bottom flask was charged with the previously synthesized amic acid (0.5g, 2.41mmol), dicarbocyclohexyldiimide (0.45g, 2.18mmol) and 5mL dichloromethane. The reaction mixture was refluxed at 40°C overnight then vacuum filtered and washed with cold dichloromethane. The precipitate was dissolved in acetonitrile and vacuum filtered again to yield a yellow-brown material. (0.46g, 81.1% yield): ^{1}H NMR (500MHz, $(CD_3)_2SO$) δ 6.83 (d, 4H), 7.02 (d, 2H), 7.35 (d, 4H), 7.74 (d, 2H), 4.85 (s, 2H).

N-(4-hydroxyphenyl maleimide): Steglich Esterification Method

A 25mL round bottom flask was charged with dicarbocyclohexyldiimide (0.45g, 2.18mmol), 4-dimethylaminopyradine (29.5mg, 0.241mmol) and 8mL dichloromethane. The previously synthesized amic acid (0.5g, 2.41mmol) was then added and the reaction mixture was allowed to stir overnight at 22°C. The resulting solution was vacuum filtered, concentrated by rotary evaporation and purified via column chromatography (75:25 ethyl acetate:hexanes) to yield a yellow-brown material (0.429g, 93.2% yield).

N-(4-hydroxyphenyl maleimide): Anhydrous Sodium Acetate-Acetic Anhydride Method

The previously synthesized amic acid (3.78g, 18.2mmol) was added to a 25mL round bottom flask containing anhydrous sodium acetate (0.65g, 7.92mmol) and acetic anhydrous (6.7mL, 70.9mmol). The reaction mixture was stirred at 100°C for 30min then cooled to room

temperature in a cold-water bath. This solution was then precipitated into an ice/water mixture and vacuum filtered. The resulting yellow solid was rinsed with ice water and dried under reduced pressure. (3.61g, 105% yield): ^{1}H NMR (500MHz, $(CD_3)_2SO$) δ 2.28 (s, 3H), 7.19 (s, 2H), 7.25 (d, 2H), 7.35 (d, 2H); ^{13}C NMR (500MHz, $(CD_3)_2SO$) δ 21.30 (s), 122.84 (s), 128.44 (s), 129.46 (s), 135.17 (s), 150.04 (s), 169.68 (s), 170.36 (s).

N-(4-hydroxyphenyl maleimide)

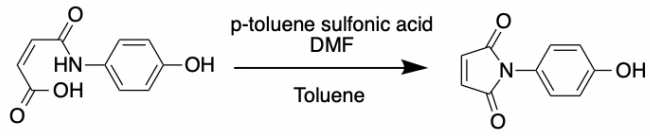

Amic acid (3.0g, 14.5mmol) was dispersed in toluene (12.8mL) in a 50mL round bottom flask. The reaction vessel was then charged with p-toluene sulfonic acid (0.197g, 1.14mmol) and N,N-dimethylformamide (2.25mL) and the mixture was refluxed at 110°C for 24h. The resulting dark brown solution was precipitated into an ice/water mixture to produce a yellow-brown solid that was isolated by vacuum filtration and washed with ice cold water. The product was dried under vacuum followed by purification via hot filtration in dichloromethane to obtain a yellow-orange powder. (1.42g, 51.8% yield): ^{1}H NMR (500MHz, $(CD_3)_2SO$) δ 6.84 (d, 2H), 7.07 (d, 2H), 7.13 (s, 2H), 9.68 (s, 1H); ^{13}C NMR (500MHz, $(CD_3)_2SO$) δ 115.89 (s), 123.00 (s), 128.86 (s), 135.00 (s), 157.50 (s), 170.77 (s).

DMF Study

To study the effect of DMF incorporation the same procedure as seen above for the production of phenolic maleimide utilizing p-toluene sulfonic acid was conducted for several different trials. The ratios of DMF, toluene and amic acid utilized for each trial can be seen in Table 1.

Steglich Esterification of N-(4-hydroxyphenyl maleimide)

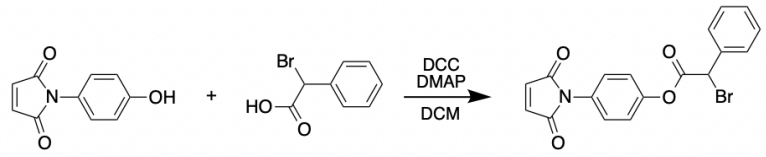

Dicyclohexylcarbodiimide (0.29g,), 4-dimethylaminopyradine (7.91mg,), α-bromophenylacetic acid(0.28g,) and dichloromethane (7.5mL) were added to a 25mL round bottom flask at 0°C in an ice bath. N-(4-hydroxyphenyl maleimide) (0.49g,) was then added and the reaction mixture was brought to room temperature and allowed to stir for 24h. The precipitate was removed via vacuum filtration and the resulting solution was condensed via rotary evaporation. ^{1}H NMR (500MHz, $(CD_3)_2SO$) δ 1.05-1.23 (m, 8H), 1.49-1.71 (m, 8H), 5.56 (d, 1H), 6.84 (d, 2H), 7.07 (d, 2H), 7.13 (s, 2H), 7.23 (s, 2H), 7.31 (d, 2H), 7.41 (d, 2H).

Exo-N-(p-hydroxyphenyl)-3,6-epoxy-4-cyclohexene-1,2-dicarboximide

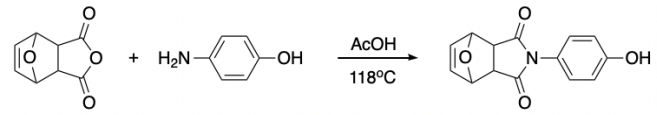

P-aminophenol (1.31g, 12.0mmol), 7-oxabicyclo[2.2.1]hept-5-ene-2,3-dicarboxylic anhydride (2.0g, 10.86mmol) and 3mL glacial acetic acid were added to a 50mL round bottom flask and

refluxed at 118°C for 1 hour to generate a precipitate. The reaction mixture was then cooled to room temperature and the solid was isolated via vacuum filtration and rinsed with water followed by drying under reduced pressure. ^{1}H NMR (500MHz, $(CD_3)_2SO$) δ 3.03 (s, 2H), 5.22 (s, 2H), 6.31 (d, 1H), 6.44 (d, 1H), 6.60 (s, 2H), 6.74 (d, 2H), 6.83 (d, 2H), 6.96 (d, 2H), 7.41 (d, 2H), 9.35 (s, 1H), 9.75 (s, 1H), 10.38 (s, 1H), 13.70 (s, 1H).

Exo-N-(p-hydroxyphenyl)-3,6-epoxy-4-cyclohexene-1,2-dicarboximide

P-aminophenol (1.31g, 12.0mmol), 7-oxabicyclo[2.2.1]hept-5-ene-2,3-dicarboxylic anhydride (2.0g, 10.86mmol) and 3mL methanol were added to a 50mL round bottom flask and refluxed at 70°C for 1 hour to generate a precipitate. The reaction mixture was then cooled to room temperature and the solid was isolated via vacuum filtration and rinsed with water followed by drying under reduced pressure. (2.02g, 72% yield): ^{1}H NMR (500MHz, $(CD_3)_2SO$) δ 5.22 (s, 2H), 6.60 (s, 2H), 6.83 (d, 2H), 6.95 (d, 2H), 9.76 (s, 1H).

Steglich Esterification of Exo-N-(p-hydroxyphenyl)-3,6-epoxy-4-cyclohexene-1,2-dicarboximide

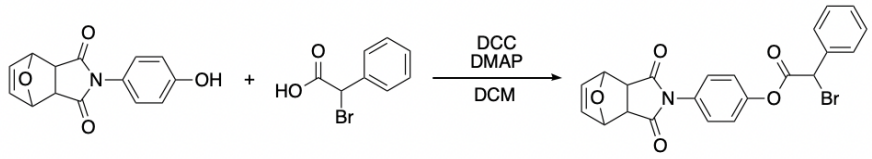

Dicyclohexylcarbodiimide (0.25g, 1.21mmol), 4-dimethylaminopyridine (6.72mg, .055mmol), α-bromophenylacetic acid(0.237g, 1.10mmol) were dissolved in 9mL of dichloromethane in a 25mL round bottom flask. *Exo*-N-(p-hydroxyphenyl)-3,6-epoxy-4-cyclohexene-1,2-dicarboximide (0.57g, 2.20mmol) was then added and the reaction mixture was allowed to stir for 24h followed by vacuum filtration to remove the precipitate. The resulting solution was

condensed via rotary evaporation and the product was isolated by column chromatography (SiO_2, 70:30 ethyl acetate: hexanes). (0.048g, 9.65% yield): ^{1}H NMR (500MHz, $(CD_3)_2SO$) δ 3.01 (s, 1H), 3.06 (s, 2H), 5.20 (s, 1H), 5.22 (s, 2H), 5.43 (s, 1H), 6.58 (s, 3H), 6.81 (d, 2H), 6.93 (d, 2H), 7.12 (d, 2H), 7.21 (d, 2H), 7.41 (m, 4H), 7.51 (d, 2H).

Esterification of N-(4-hydroxyphenyl maleimide)

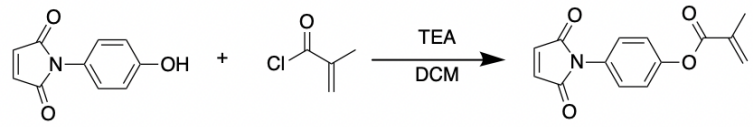

N-(4-hydroxyphenyl maleimide) (1g, 5.29mmol) was dissolved in 41.13mL dichloromethane in a 100mL round bottom flask and brought to 0°C by placing in an ice bath. Triethylamine (0.81mL, 5.81mmol) was then added dropwise to the stirring solution which was subsequently sparged with argon gas for 15min. Methacryloyl chloride (0.61g, 5.84mmol), previously purified by vacuum filtration, was then added dropwise via syringe to the solution at 0°C. The reaction was allowed to stir for 24h was then washed with 0.1M HCl (3x30mL), saturated sodium bicarbonate (2x30mL) and brine (1x35mL). The organic layer was dried with anhydrous magnesium sulfate which was removed by vacuum filtration and the resulting solution was concentrated via rotary evaporation and dried in a vacuum oven to obtain a yellow powder. (1.31g, 96% yield): ^{1}H NMR (500MHz, $(CD_3)_2SO$) δ 2.02 (s, 3H), 5.93 (s, 1H), 6.31 (s, 1H), 7.20 (s, 2H), 7.31 (d, 2H), 7.39 (d, 2H); ^{13}C NMR (500MHz, $(CD_3)_2SO$) δ 18.50 (s), 122.82 (s), 128.44 (s), 128.48 (s), 129.58 (s), 135.19 (s), 135.63 (s), 150.14 (s), 165.73 (s), 170.16 (s).

ATRC-Capable Diels-Alder Adduct

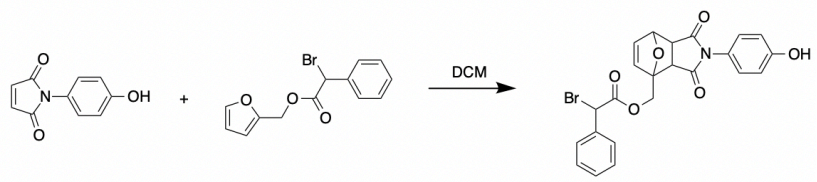

A 25mL round bottom flask was charged with N-(4-hydroxyphenyl maleimide) (0.53g, 2.80mmol) and α-bromo-2-furanylmethylester-benzeneacetic acid (0.90g, 3.06mmol). Dichloromethane (7mL) was then added and the reaction mixture was stirred at 40°C with a condenser attachment for six days. The resulting product was isolated via rotary evaporation and purified by column chromatography (SiO_2, 60:40 Ethyl Acetate:Hexanes). The resulting solution was condensed by rotary evaporation to generate a tan solid. (0.62g, 46%yield): (*Endo*) ^{1}H NMR (500MHz, $(CD_3)_2SO$) δ 3.54 (d, 1H), 3.78 (m, 1H), 4.75 (m, 1H), 4.88 (m, 1H), 5.37 (m, 1H), 6.01 (d, 1H), 6.46-6.50 (m, 1H), 6.64 (m, 0.98), 6.81 (d, 2H), 6.90 (d, 2H), 7.38 (m, 3H), 7.57 (d, 2H), 9.73 (s, 1H); ^{13}C NMR (500MHz, $(CD_3)_2SO$) δ 21.19 (s), 46.48-47.69 (q), 63.91 (s), 79.65 (s), 89.78 (s), 115.84 (s), 123.37 (s), 128.56 (s), 129.26 (d), 129.68 (d), 134.57 (s), 136.38-136.55 (q), 157.93 (s), 168.22 (d), 174.60 (d). (*Exo*) ^{1}H NMR (500MHz, $(CD_3)_2SO$) δ 3.11 (d, 1H), 3.19 (d, 1H), 4.51 (t, 1H), 4.99 (t, 1H), 5.22 (s, 1H), 5.92 (d, 1H), 6.38-6.44 (m, 1H), 6.62 (m, 1H), 6.84 (d, 2H), 6.98 (d, 2H), 7.37 (m, 3H), 7.54 (d, 2H), 9.75 (s, 1H); ^{13}C NMR (500MHz, $(CD_3)_2SO$) δ 21.24 (s), 46.80-47.08 (d) 48.88 (s), 50.19 (s), 63.89 (s), 81.37 (s), 89.32 (s), 115.90 (s), 123.56 (s), 128.55 (s), 129.16-129.21 (t), 129.29 (s), 136.50 (d), 157.86 (s), 168.19 (s), 174.72 (s), 176.02 (s).

Reaction Time Investigation

A 25mL round bottom flask was charged with N-(4-hydroxyphenyl maleimide) (0.195g, 1.03mmol) and α-bromo-2-furanylmethylester-benzeneacetic acid (0.34g, 1.15mmol). Dichloromethane (2mL) was then added and the reaction mixture was stirred at 40°C with a condenser attachment for a specified amount of time. The resulting product was isolated via rotary evaporation and purified by column chromatography (60:40 Ethyl Acetate:Hexanes) to generate a tan solid.

ATRC-Capable Diels-Alder Esterification

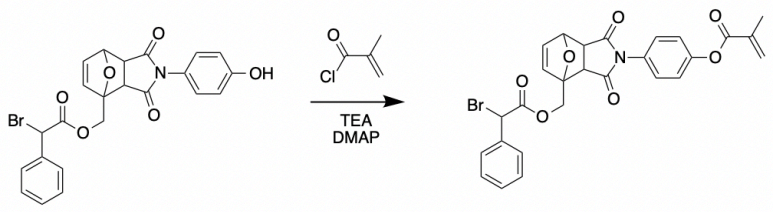

Attempt 1:

In an oven dried 100mL round bottom flask, the Diels-Alder adduct (0.18g, 0.37mmol) was dissolved in tetrahydrofuran (5.44mL) and the reaction vessel was brought to 0°C in an ice bath. 4-Dimethylaminopyridine (1.0mg, 0.0082mmol) and triethylamine (0.055mL, 0.40mmol) were added and the solution was bubbled with Argon gas for 15 minutes. Methacryloyl chloride (0.08mL, 0.82mmol) was then added in 1mL tetrahydrofuran dropwise while stirring. The reaction was allowed to stir for 24h before quenching with air and removing the tetrahydrofuran via rotary evaporation. The resulting brown material was dissolved in dichloromethane and washed with 1M hydrochloric acid (2x20mL), saturated sodium bicarbonate (2x20mL), and brine (1x25mL). The organic layer was dried with anhydrous

magnesium sulfate which was removed by vacuum filtration then concentrated via rotary evaporation to produce a light brown liquid that was further purified by column chromatography. (0.25, 125% yield): ^{1}H NMR (500MHz, $(CD_3)_2SO$) δ 3.15 (m, 1H), 3.24 (d, 1H), 3.76 (m, 8H), 4.26 (m, 1H), 4.55 (m, 1H), 5.02 (m, 1H), 5.23 (s, 1H), 5.38 (d, 3H), 5.56-5.61 (m, 1H), 5.93 (s, 1H), 5.94 (s, 1H), 6.31 (s, 1H), 6.58-6.62 (m, 1H), 7.30 (s, 4H), 7.40 (s, 3H), 7.48 (s, 2H), 11.69 (s, 3H).

Attempt 2 (without DMAP):

In an oven dried 100mL round bottom flask, the Diels-Alder adduct (0.5g, 1.03mmol) was dissolved in tetrahydrofuran (14.26mL) and the reaction vessel was brought to 0°C in an ice bath. Triethylamine (0.12mL, 1.19mmol) were added and the solution was bubbled with Argon gas for 15 minutes. Methacryloyl chloride (0.216mL, 2.06mmol) was added in a solution of tetrahydrofuran (1mL) while stirring using an addition funnel. The reaction was allowed to run for 24h before quenching with air and removing the acetonitrile via rotary evaporation. The resulting brown material was dissolved in dichloromethane and washed with 1M hydrochloric acid (2x20mL), saturated sodium bicarbonate (2x20mL), and brine (1x25mL). The organic layer was dried with anhydrous magnesium sulfate which was removed by vacuum filtration then concentrated via rotary evaporation to produce a light brown liquid. ^{1}H NMR (500MHz, $(CD_3)_2SO$) δ 1.66 (t, 3H), 1.94 (s, 2H), 2.02 (s, 3H), 3.18 (m, 1H), 3.25 (m, 1H), 4.54 (m, 1H), 5.03 (m, 1H), 5.26 (d, 1H), 5.93 (s, 1H), 5.95 (s, 1H), 6.02 (s, 1H), 6.31 (s, 1H), 6.39-6.46 (m, 1H), 6.64 (m, 1H), 7.20-7.27 (m, 2H), 7.31 (s, 2H), 7.38-7.39 (m, 3H), 7.48 (m, 1H), 7.55 (m, 2H).

Attempt 3 (Reduction of methacryloyl chloride):

In an oven dried 100mL round bottom flask, the Diels-Alder adduct (0.5g, 1.03mmol) was dissolved in tetrahydrofuran (14.26mL) and the reaction vessel was brought to 0°C in an ice bath. Triethylamine (0.12g, 1.19mmol) was added dropwise and the solution was bubbled with Argon gas for 15 minutes. Methacryloyl chloride (0.108g, 1.03mmol) was added in a solution of tetrahydrofuran (1mL) while stirring using an addition funnel. The reaction was allowed to run for 24h before quenching with air and removing the acetonitrile via rotary evaporation. The resulting brown material was dissolved in dichloromethane and washed with 1M hydrochloric acid (2x20mL), saturated sodium bicarbonate (2x20mL), and brine (1x25mL). The organic layer was dried with anhydrous magnesium sulfate which was removed by vacuum filtration then concentrated via rotary evaporation to produce a light brown liquid. ^{1}H NMR (500MHz, $(CD_3)_2SO$) δ 1.66 (s, 1H), 1.69 (s, 1H), 1.94 (s, 2H), 2.02 (s, 3H), 3.18 (m, 1H), 3.25 (m, 1H), 4.54 (t, 1H), 5.02 (t, 1H), 5.25 (s, 1H), 5.93 (s, 1H), 5.94 (s, 1H), 6.30 (s, 1H), 6.38-6.45 (m, 1H), 6.44 (m, 1H), 7.25 (m, 2H), 7.31 (s, 2H), 7.38 (m, 3H), 7.55 (m, 2H).

Diels-Alder Solvent Study for ATRC-Capable Monomer

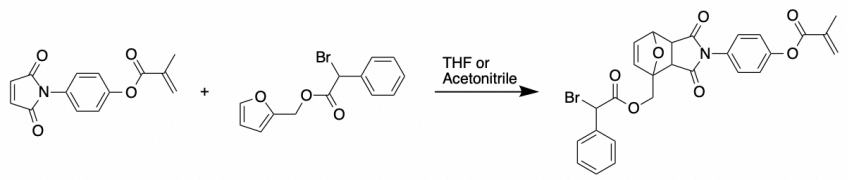

Acetonitrile

A 50mL round bottom flask was charged with N-(4-hydroxyphenyl maleimide) (1g, 3.88mmol) which was dissolved in minimal amounts of tetrahydrofuran (4mL) at 45°C. α-Bromo-2-

furanylmethylester-benzeneacetic acid (1.38g, 4.68mmol) was then added and the reaction was allowed to stir at 45°C for 48h. Targeted precipitation of the adduct over this time was not achieved. However, the product was obtained by concentration via rotary evaporation followed by purification by column chromatography (SiO_2, 50:50 Hex: EtOAc) to yield a tan oil. ^1H NMR (500MHz, $(CD_3)_2SO$) δ 2.01 (d, 6H), 3.18 (t, 1H), 3.26 (t, 1H), 3.60 (t, 1H), 3.83 (m, 1H), 4.55 (3, 1H), 4.73 (q, 1H), 4.92 (q, 1H), 5.02 (t, 1H), 5.26 (s, 1H), 5.40 (t, 1H), 5.92 (d, 2H), 6.03 (d, 2H), 6.31 (d, 2H), 6.40-6.55 (m, 2H), 6.66 (m, 2H), 7.20 (d, 4H), 7.31 (t, 4H), 7.39 (m, 6H), 7.57 (m, 4H).

Tetrahydrofuran

A 50mL round bottom flask was charged with N-(4-hydroxyphenyl maleimide) (1g, 3.88mmol) which was dissolved in minimal amounts of acetonitrile (3.7mL) at 45°C. α-Bromo-2-furanylmethylester-benzeneacetic acid (1.38g, 4.68mmol) was then added and the reaction was allowed to stir at 45°C for 48h. Targeted precipitation of the adduct over this time was not achieved. However, the product was obtained by concentration via rotary evaporation followed by purification by column chromatography (50:50 Hex: EtOAc) to yield a tan oil (1.82g, 62% yield).

Diels-Alder Crosslinker

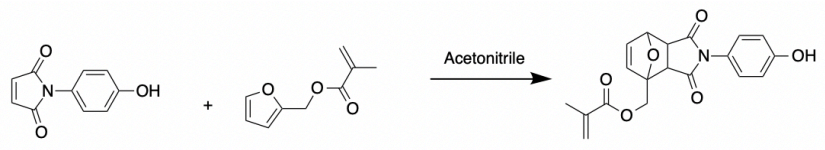

A 25mL round bottom flask was charged with N-(4-hydroxyphenyl maleimide) (1.06g, 5.60mmol) and furfuryl methacrylate (1.03g, 6.20mmol). Acetonitrile (8mL) was then added

and the reaction mixture was stirred at 45°C with a condenser attachment for six days. The resulting product was isolated via column chromatography (60:40 Ethyl Acetate:Hexanes) followed by rotary evaporation to generate a tan solid. (1.40g, 69.8% yield): (*Endo*) ^{1}H NMR (500MHz, $(CD_3)_2SO$) δ 1.90 (s, 3H), 3.61 (d, 1H), 3.81 (t, 1H), 4.67 (d, 1H), 4.81 (d, 1H), 5.37 (d, 1H), 5.72 (s, 1H), 6.08 (s, 1H), 6.56 (d, 1H), 6.64 (d, 1H), 6.81 (d, 2H), 6.89 (d, 2H), 9.73 (s, 1H). (*Exo*) ^{1}H NMR (500MHz, $(CD_3)_2SO$) δ 1.86 (s, 3H), 3.14 (d, 1H), 3.21 (d, 1H), 4.51 (d, 1H), 4.85 (d, 1H), 5.23 (s, 1H), 5.69 (s, 1H), 6.01 (s, 1H), 6.55 (s, 1H), 6.64 (s, 1H), 6.84 (d, 2H0, 6.98 (d, 2H), 9.75 (s, 1H); (*Endo*) ^{13}C NMR (500MHz, $(CD_3)_2SO$) δ 14.56 (s), 18.41 (s), 21.24 (s), 46.80 (s), 47.78 (s), 60.23 (s), 62.56 (s), 79.58 (s), 89.56 (s), 115.86 (s), 123.40 (s), 126.40 (s), 128.58 (s), 134.98 (s), 135.92 (s), 136.33 (s), 157.90 (s), 166.59 (s), 170.81 (s), 174.63 (d). (*Exo*) ^{13}C NMR (500MHz, $(CD_3)_2SO$) δ 18.36 (s), 48.79 (s), 50.26 (s), 62.25 (s), 81.31 (s), 89.60 (s), 115.90 (s), 126.75 (s), 128.54 (s), 157.85 (s).

Esterification of Diels-Alder Adducts

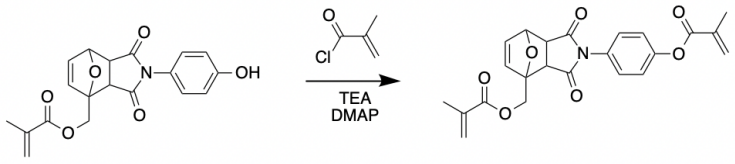

In an oven dried 100mL round bottom flask, the Diels-Alder adduct (1.44g, 4.05mmol) was dissolved in acetonitrile (41.16mL) and the reaction vessel was brought to 0°C in an ice bath. 4-dimethylaminopyridine (9.92mg, 0.081mmol) and triethylamine (0.636mL, 4.56mmol) were added and the solution was bubbled with Argon gas for 15 minutes. Methacryloyl chloride (0.87mL, 8.90mmol) was added in a solution of acetonitrile (2mL) while stirring using an

addition funnel. The reaction was allowed to run for 24h before quenching with air and removing the acetonitrile via rotary evaporation. The resulting brown material was dissolved in dichloromethane and washed with 1M hydrochloric acid (2x20mL), saturated sodium bicarbonate (2x20mL), and brine (1x25mL). The organic layer was dried with anhydrous magnesium sulfate which was removed by vacuum filtration then concentrated via rotary evaporation to produce a light brown liquid. (1.8079g, 105.4% yield): (*Endo*) ^{1}H NMR (500MHz, $(CD_3)_2SO$) δ 1.91 (s, 3H), 2.01 (s, 2H), 3.67 (d, 1H), 3.87 (t, 1H), 4.69 (d, 1H), 4.82 (d, 1H), 5.41 (d, 1H), 5.73 (s, 1H), 5.92 (s, 1H), 6.09 (s, 1H), 6.25-6.29 (d, 1H), 6.62 (1H), 6.69 (d, 1H), 7.21 (t, 2H), 7.28 (d, 2H). (*Exo*) 1.87 (s, 3H), 2.02 (s, 3H), 3.21 (d, 1H), 3.27 (d, 1H), 4.55 (d, 1H), 4.89 (d, 1H), 5.28 (s, 1H), 5.68 (s, 1H), 5.92 (s, 1H), 6.02 (s, 1H), 6.31 (s, 1H), 5.65 (d, 1H), 6.66 (d, 1H), 7.21 (s, 4H); (*Endo*) ^{13}C NMR (500MHz, $(CD_3)_2SO$) δ 17.93 (s), 18.40 (s), 18.47 (s), 47.03 (s), 47.99 (s), 55.37 (s), 62.54 (s), 79.64 (s), 90.04 (s), 122.92 (s), 126.96 (s), 128.57 (d), 129.77 (s), 130.80 (s), 133.35 (m), 136.42 (s), 150.74 (s), 165.65 (s), 166.58 (s), 174.24 (d). (*Exo*) ^{13}C NMR (500MHz, $(CD_3)_2SO$) δ 17.93 (s), 18.48 (m), 24.49 (d), 25.49 (s), 30.45 (s), 30.61 (s), 49.01 (s), 50.51 (s), 55.36 (s), 62.21 (s), 81.39 (t), 89.71 (s), 103.26 (s), 122.64 (s), 122.93 (s), 126.72 (s), 128.50 (s), 129.33 (s), 130.78 (s), 135.60 (m), 137.46 (s), 137.94 (s), 150.68 (s), 163.55 (s), 165.65 (s), 166.58 (s), 173.74 (s), 174.41 (s), 175.78 (s).

Copolymerization of Methyl Methacrylate and ATRC-Capable Monomer via RAFT

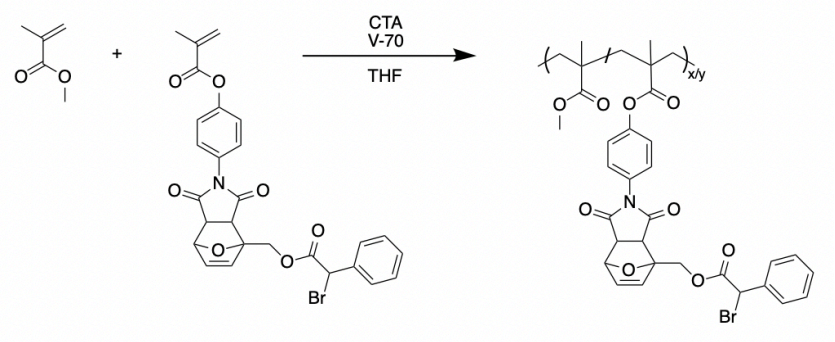

A stock solution of initiator and chain transfer agent was created by dissolving 2,2'-azobis(2,4-dimethylvaleronitrile) (V-70)(7.6mg, 0.0248mmol) and 4-cyano-4-[(dodecylsulfanylthiocarbonyl)sulfanyl]pentanoic acid (0.1g, 0.248mmol) in 1mL tetrahydrofuran in a 15mL round bottom flask. An oven dried, 25mL round bottom flask was then charged with bpDA, deinhibited methyl methacrylate, stock solution and tetrahydrofuran in amounts according to Table 3 dependent on targeted molecular weight and incorporation and was bubbled with argon for 50 minutes at 0°C in an ice bath. The reaction mixture was then transferred to a 35°C oil bath and stirred for 24h. The resulting solution was precipitated by addition of cold methanol, allowing precipitate to settle, then extracting the resulting solution and drying remaining precipitate under reduced pressure which was repeated three times. ^{1}H NMR (500MHz, $(CD_3)_2SO$) δ 0.88 (s, 3H), 1.25 (s, 24H), 1.55 (s, 16H), 3.04 (d, 1H), 3.13 (t, 1H), 4.62 (q, 1H), 5.10 (q, 1H), 5.39 (t, 2H), 5.77 (s, 1H), 6.35 (s, 1H), 6.36-6.44 (q, 1H), 6.56-6.60 (q, 1H), 7.24 (t, 4H), 7.30-7.34 (m, 3H). 7.53 (d, 2H).

Table 3: Reaction conditions for the copolymerization of ATRC capable monomer and methyl methacrylate via RAFT

Targeted MW (kDa)	Diels-Alder Monomer Incorporation	ATRC Capable Diels-Alder Monomer (g)	Methyl Methacrylate (g)	Additional THF (mL)	Stock Solution (mL)
25	5 mol%	0.11	0.38	0.92	0.08
25	10 mol%	0.19	0.30	0.92	0.08
25	15 mol%	0.24	0.25	0.92	0.08
20	5 mol%	0.11	0.38	0.79	0.20
20	10 mol%	0.18	0.30	0.79	0.20

25 kDa Homopolymerization of Methyl Methacrylate or Homopolymerization of ATRC-Capable Monomer

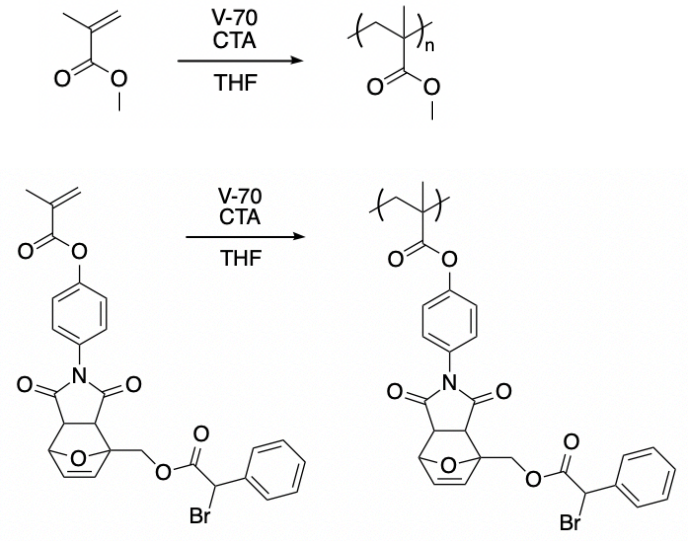

A stock solution of initiator and chain transfer agent was created by dissolving 2,2'-azobis(2,4-dimethylvaleronitrile) (V-70)(7.6mg, 0.0248mmol) and 4-cyano-4-[(dodecylsulfanylthiocarbonyl)sulfanyl]pentanoic acid (0.1g, 0.248mmol) in 1mL tetrahydrofuran in a 15mL round bottom flask. An oven dried, 25mL round bottom flask was then charged with deinhibited methyl methacrylate or ATRC-capable monomer (0.25g, 2.50mmol or 0.453mmol respectively), stock solution (0.04mL) and tetrahydrofuran (0.46mL) and was bubbled with argon for 50 minutes at 0°C in an ice bath. The reaction mixture was then

transferred to a 35°C oil bath and stirred for 24h. An aliquot was taken for ^{1}H NMR evaluation. (Methyl Methacrylate) ^{1}H NMR (500MHz, $(CD_3)_2SO$) δ 1.95 (s, 3H), 3.75 (s, 3H), 5.56 (s, 1H), 6.10 (s, 1H).

APPENDIX

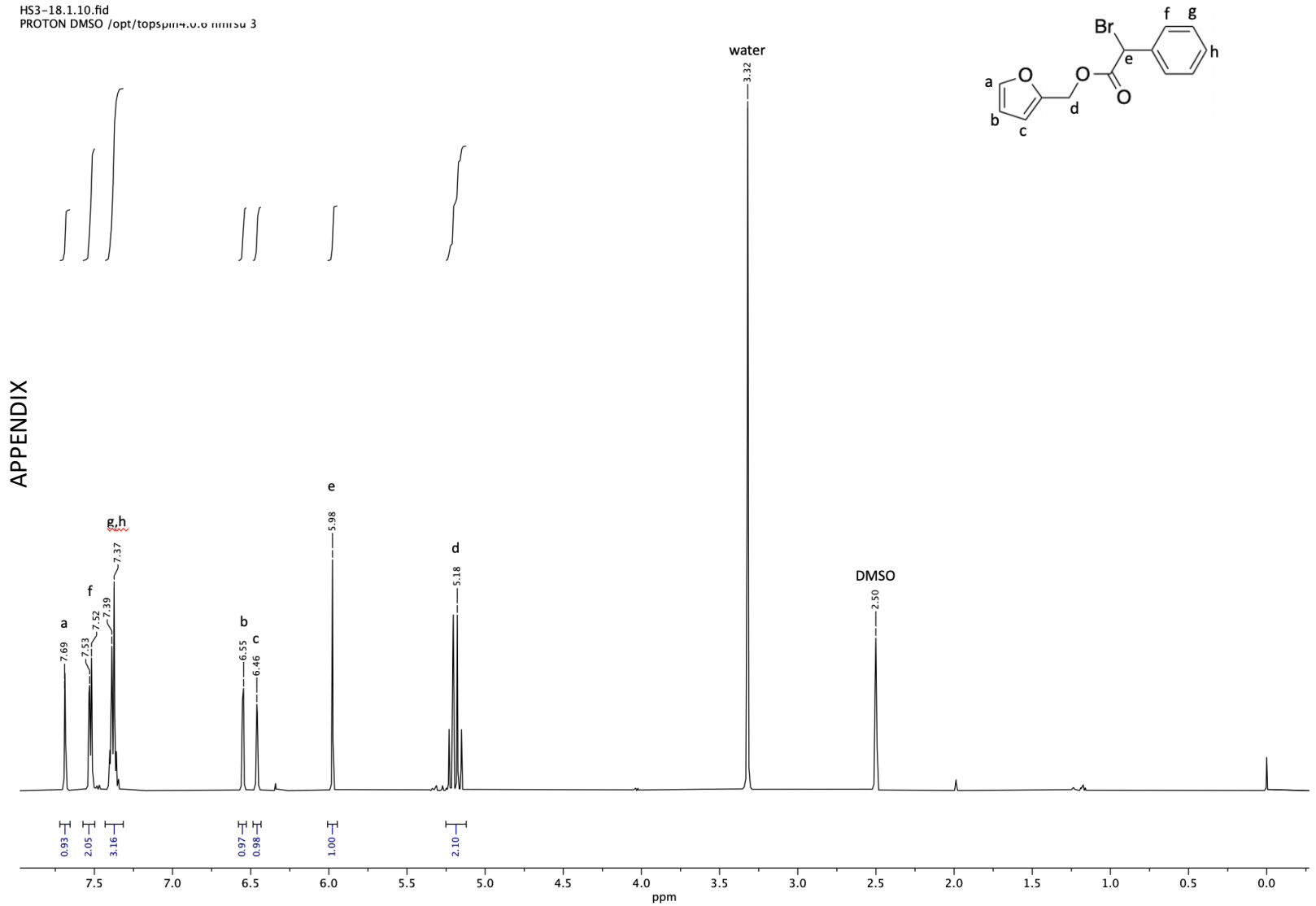

A 1: α-Bromo-2-furanylmethylester-benzeneacetic acid ^{1H}H NMR

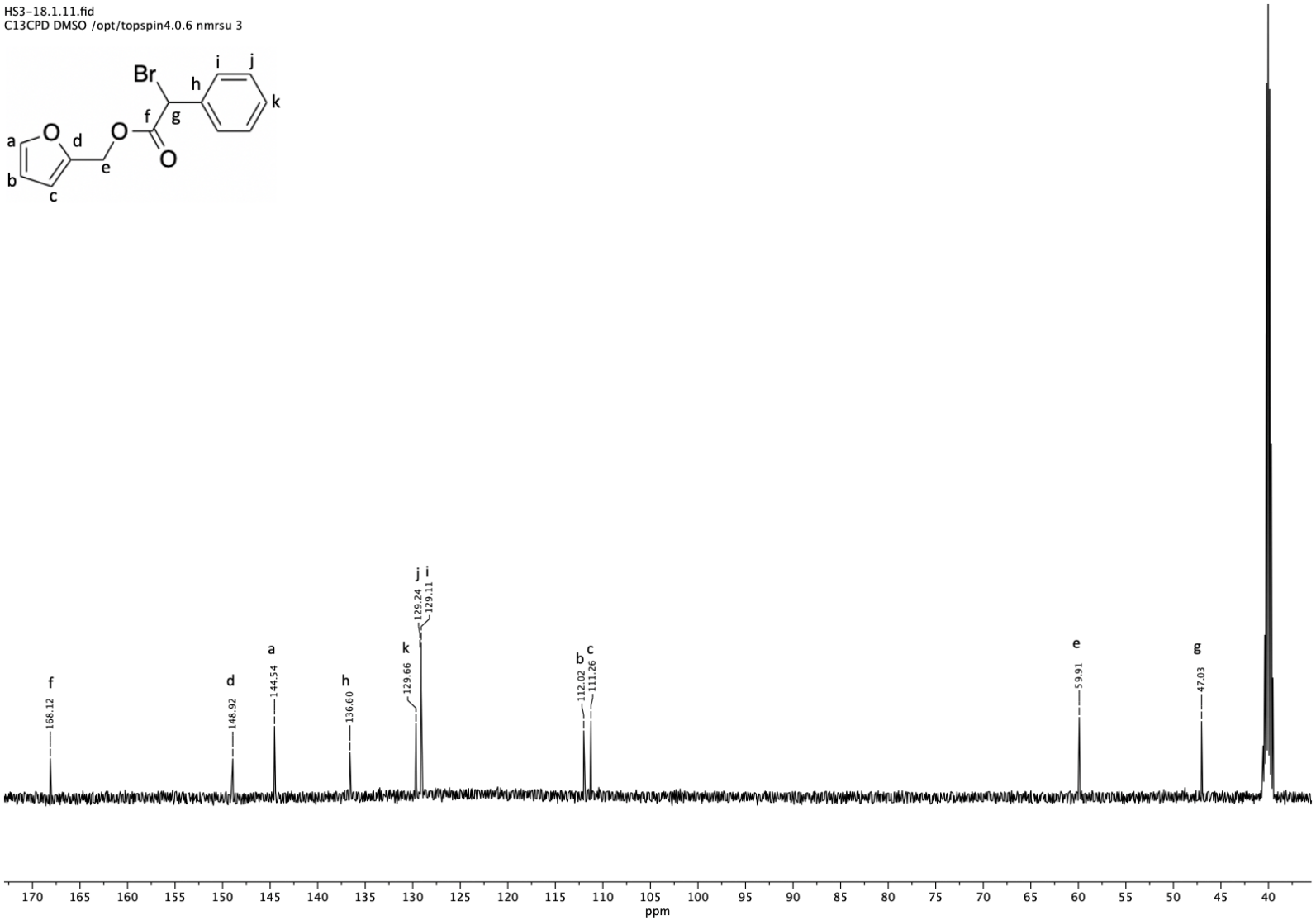

A 2: α-Bromo-2-furanylmethylester-benzeneacetic acid ^{13}C NMR

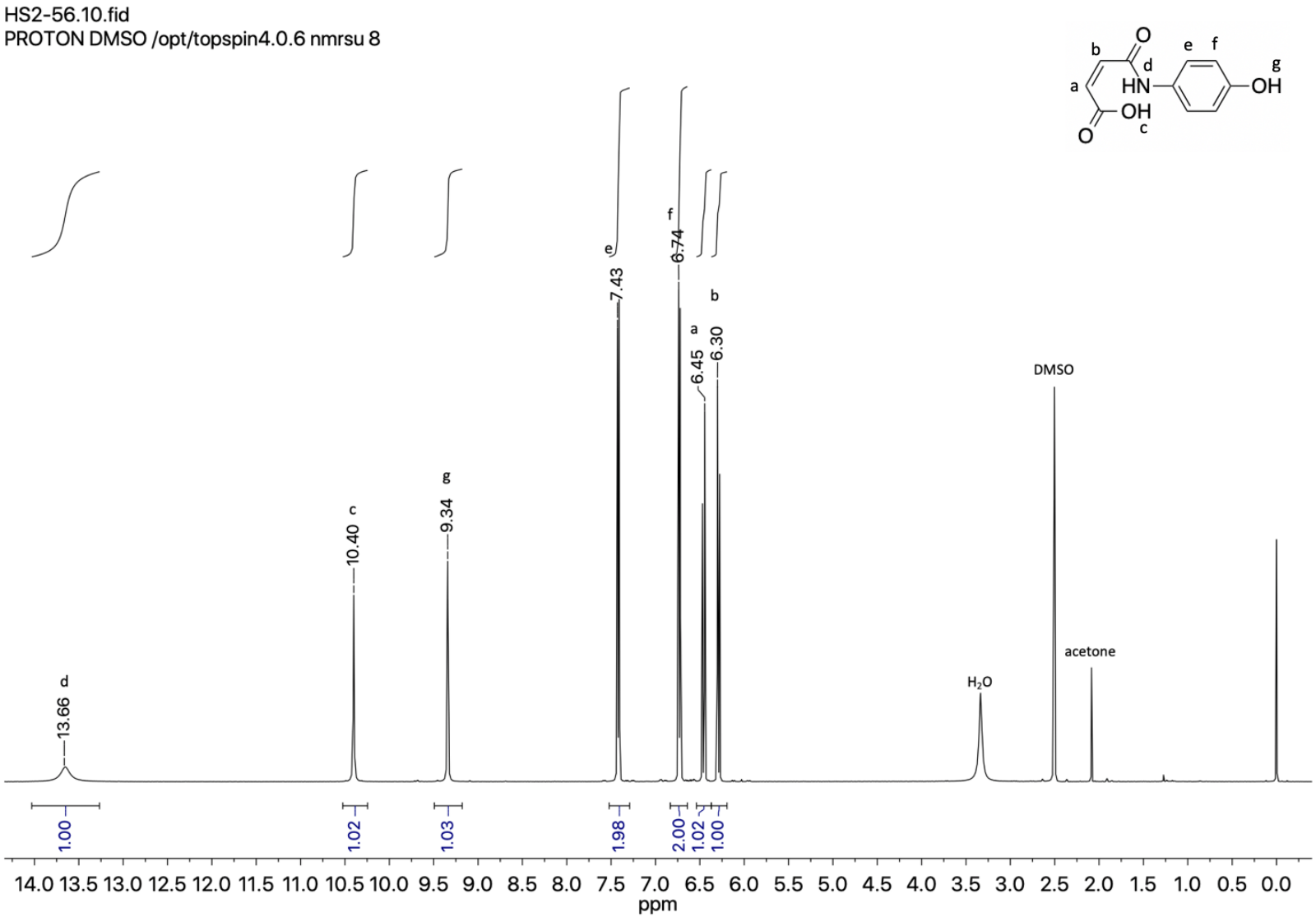

A 3: Amic Acid ^{1}H NMR

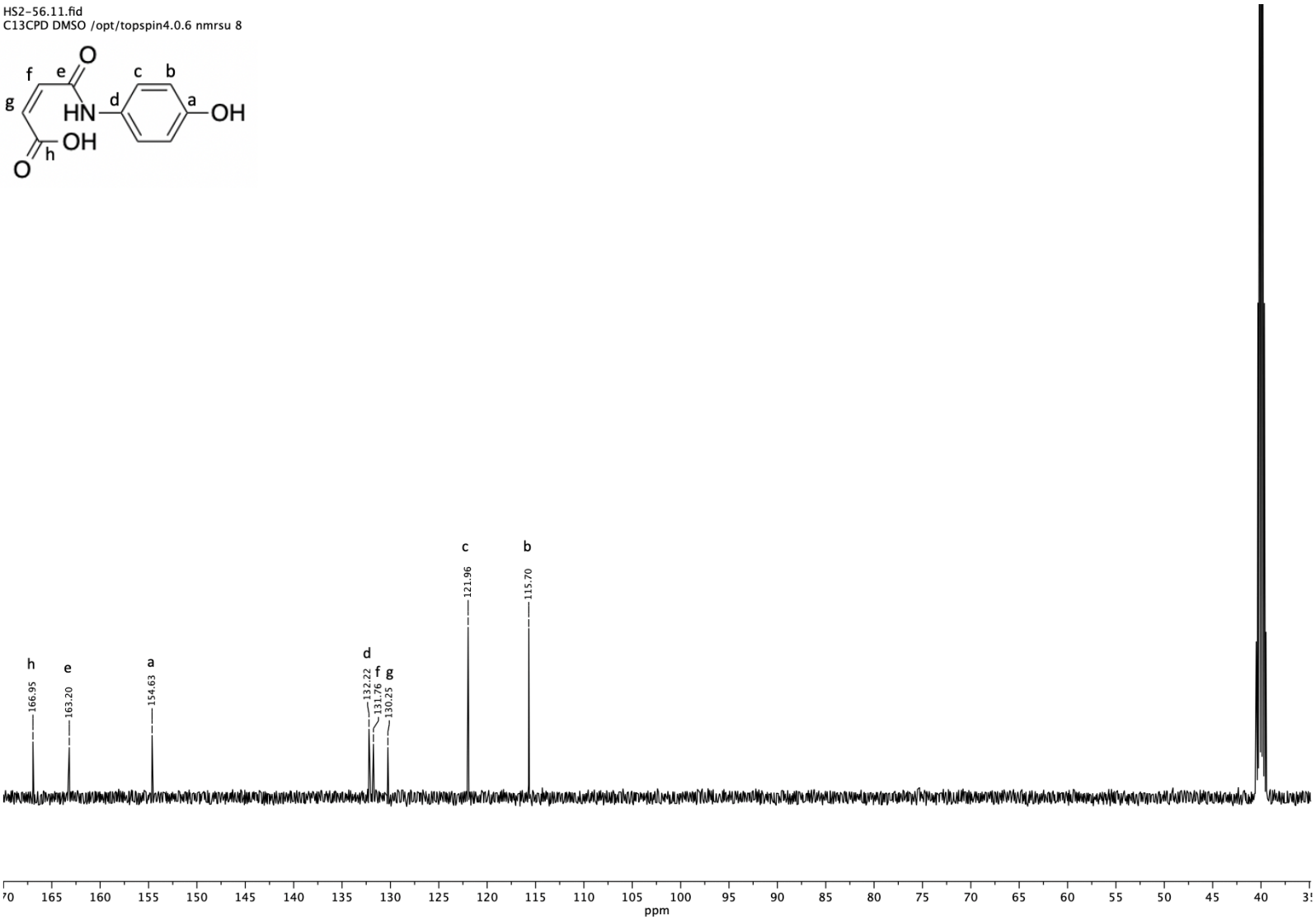

A 4: Amic Acid ^{13}C NMR

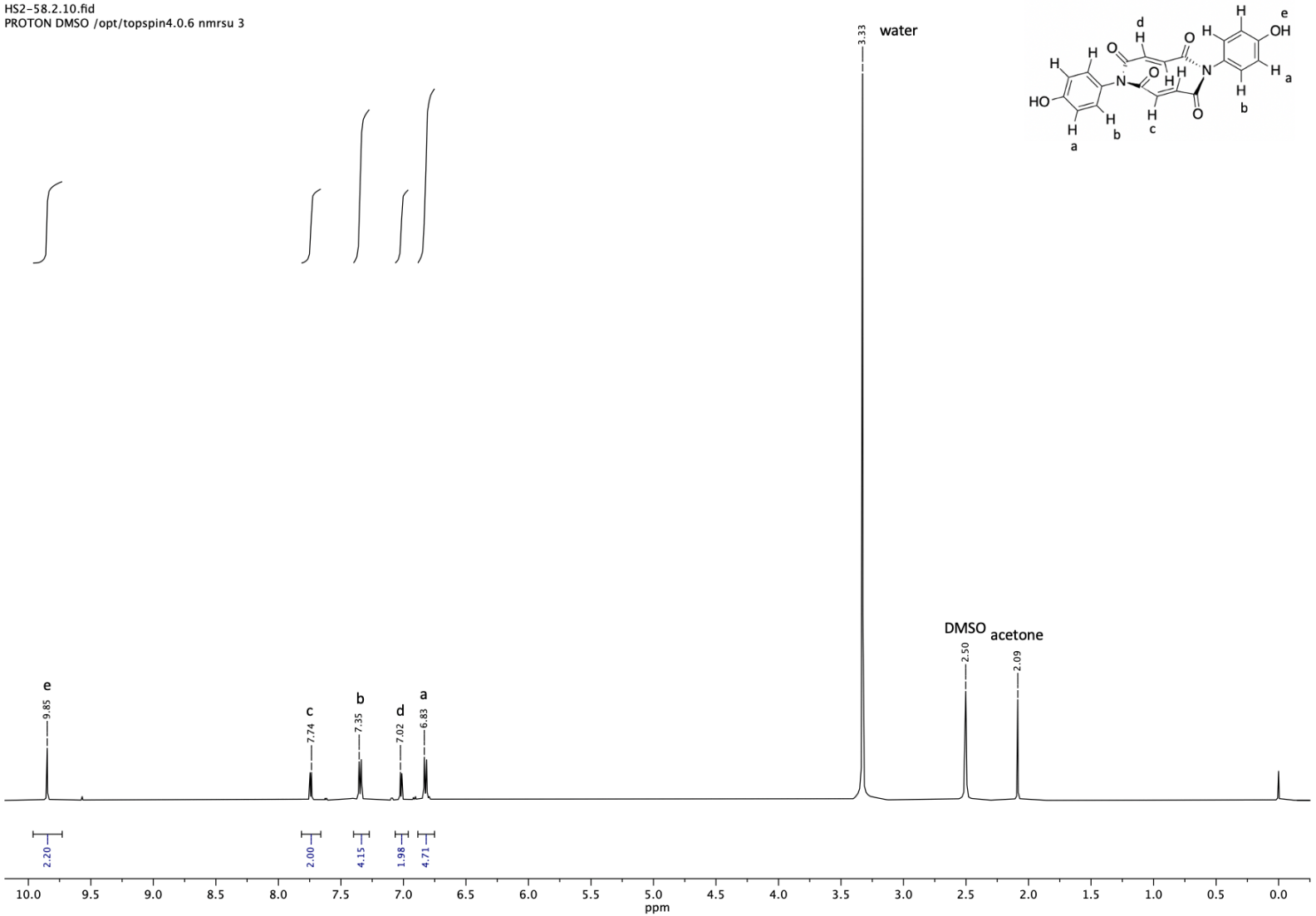

A 5: Synthesis of N-(4-hydroxyphenyl) maleimide from amic acid precursor employing dicyclohexylcarbodiimide ^{1}H NMR

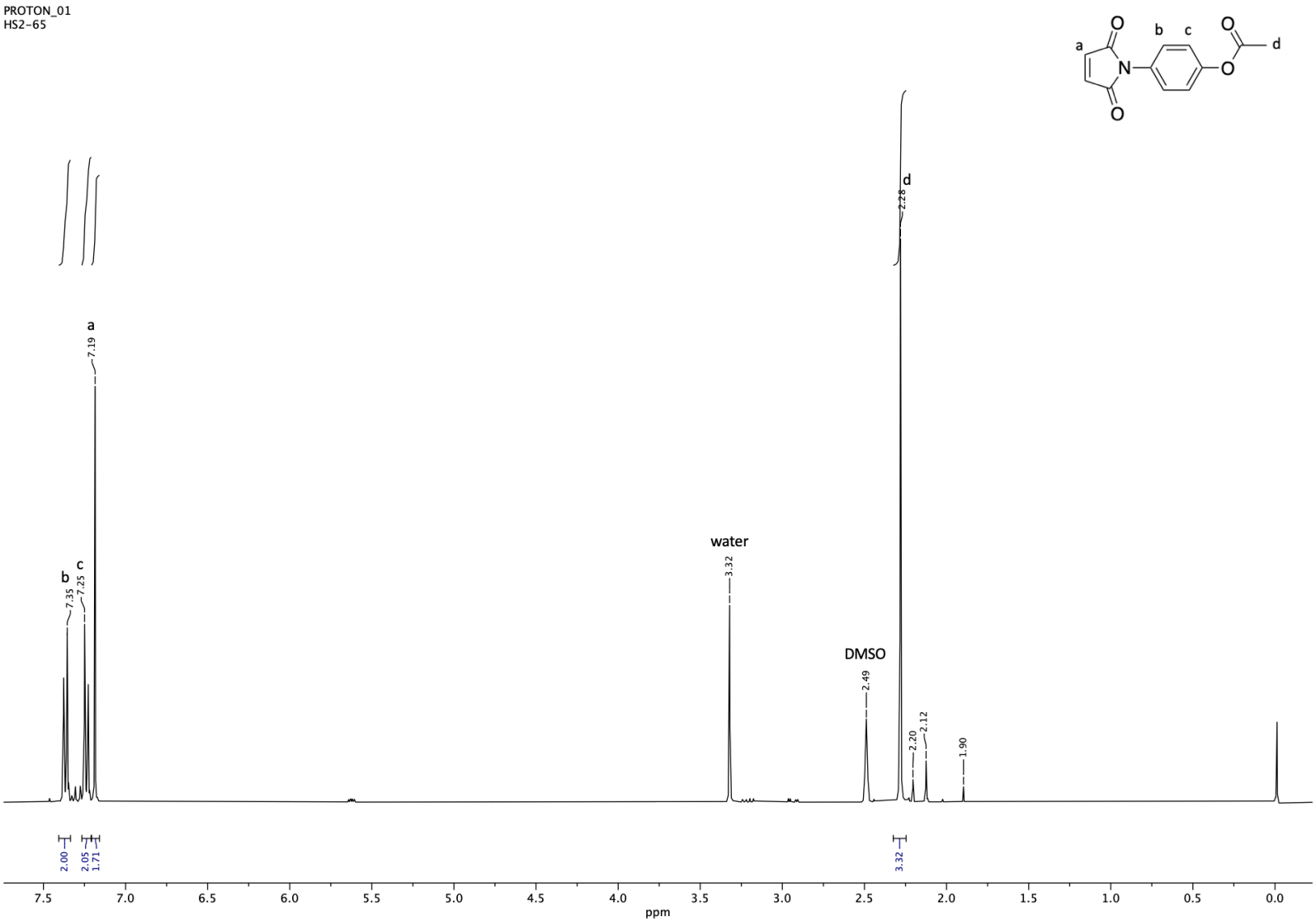

A 6: Synthesis of N-(4-hydroxyphenyl) maleimide from amic acid precursor employing anhydrous sodium acetate and acetic anhydride ^{1}H NMR

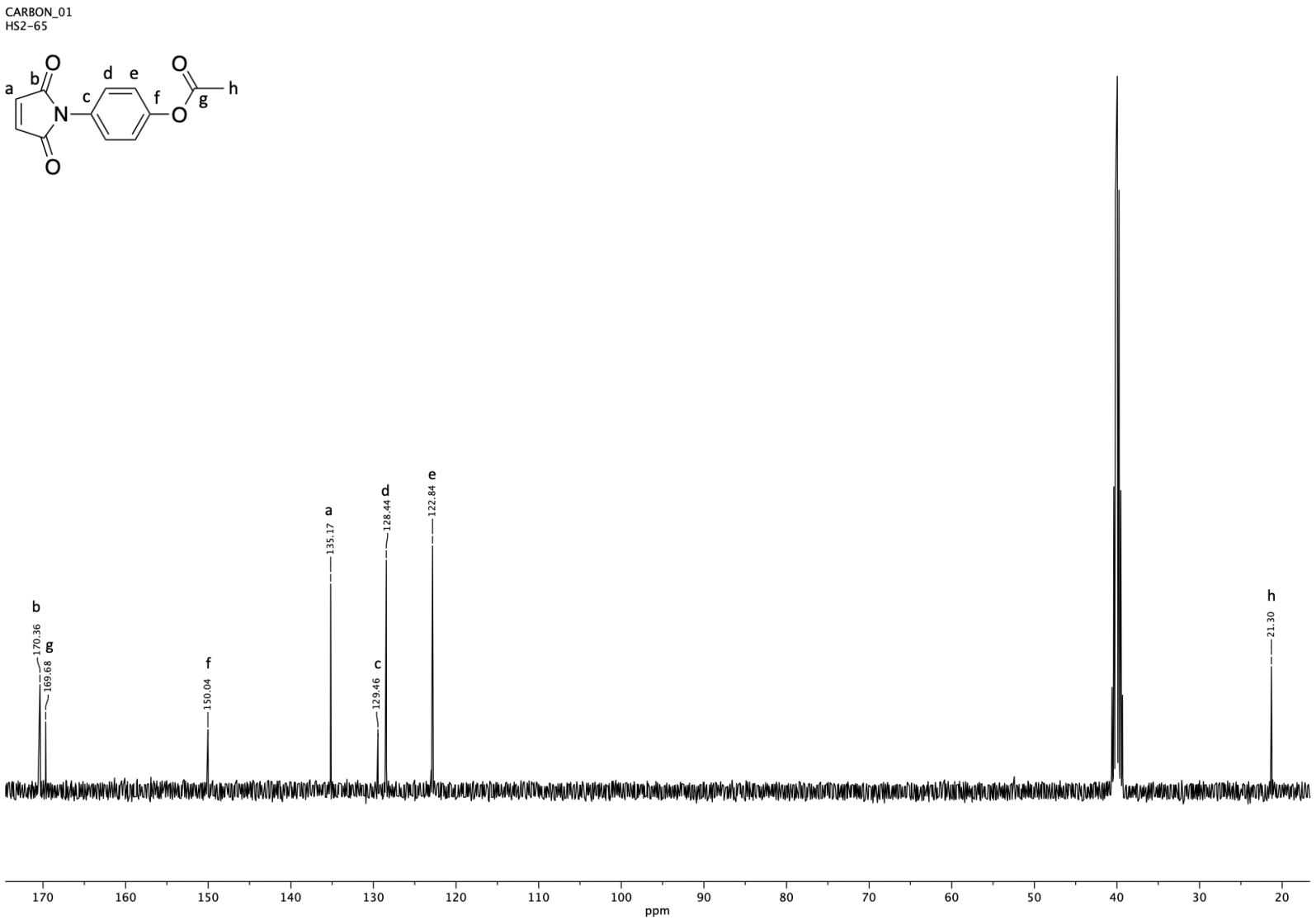

A 7: Synthesis of N-(4-hydroxyphenyl) maleimide from amic acid precursor employing anhydrous sodium acetate and acetic anhydride ^{13}C NMR

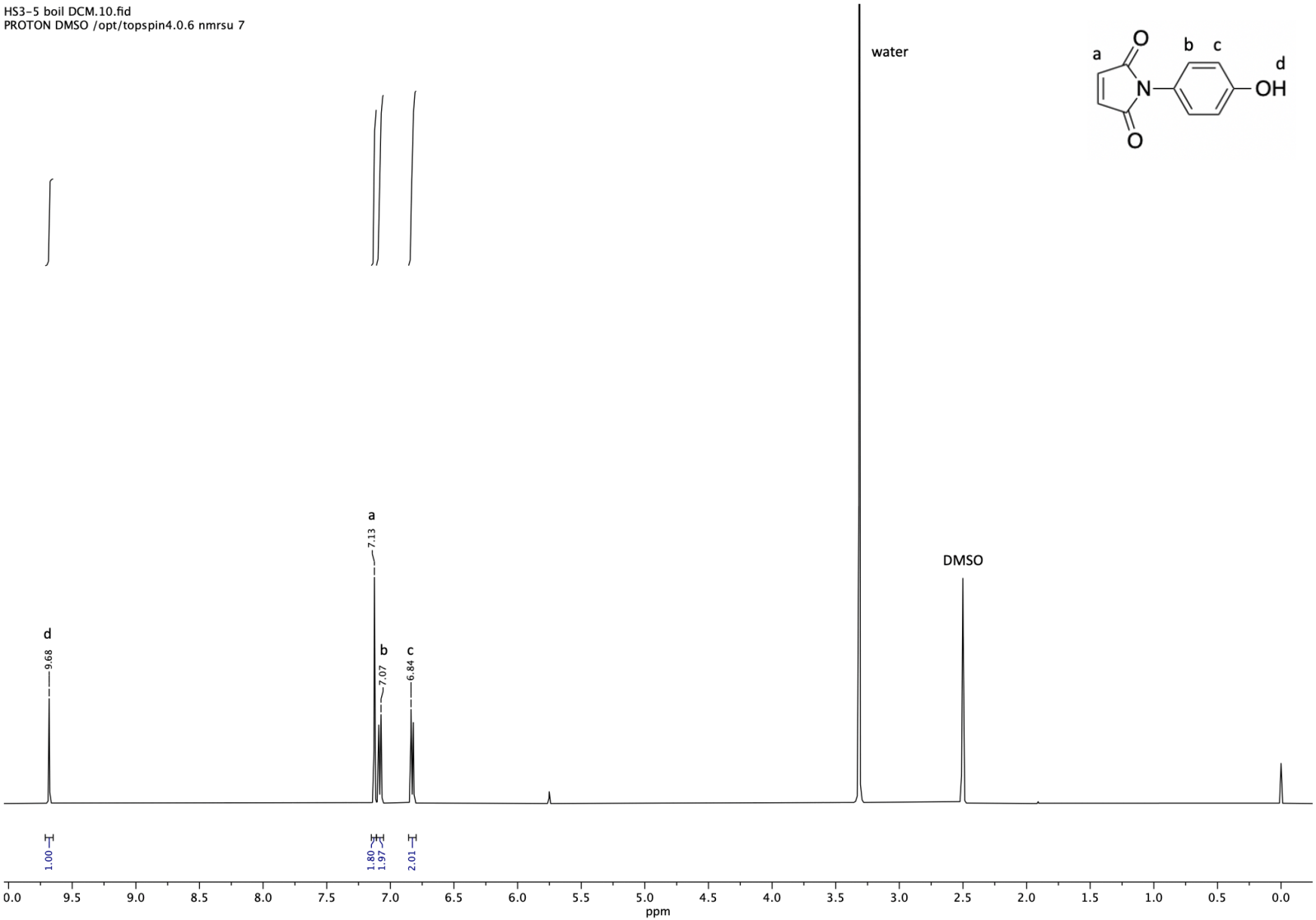

A 8: N-(4-hydroxyphenyl) maleimide ^{1}H NMR

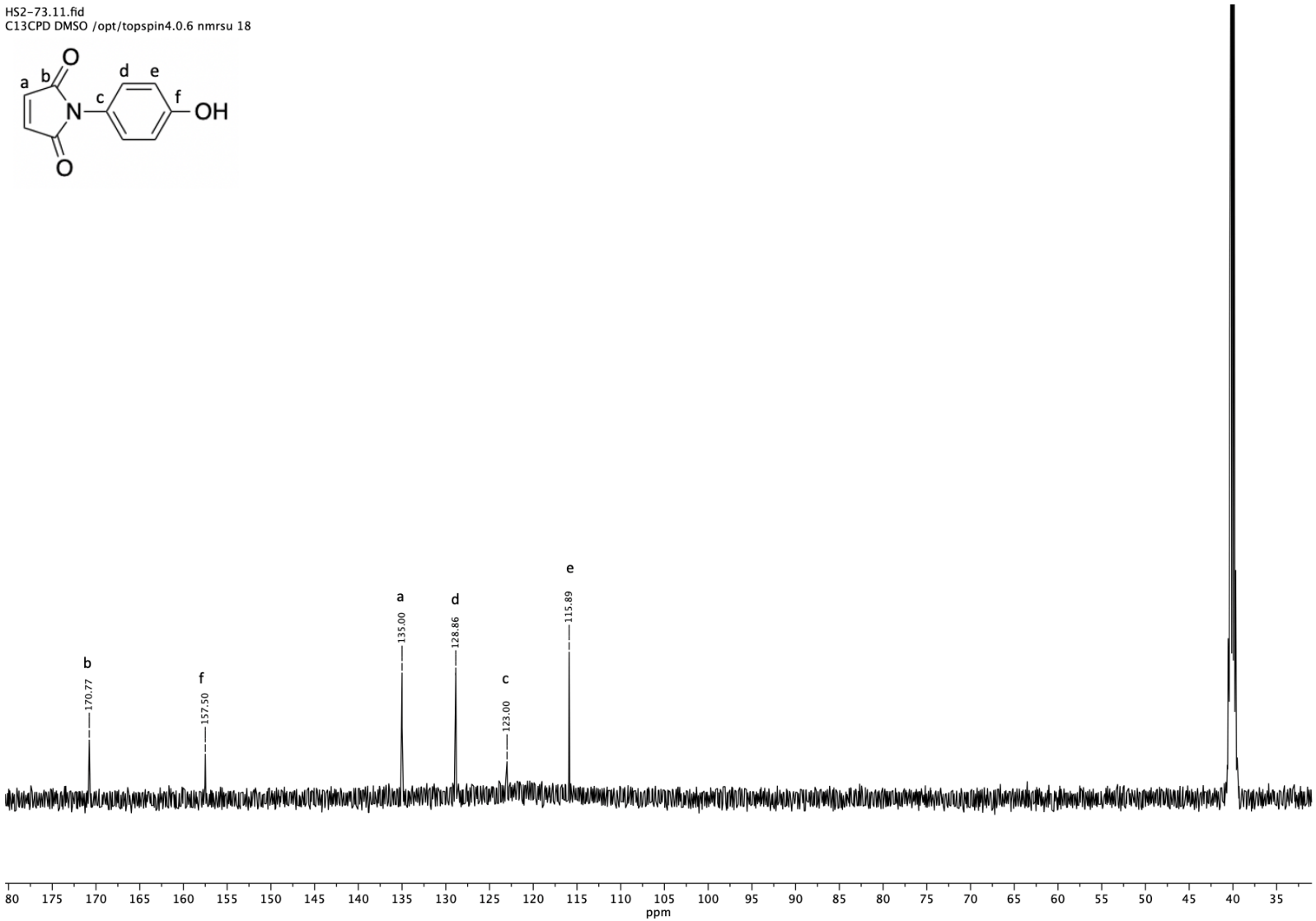

A 9: N-(4-hydroxyphenyl) Maleimide ^{13}C NMR

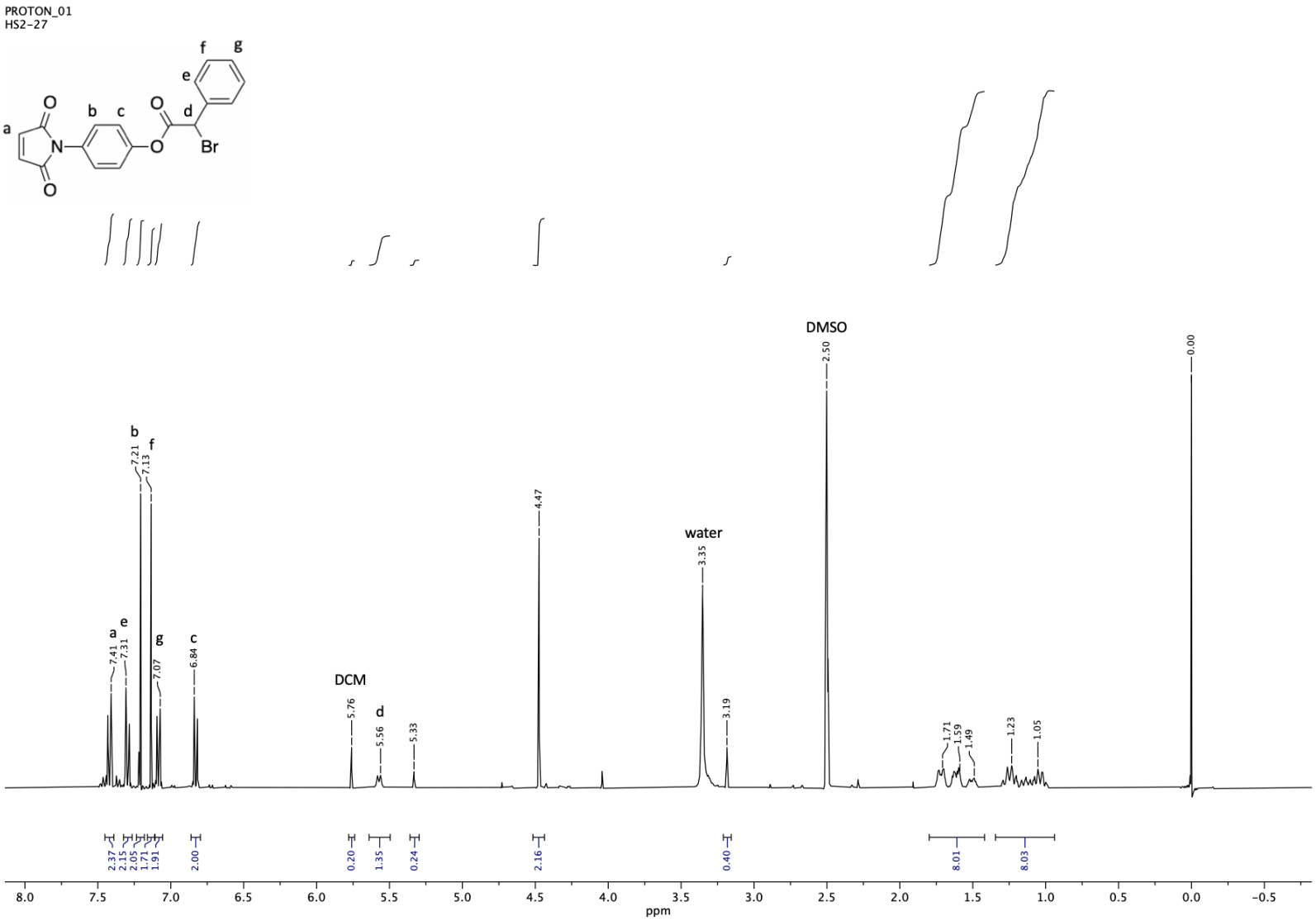

A 10: ATRC-functionalization of N-(4-hydroxyphenyl) maleimide via a steglich esterification ^{1}H NMR

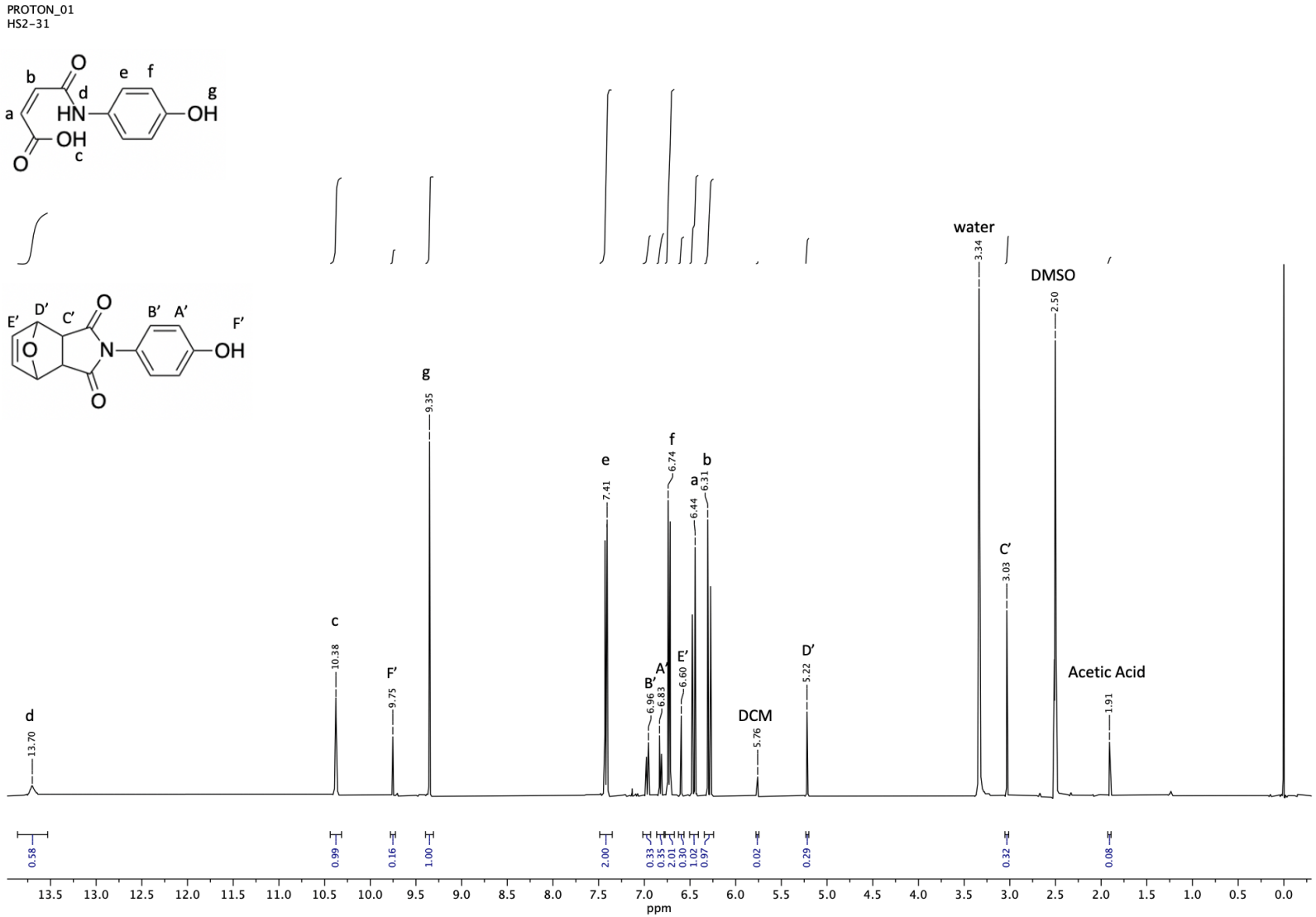

A 11: Protected N-(4-hydroxyphenyl) maleimide synthesis (118 ℃) ^{1}H NMR

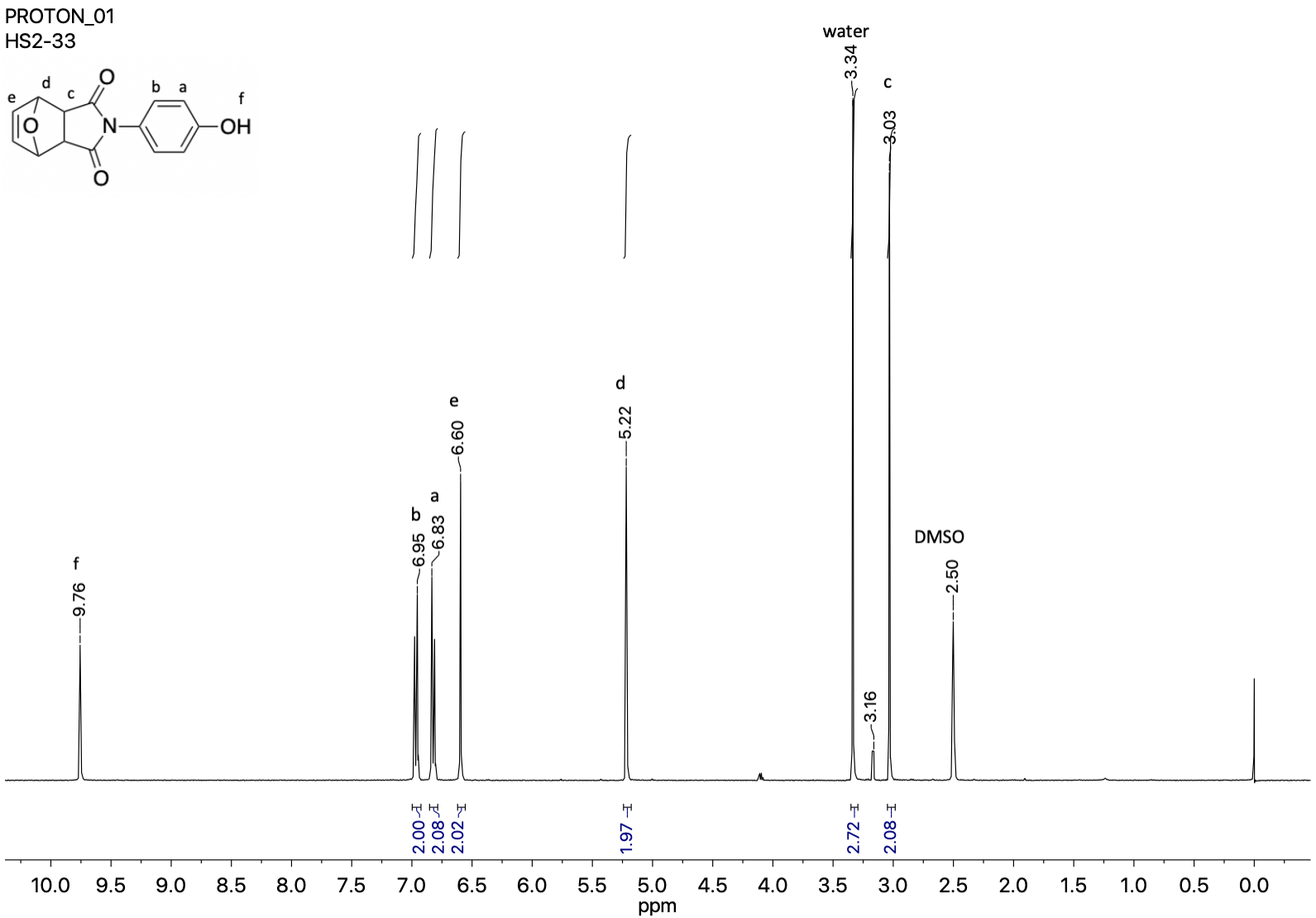

A 12: Protected N-(4-hydroxyphenyl) maleimide synthesis (70℃) ^{1}H NMR

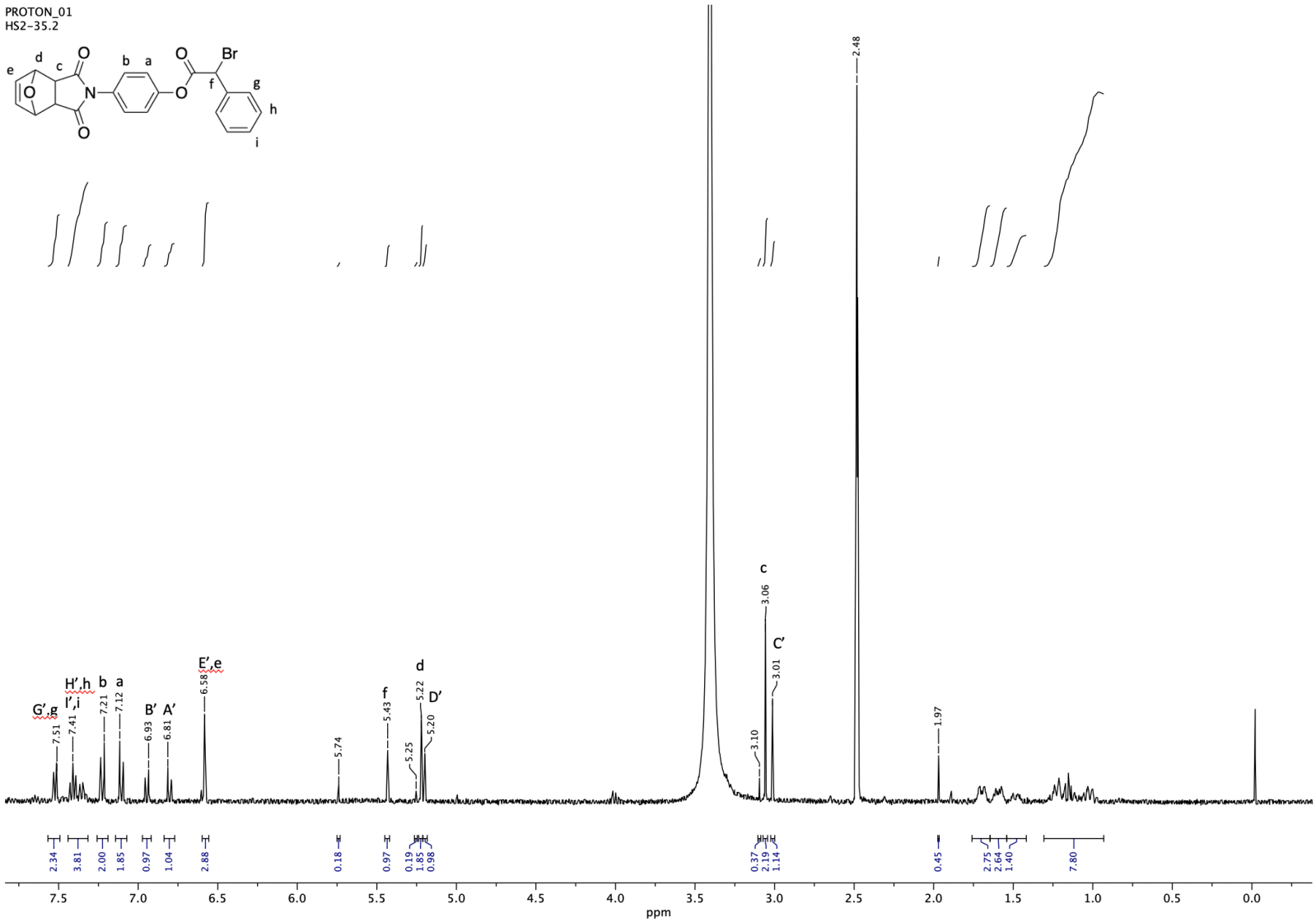

A 13: ATRC-functionalized protected N-(4-hydroxyphenyl) maleimide ^{1}H NMR: Uppercase alphabet = exo, lowercase alphabet = endo

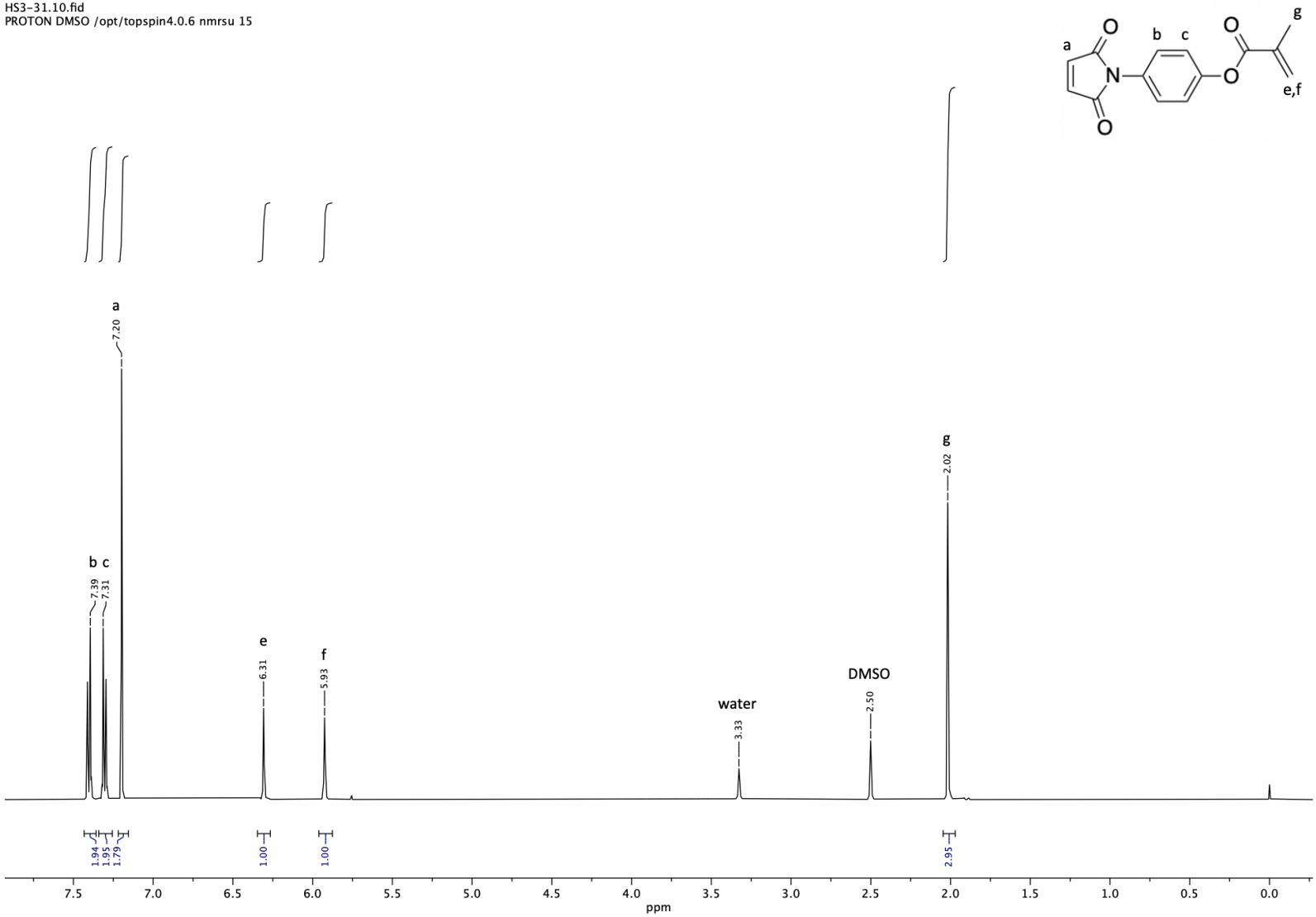

A 14: Esterification of N-(4-hydroxyphenyl) maleimide with methacryloyl chloride ^{1}H NMR

HS3-31.11.fid
C13CPD DMSO /opt/topspin4.0.6 nmrsu 15

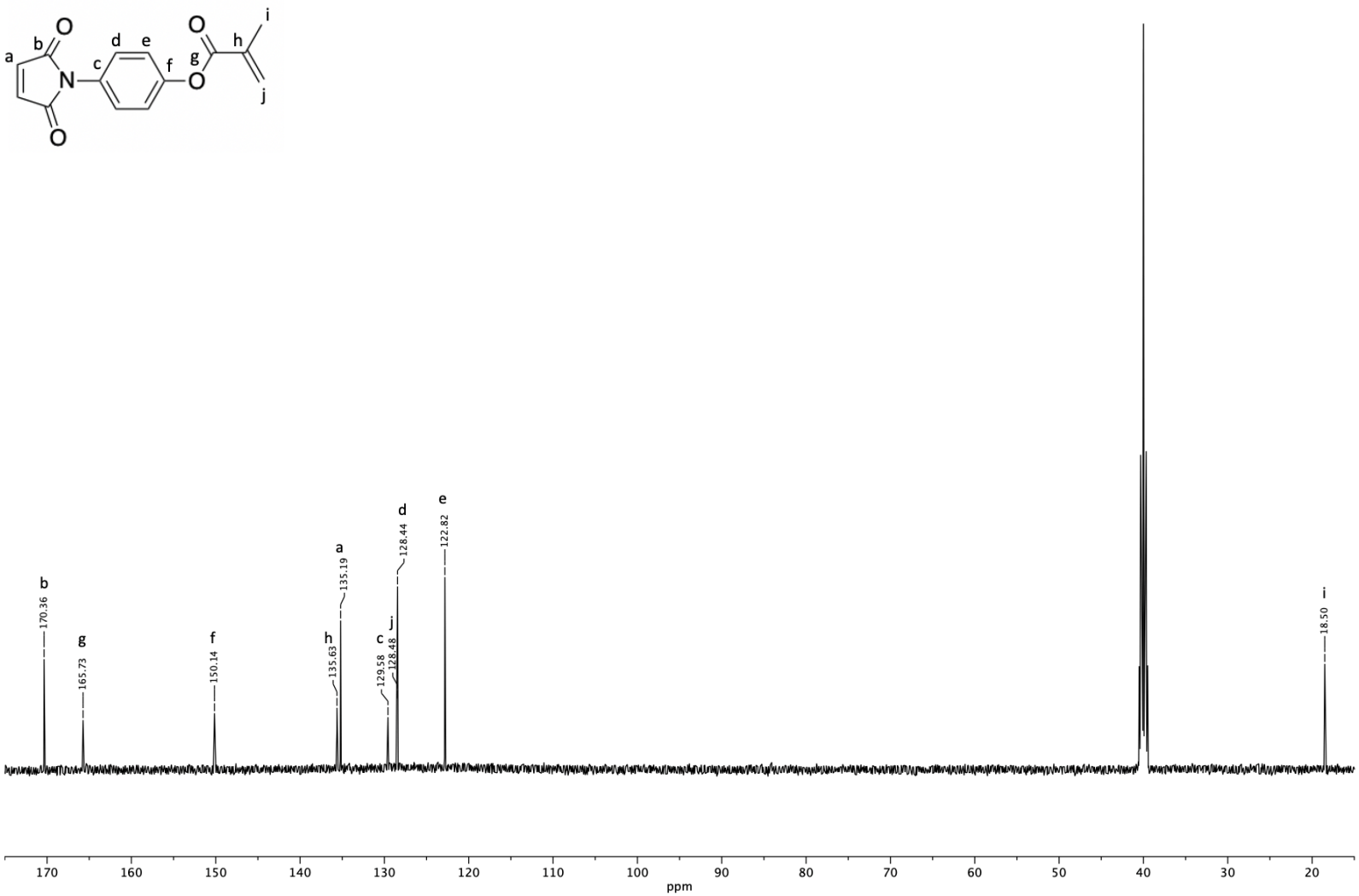

A 15: Esterification of N-(4-hydroxyphenyl) maleimide with methacryloyl chloride ^{13}C NMR

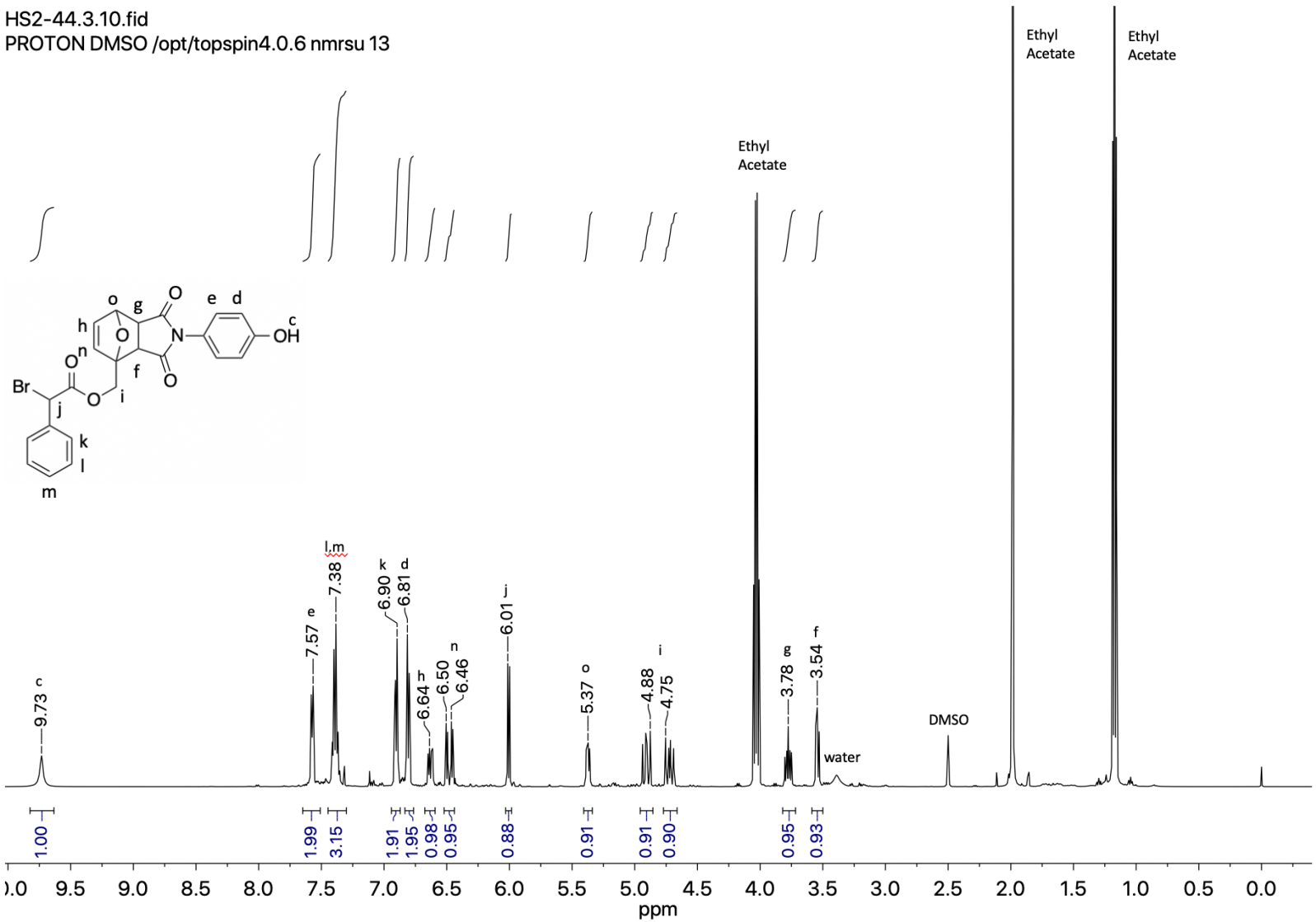

A 16: ATRC-capable Diels-Alder adduct synthesized in acetonitrile ^{1}H NMR

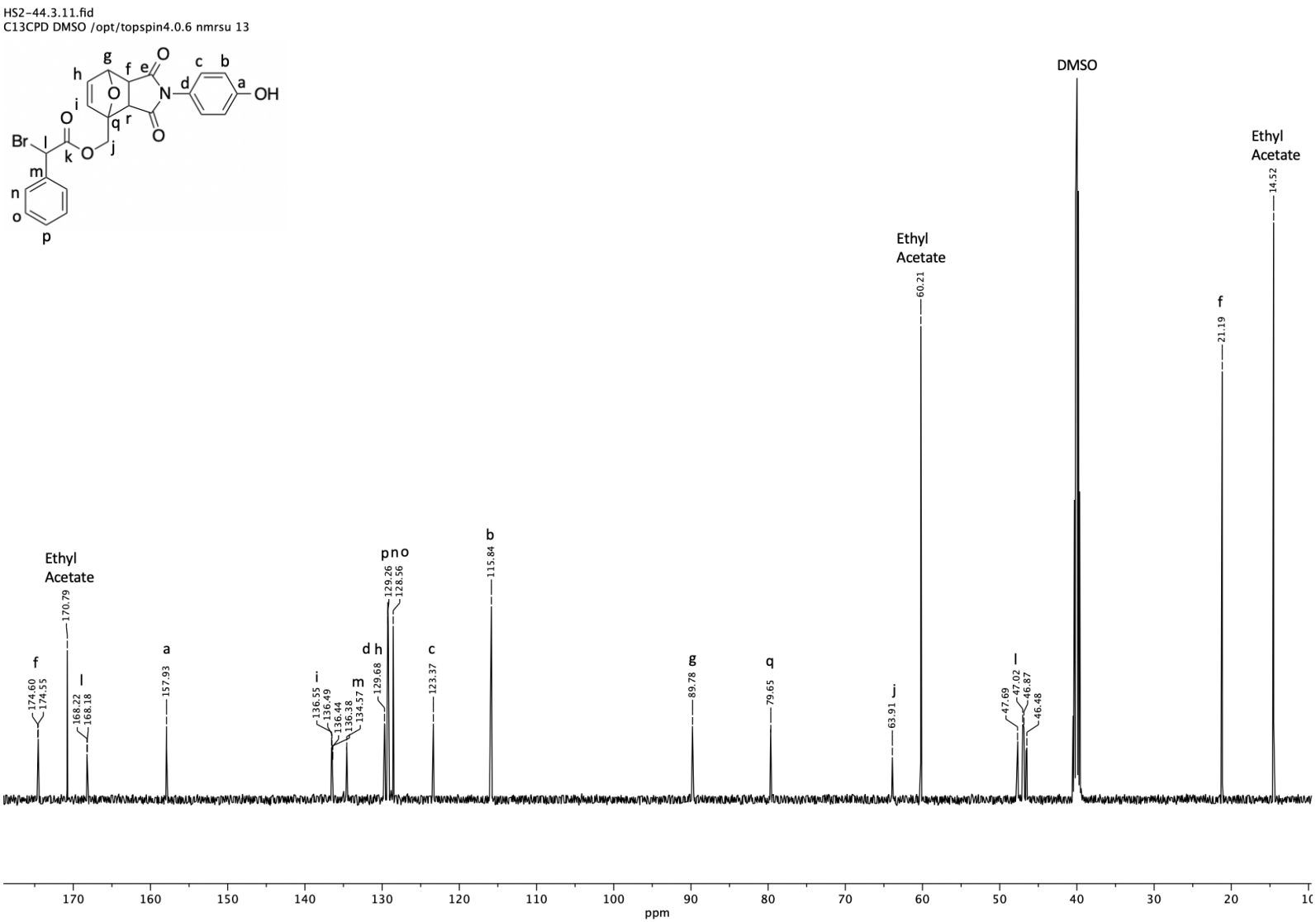

A 17: ATRC-capable Diels-Alder adduct synthesized in acetonitrile ^{13}C NMR

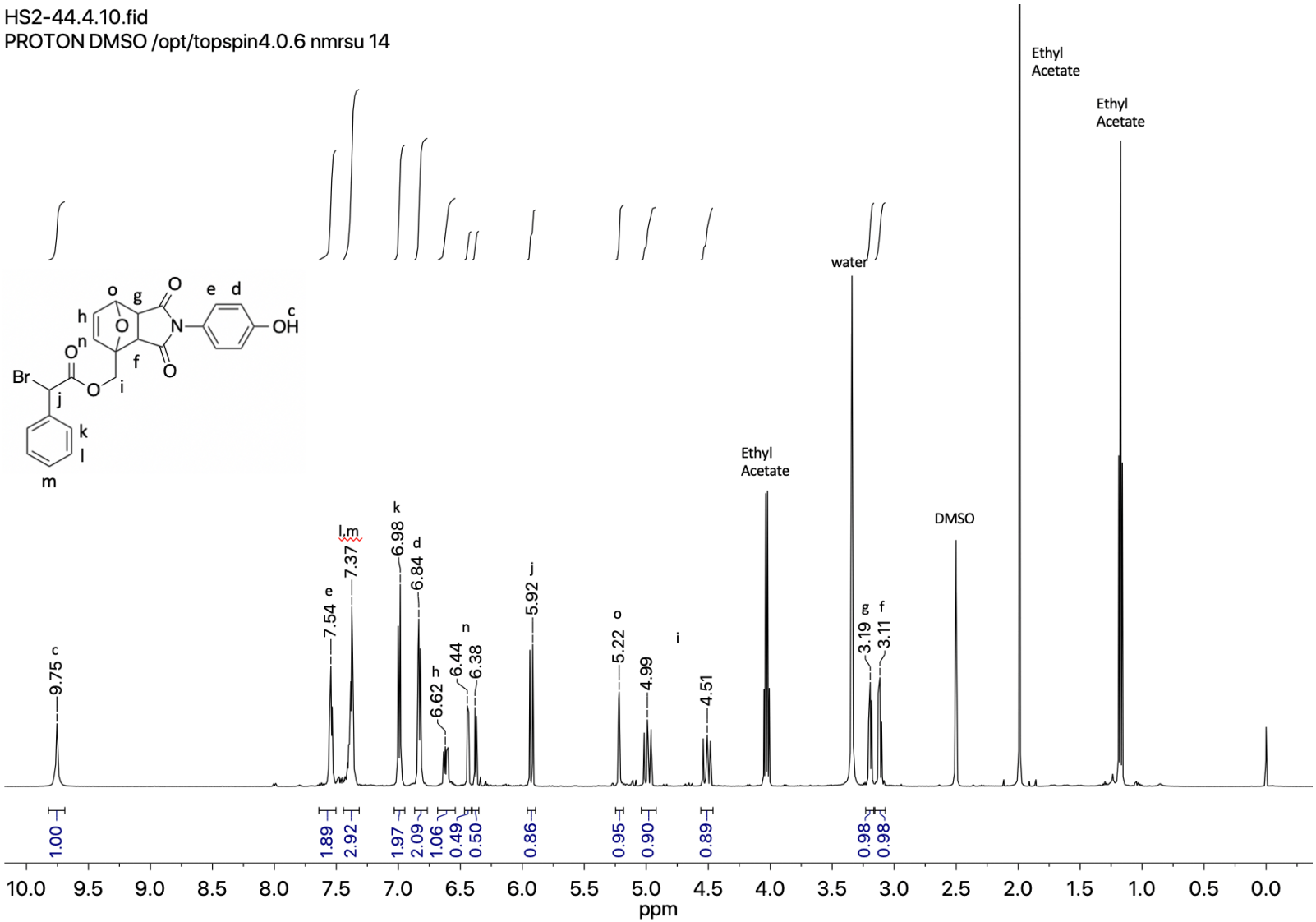

A 18: ATRC-capable Diels-Alder adduct synthesized in dichloromethane ^{1}H NMR

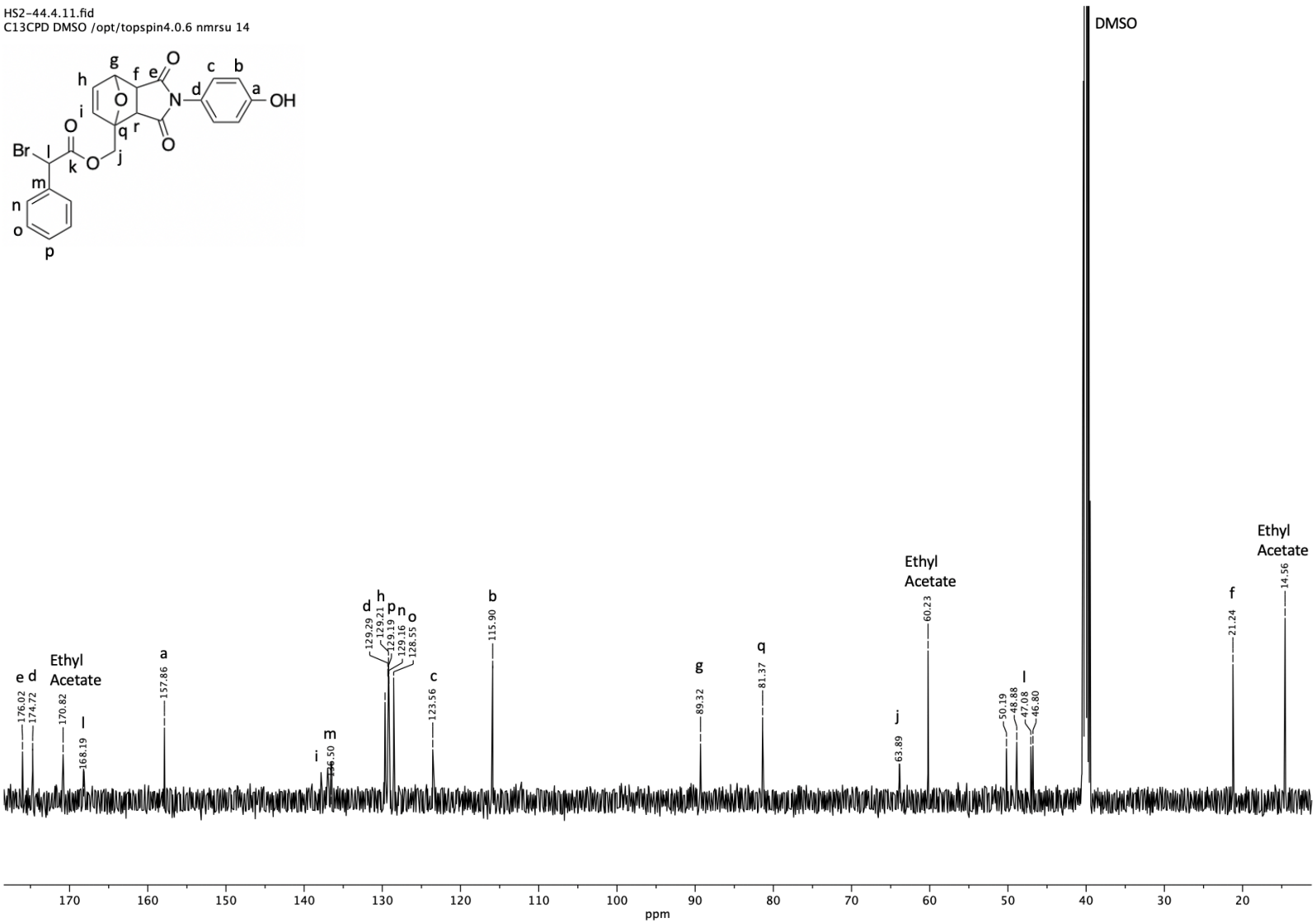

A 19: ATRC-capable Diels-Alder adduct synthesized in dichloromethane ^{13}C NMR

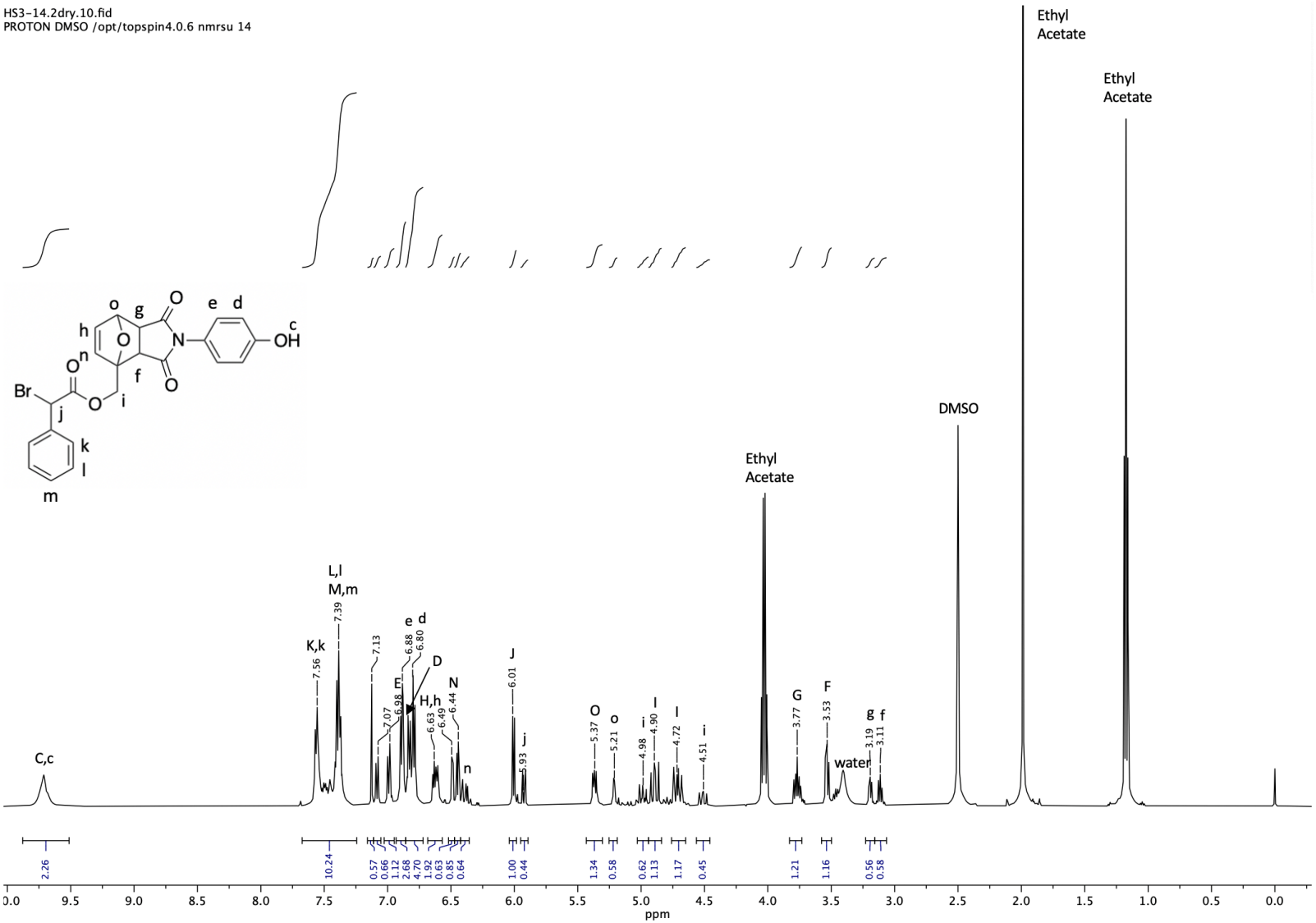

A 20: One day reaction time of the ATRC-capable monomer resulting in 70mol% endo, 30mol% exo (uppercase alphabet = endo, lowercase alphabet = exo) ^1H NMR

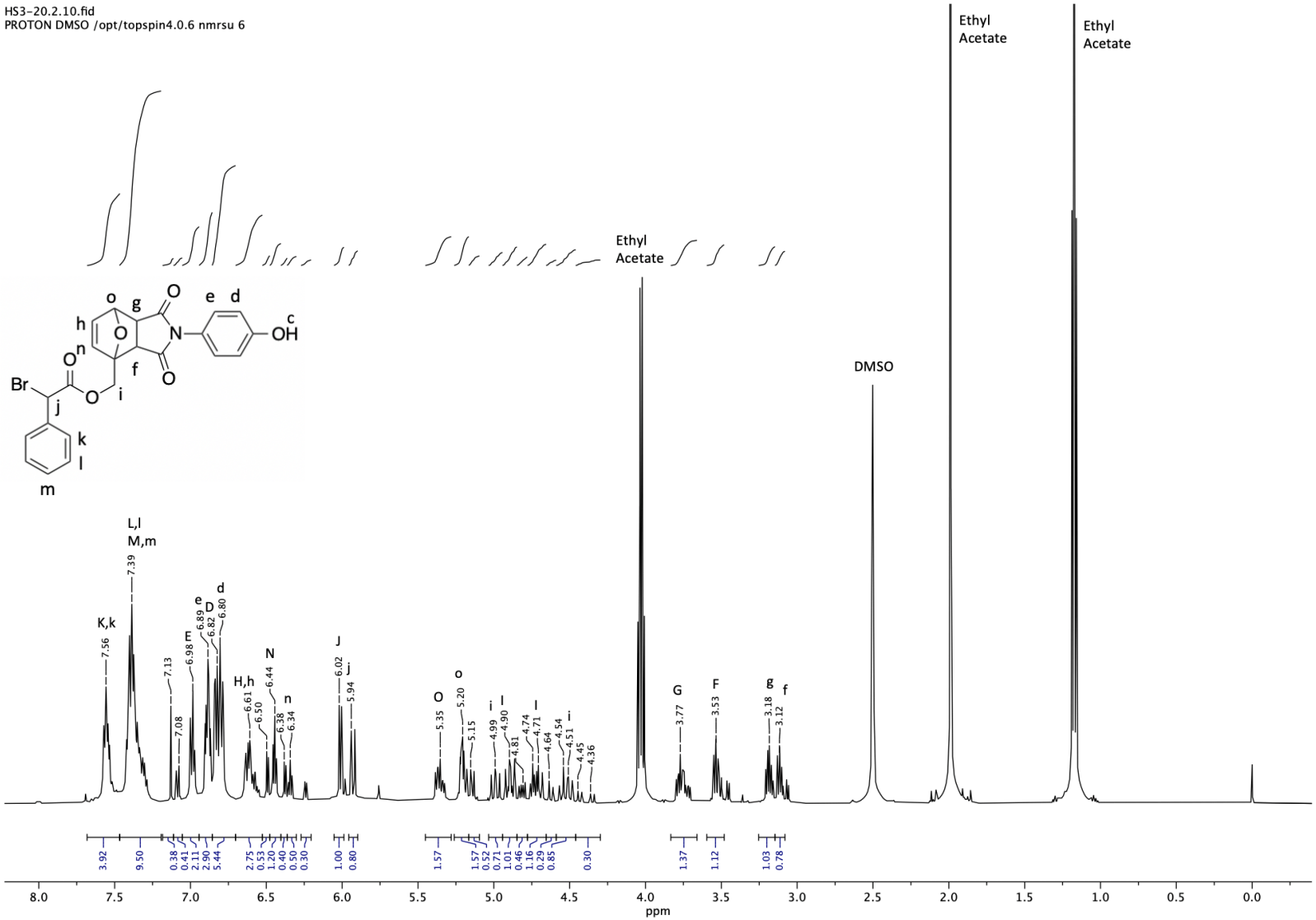

A 21: Three day reaction time of the ATRC-capable monomer resulting in 55mol% endo, 45mol% exo (uppercase alphabet = endo, lowercase alphabet = exo) ^{1}H NMR

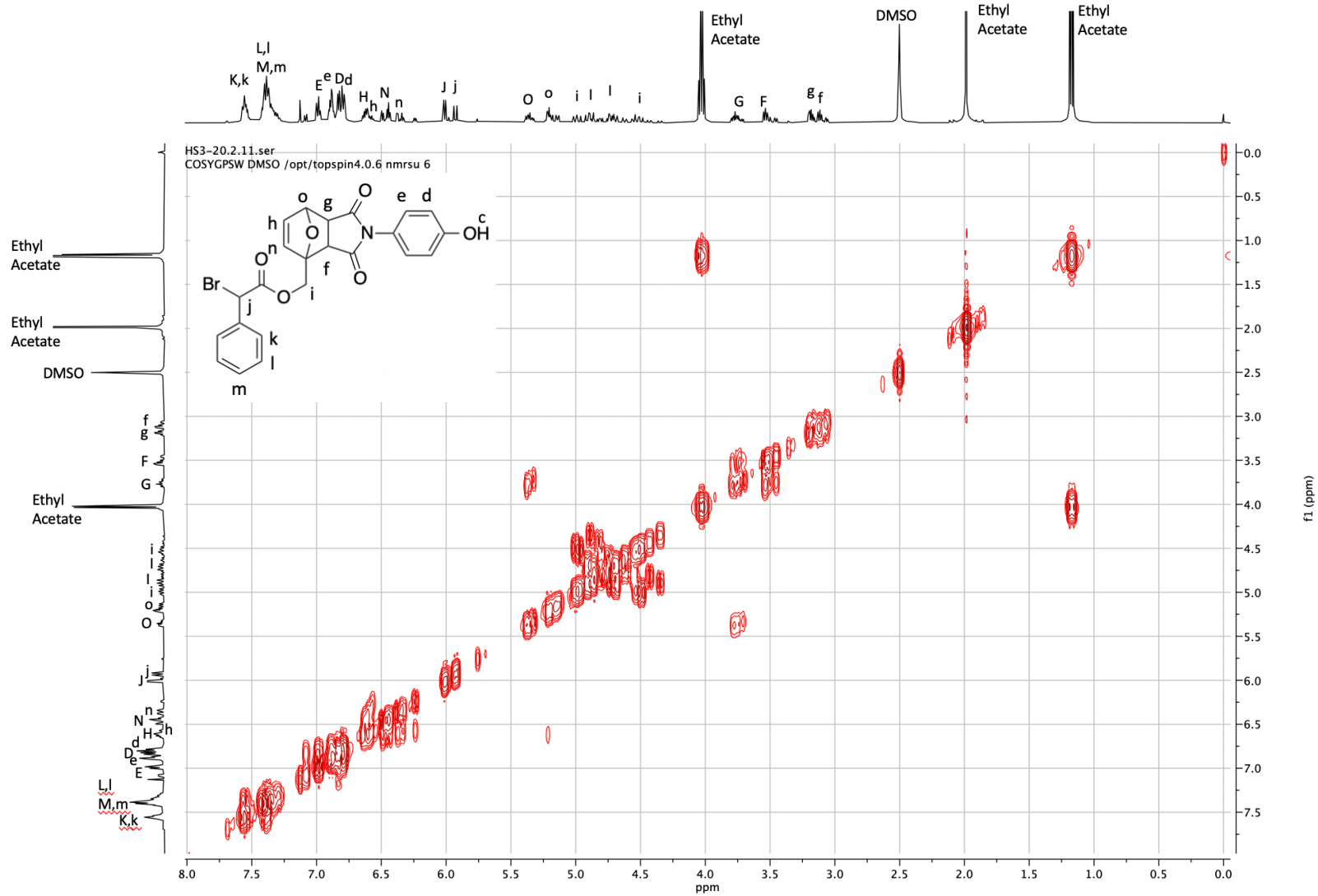

A 22: Three day reaction time ATRC-capable Diels-Alder gCOSY

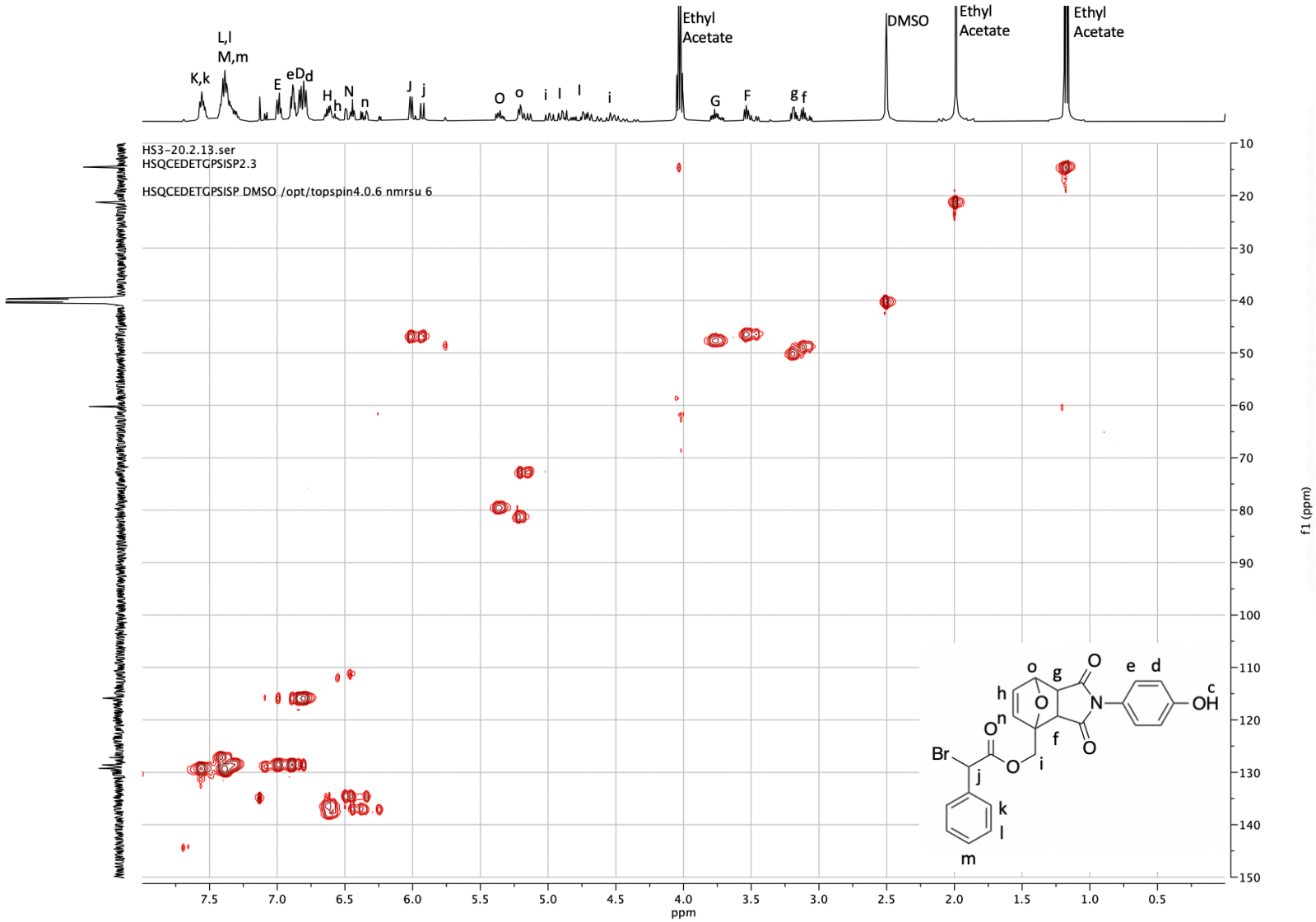

A 23: Three day reaction time ATRC-capable Diels-Alder HSQC

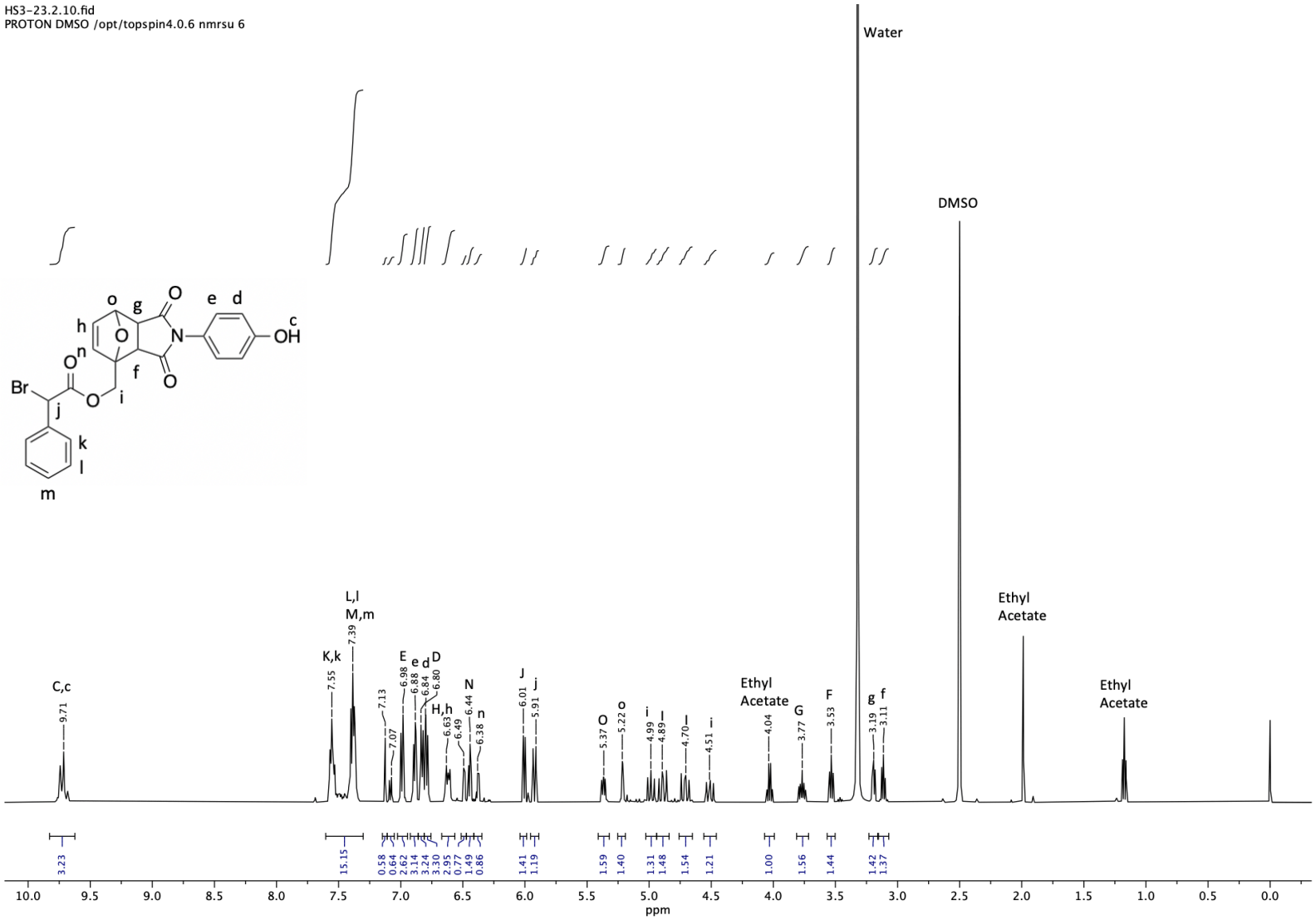

A 24: Four day reaction time of the ATRC-capable Diels-Alder resulting in 54mol% endo, 46mol% exo (uppercase alphabet = endo, lowercase alphabet = exo) ^{1}H NMR

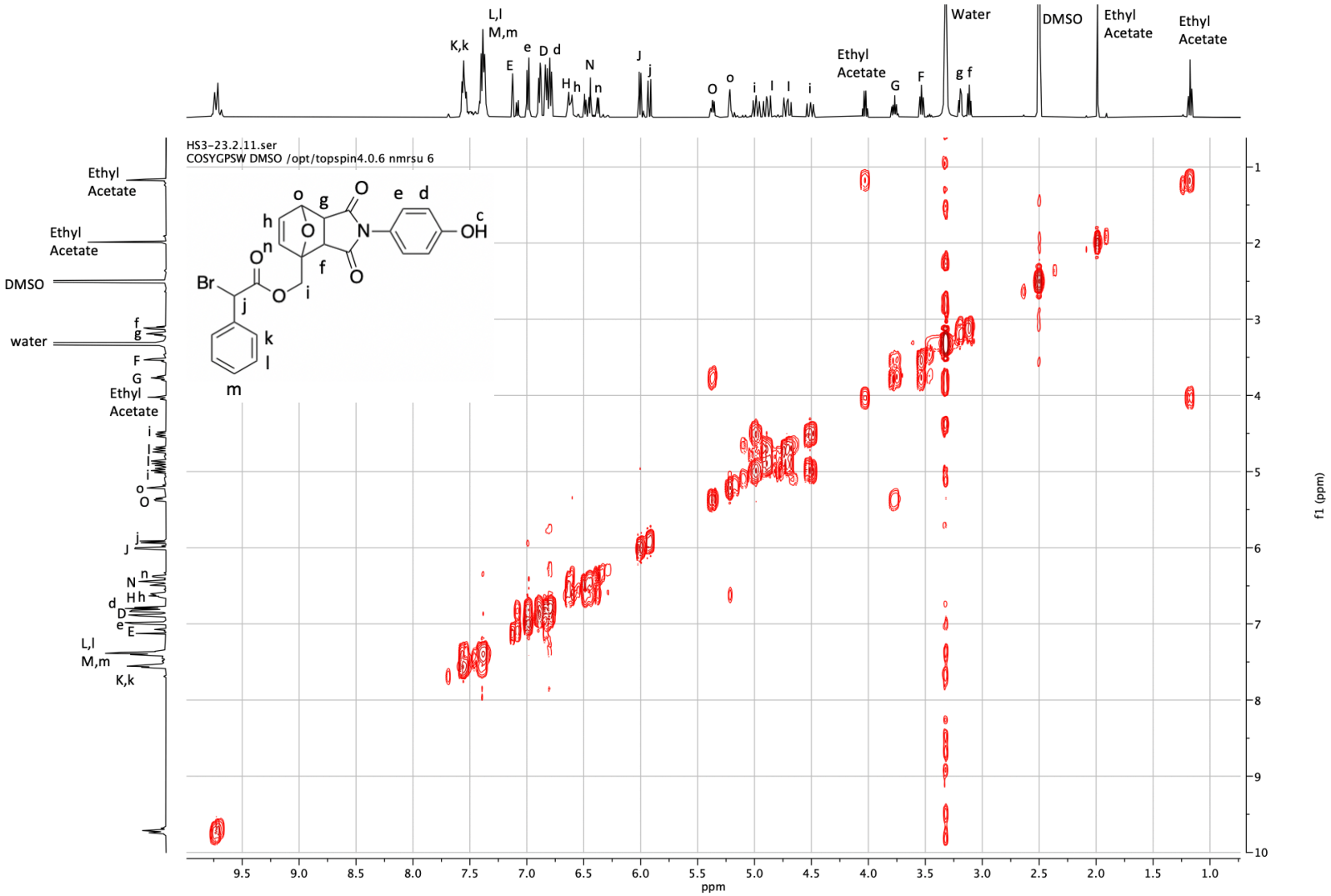

A 25: Four day reaction time ATRC-capable Diels-Alder gCOSY

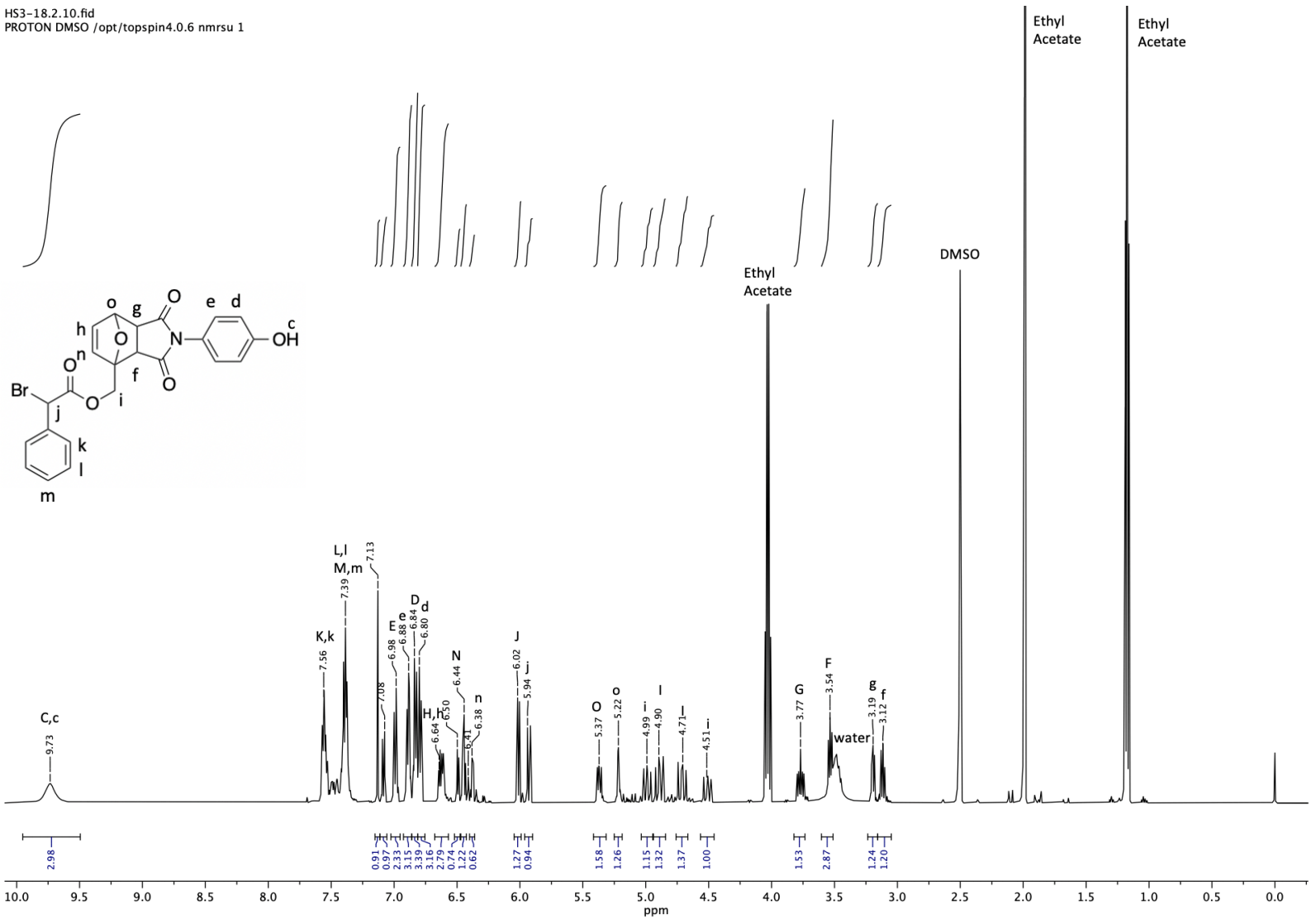

A 26: Five day reaction time of the ATRC-capable Diels-Alder resulting in 56mol% endo, 44mol% exo (uppercase alphabet = endo, lowercase alphabet = exo) ^{1}H NMR

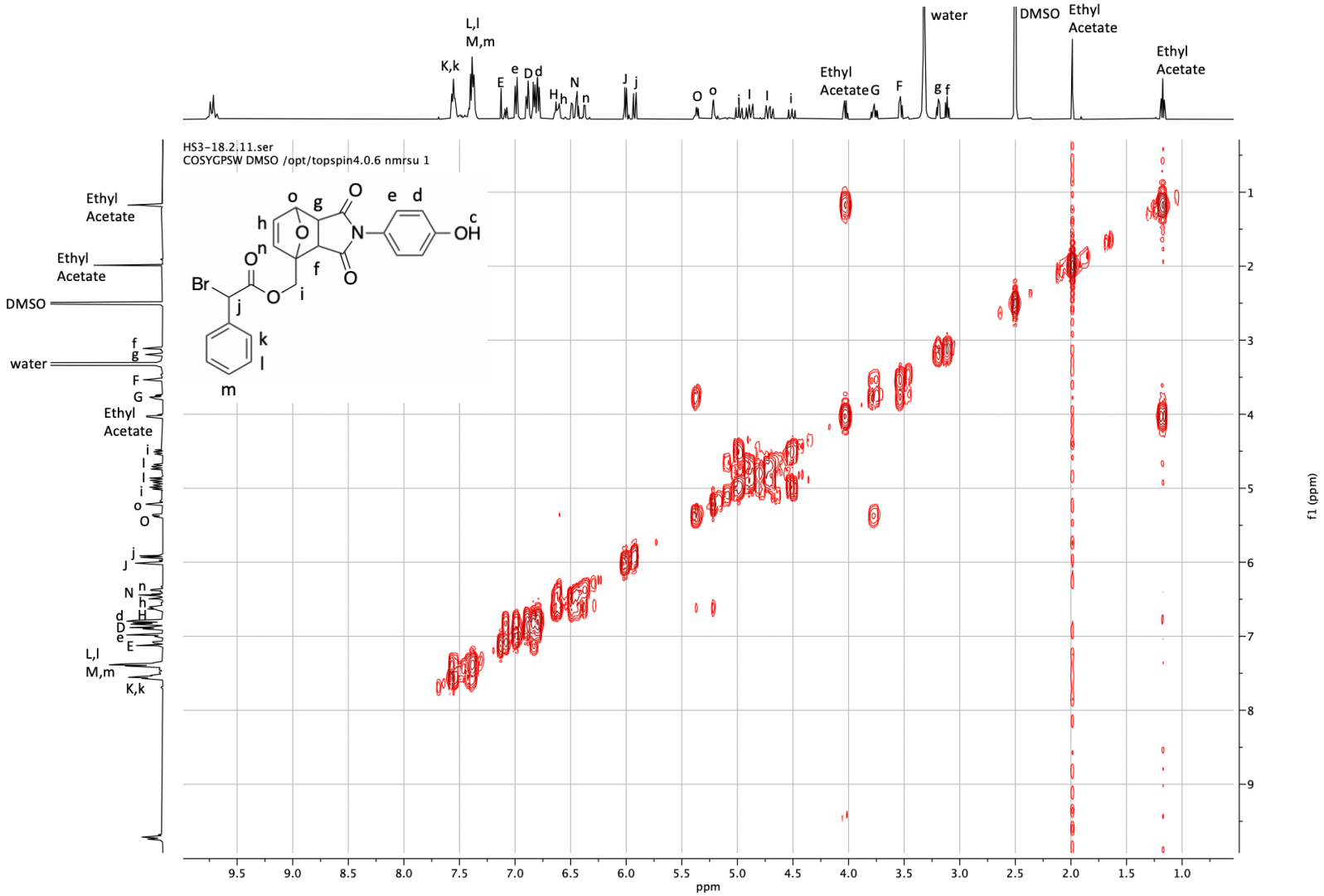

A 27: Five day reaction time ATRC-capable Diels-Alder gCOSY

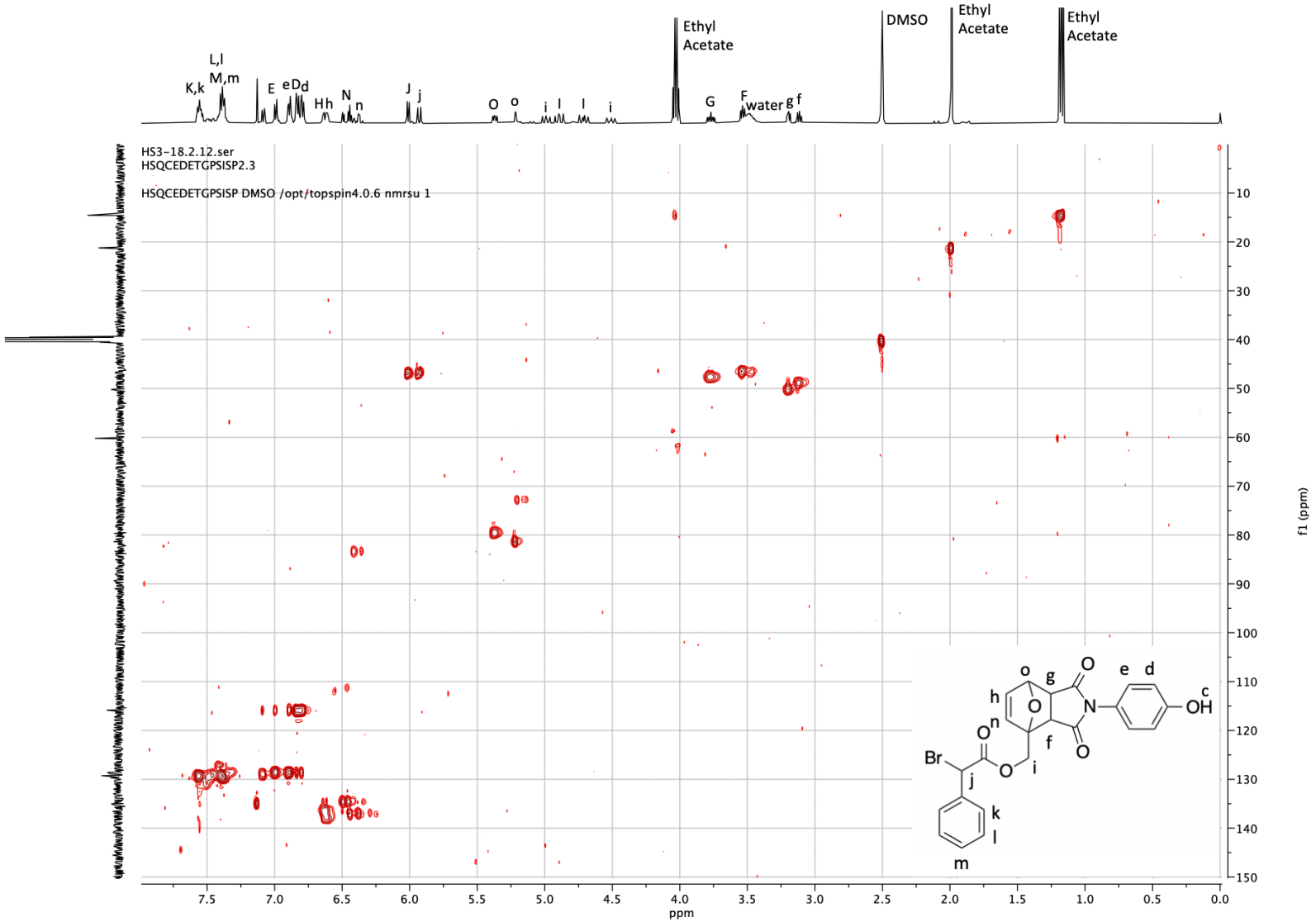

A 28: Five day reaction time ATRC-capable Diels-Alder HSQC

HS3-19.2.10.fid
PROTON DMSO /opt/topspin4.0.6 nmrsu 3

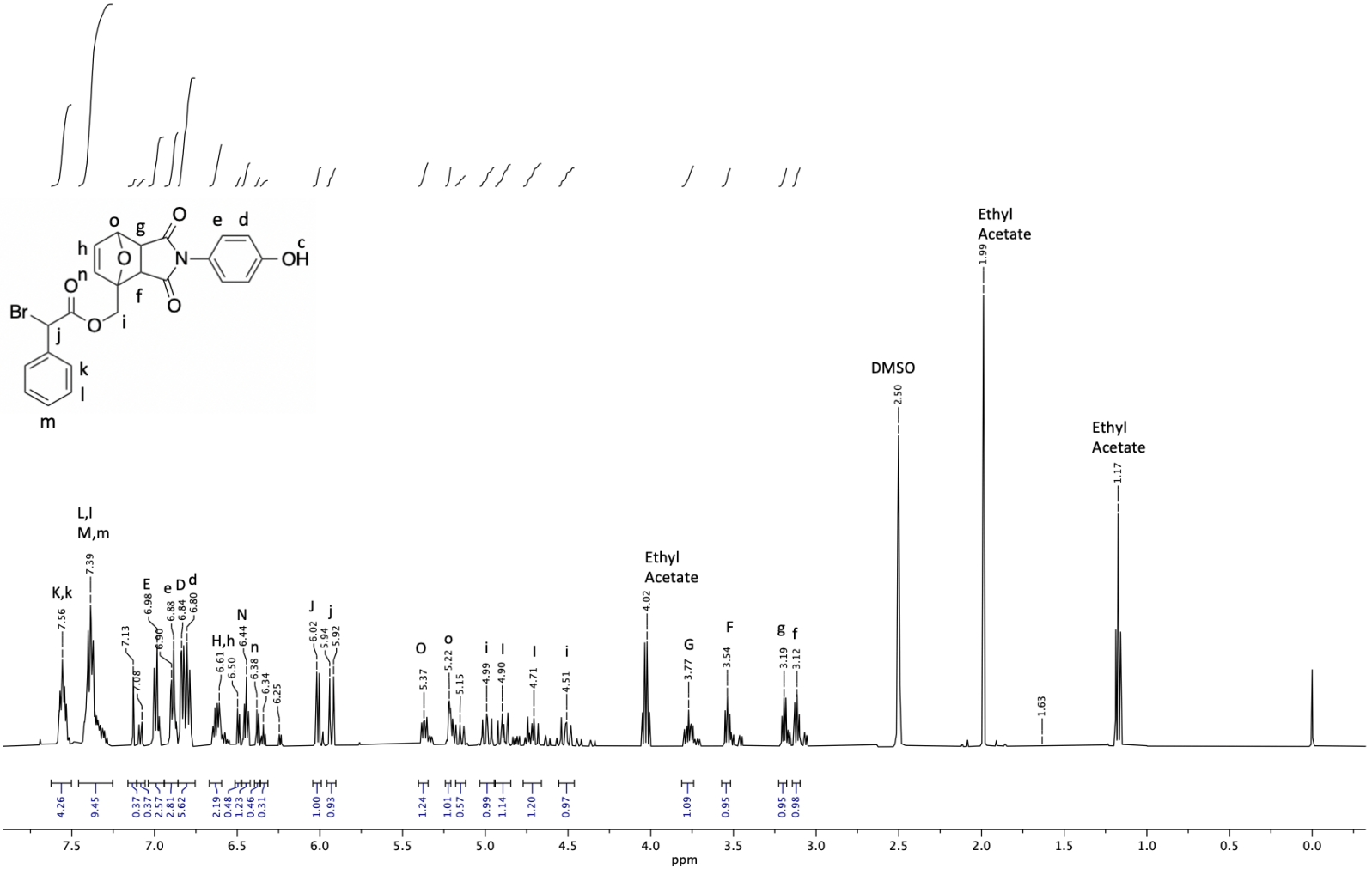

A 29: Six day reaction time of the ATRC-capable Diels-Alder resulting in 52mol% endo, 48mol% exo (uppercase alphabet = endo, lowercase alphabet = exo) ^{1}H NMR

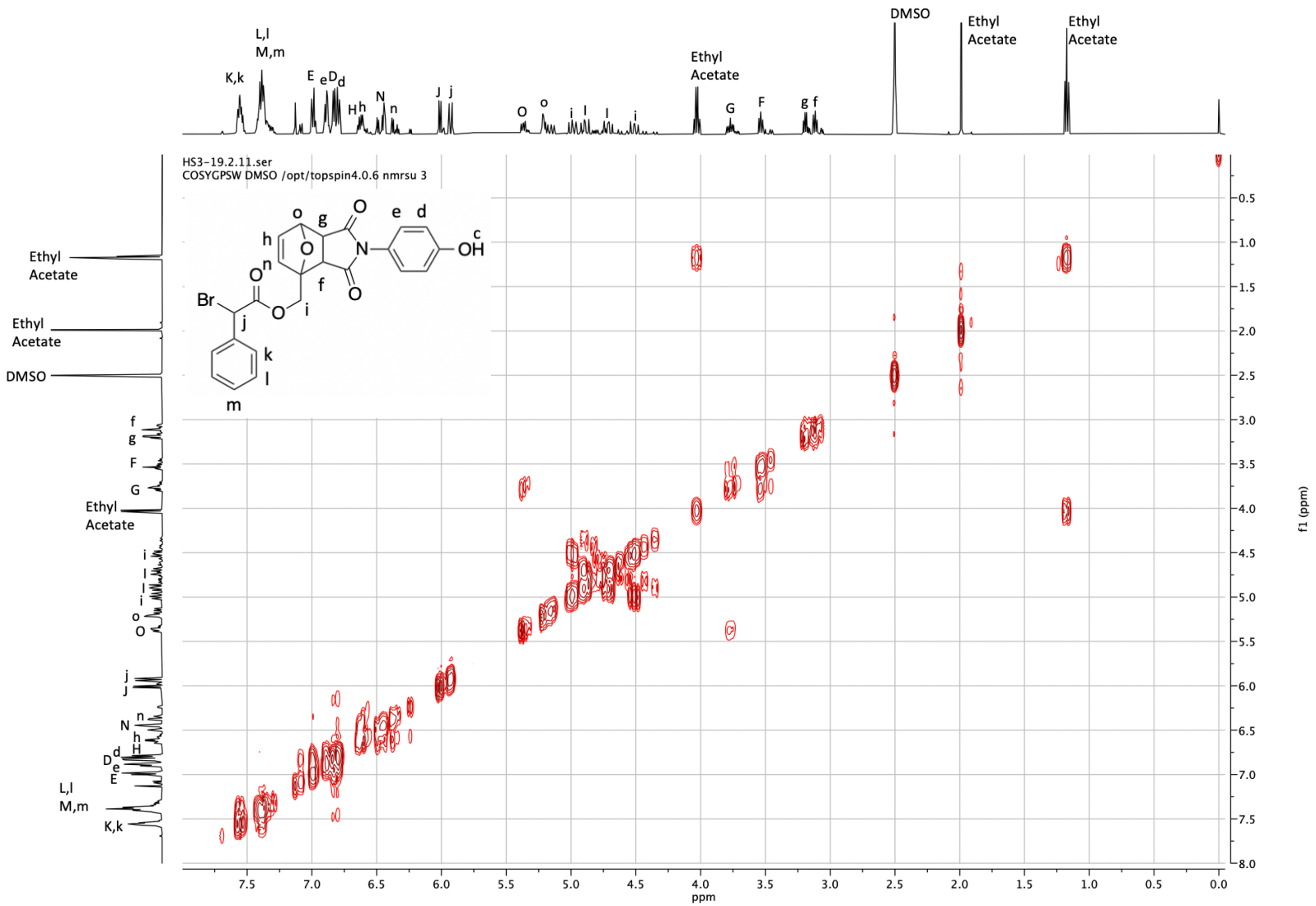

A 30: Six day reaction time ATRC-capable Diels-Alder gCOSY

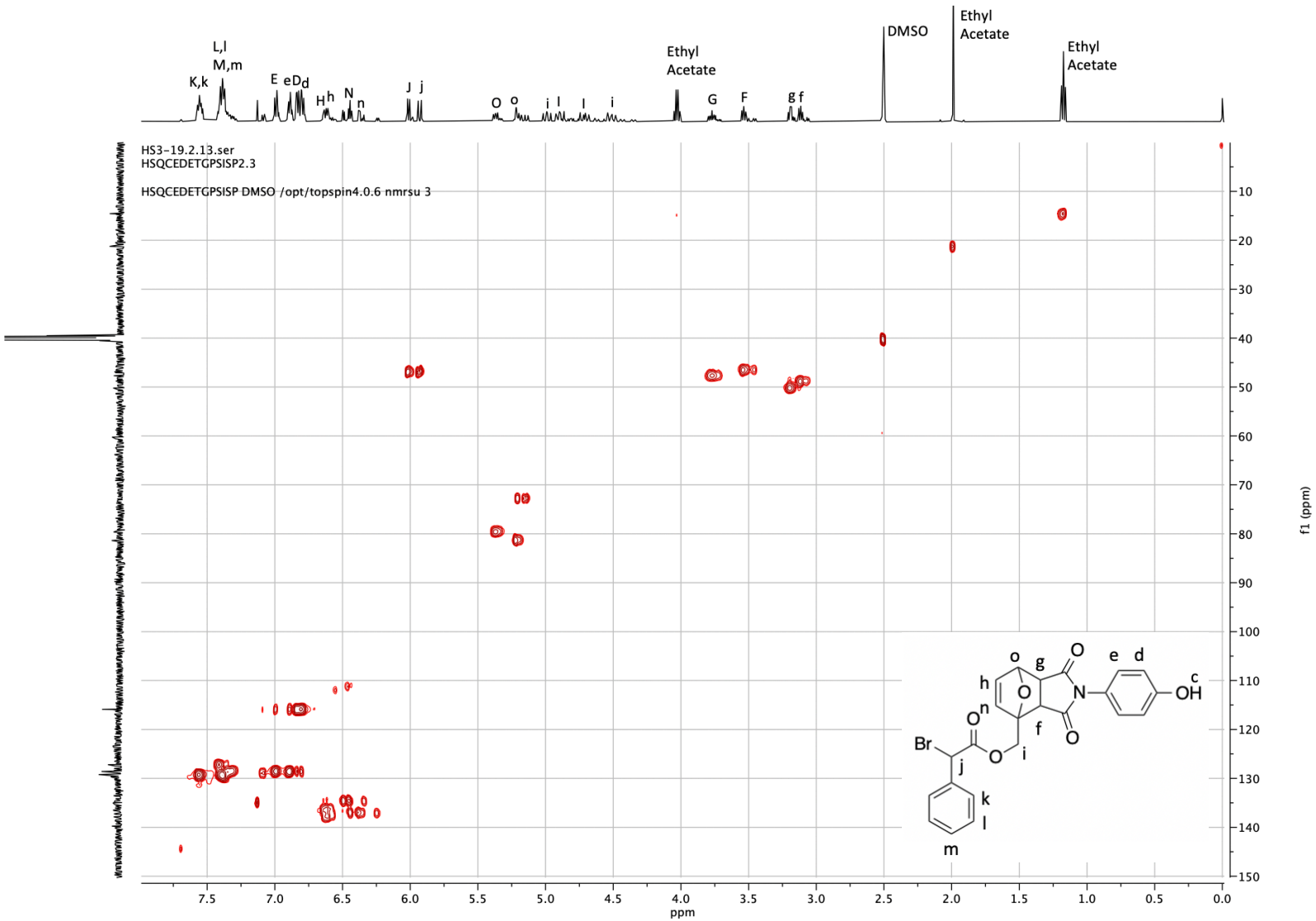

A 31: Six day reaction time ATRC-capable Diels-Alder HSQC

HS3-4B.10.fid
PROTON DMSO /opt/topspin4.0.6 nmrsu 12

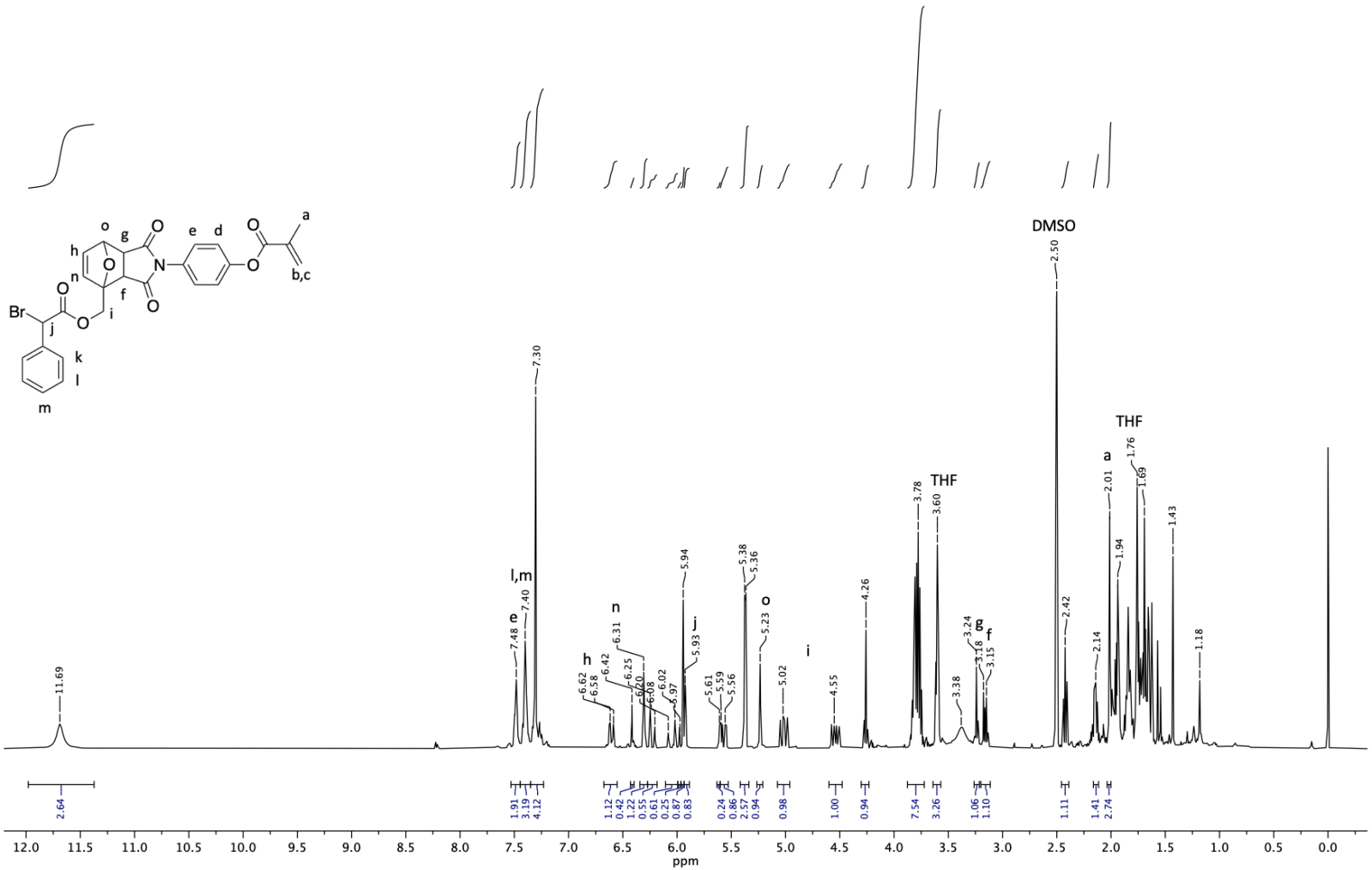

A 32: ATRC-Capable Diels-Alder adduct esterification employing triethylamine and DMAP ^{1}H NMR

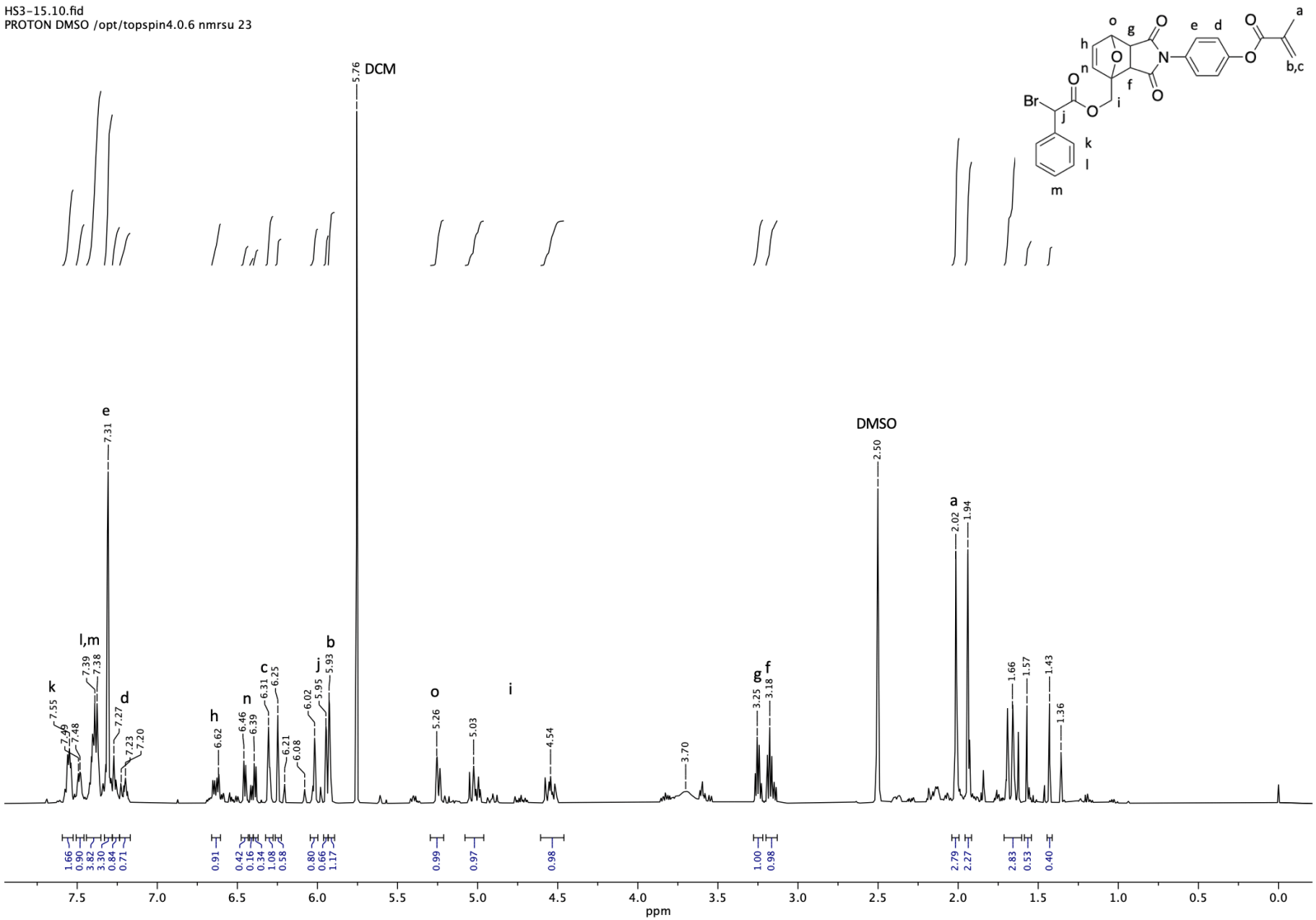

A 33: ATRC-capable Diels-Alder adduct esterification (utilizing 2eq methacryloyl chloride) ^{1}H NMR

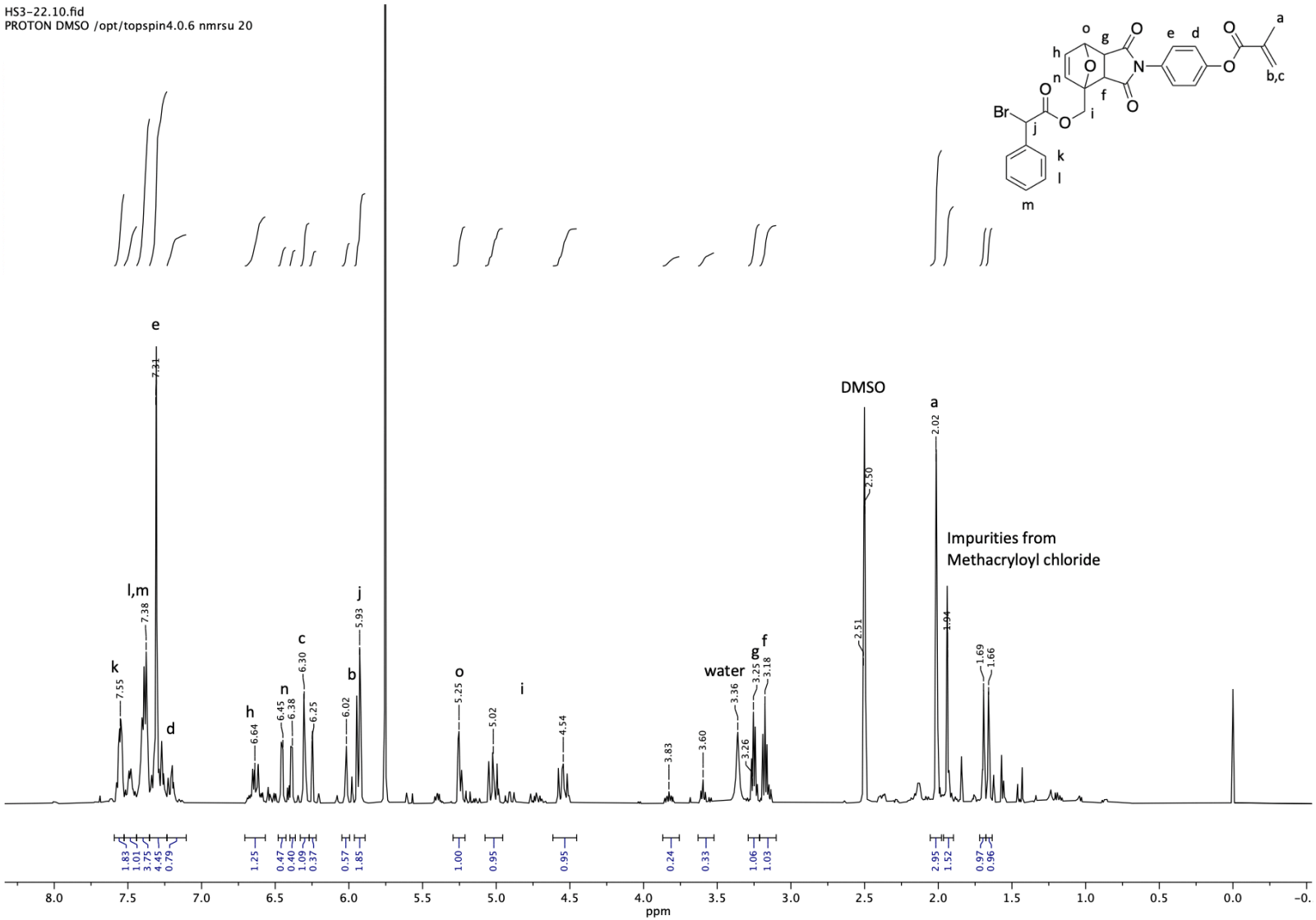

A 34: ATRC-capable Diels-Alder adduct esterification (utilizing 1eq methacryloyl chloride) ^{1}H NMR

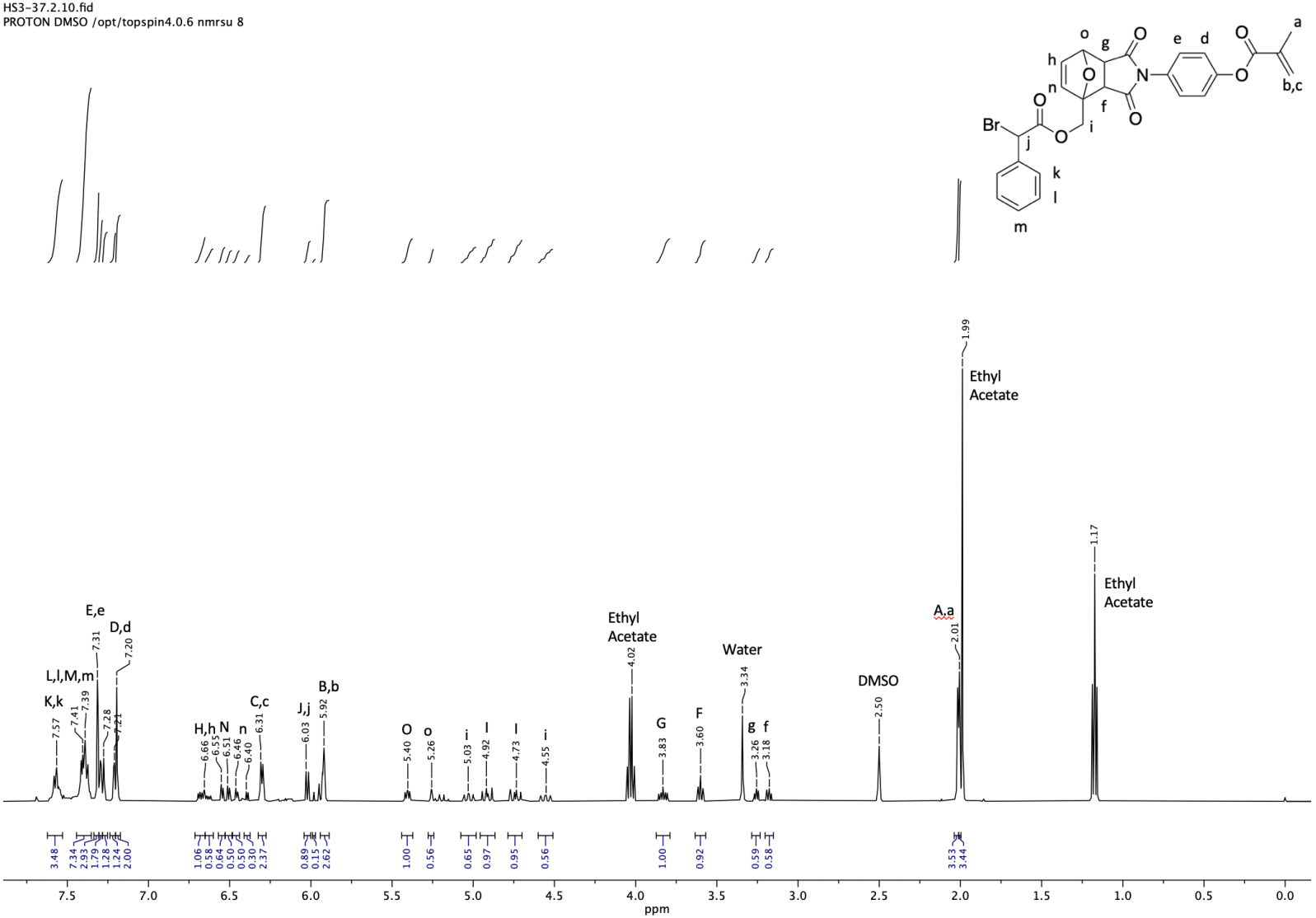

A 35: Diels-Alder synthesis utilizing methacrylate functionalized N-(4-hydroxyphenyl) maleimide ^{1}H NMR

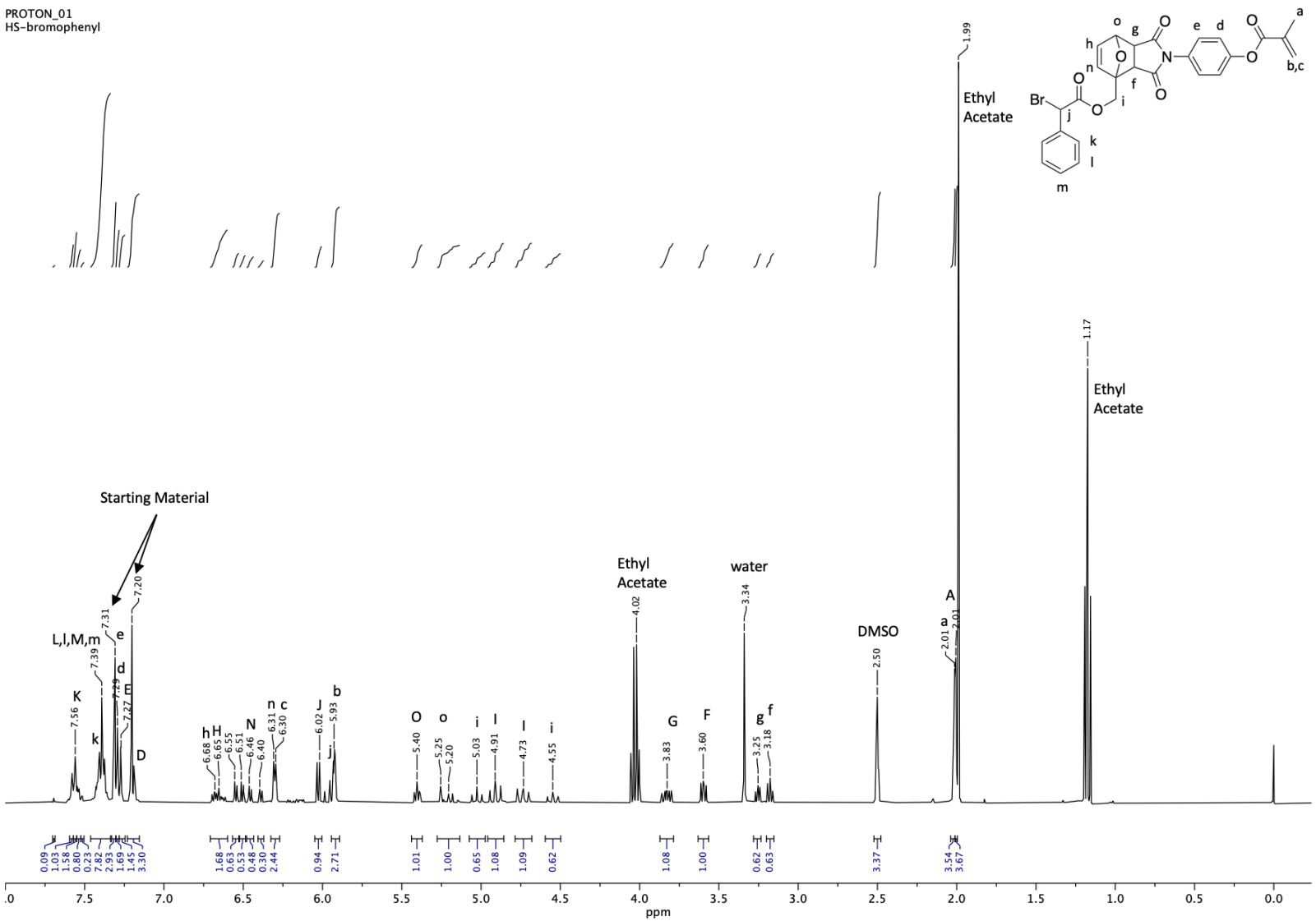

A 36: ATRC-capable monomer variable temperature ^{1}H NMR - Room Temperature (21.8℃)

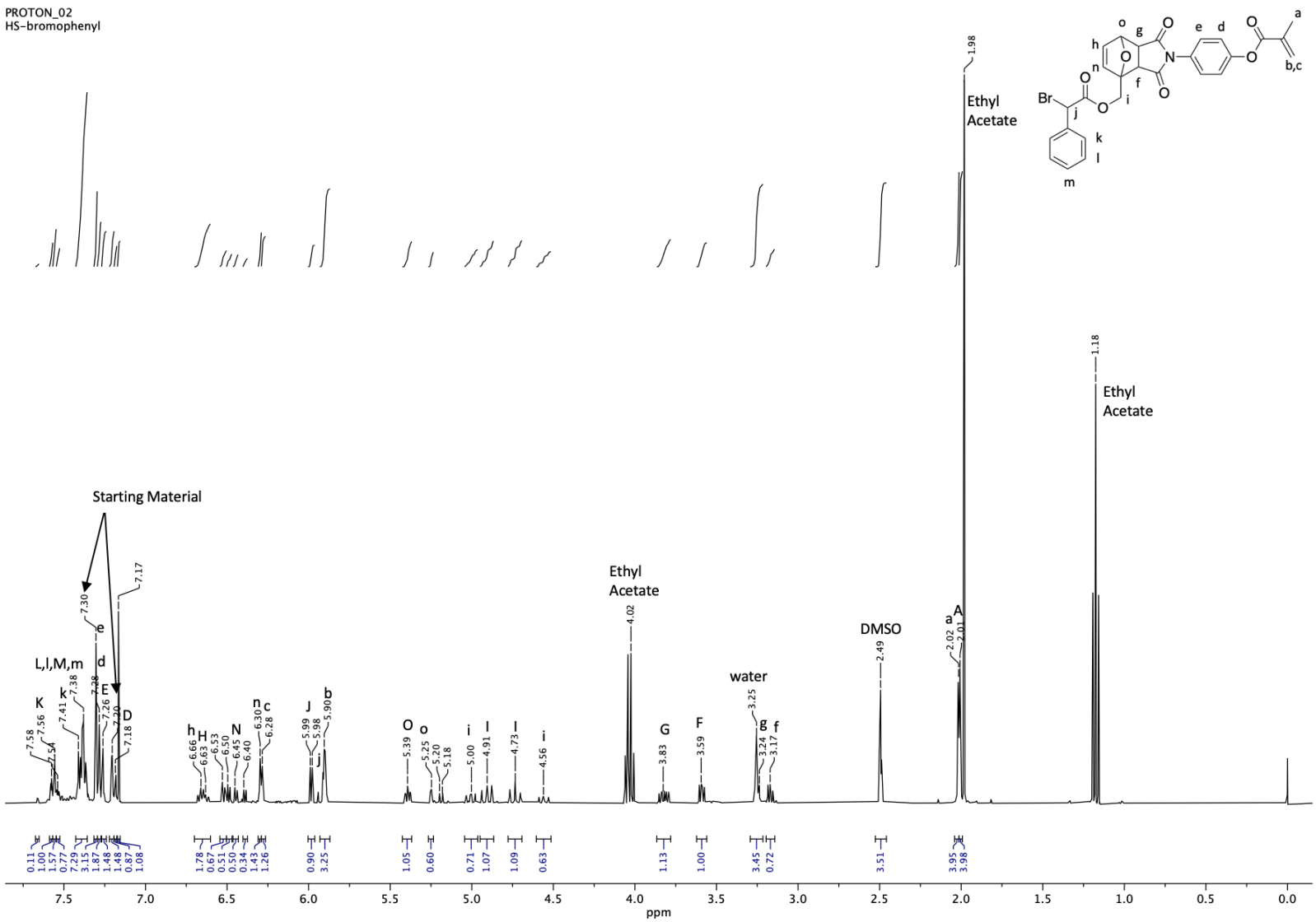

A 37: ATRC-capable monomer variable Temperature 1H NMR - 45 ℃

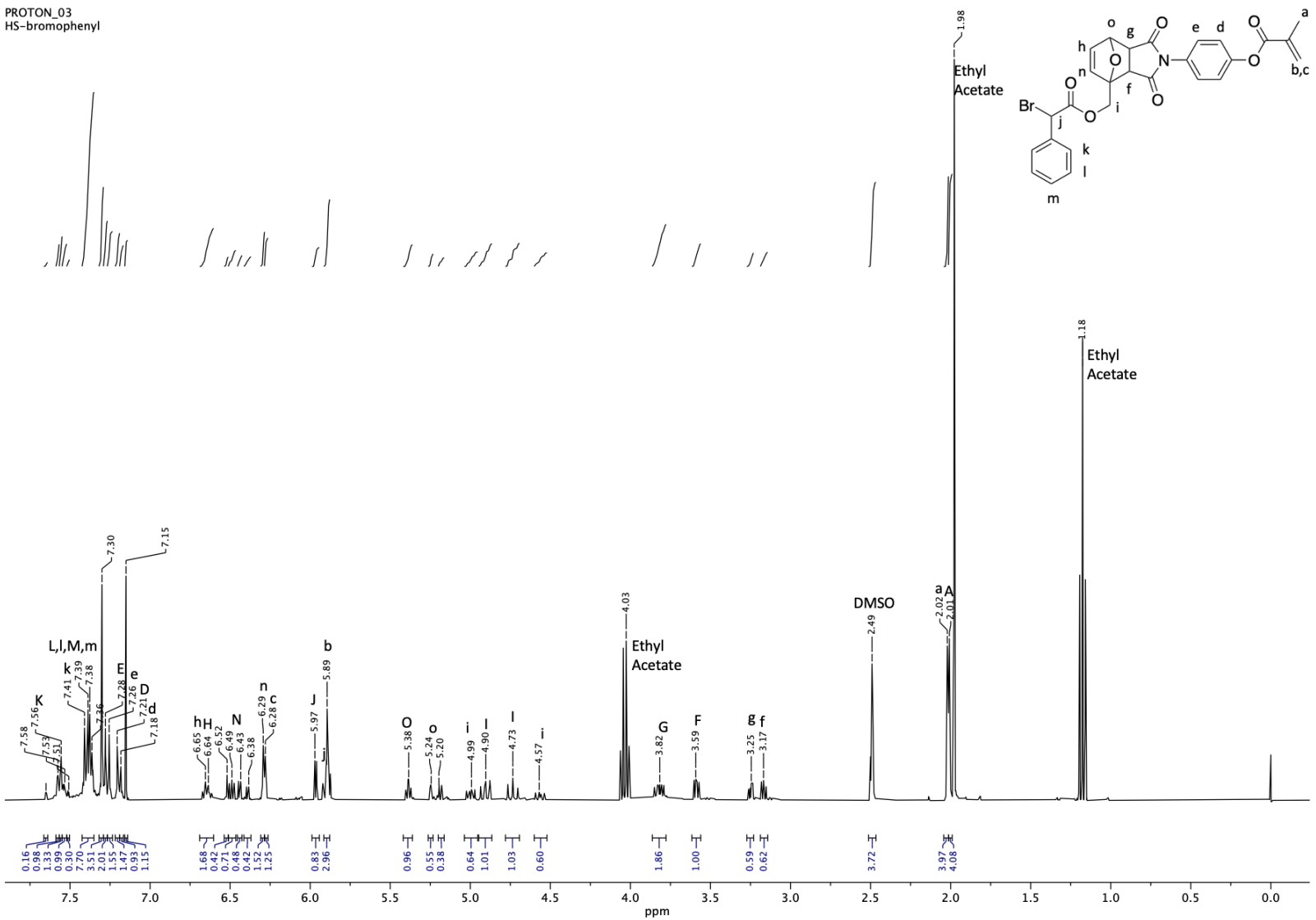

A 38: ATRC-capable monomer variable Temperature ^{1}H NMR - 55 ℃

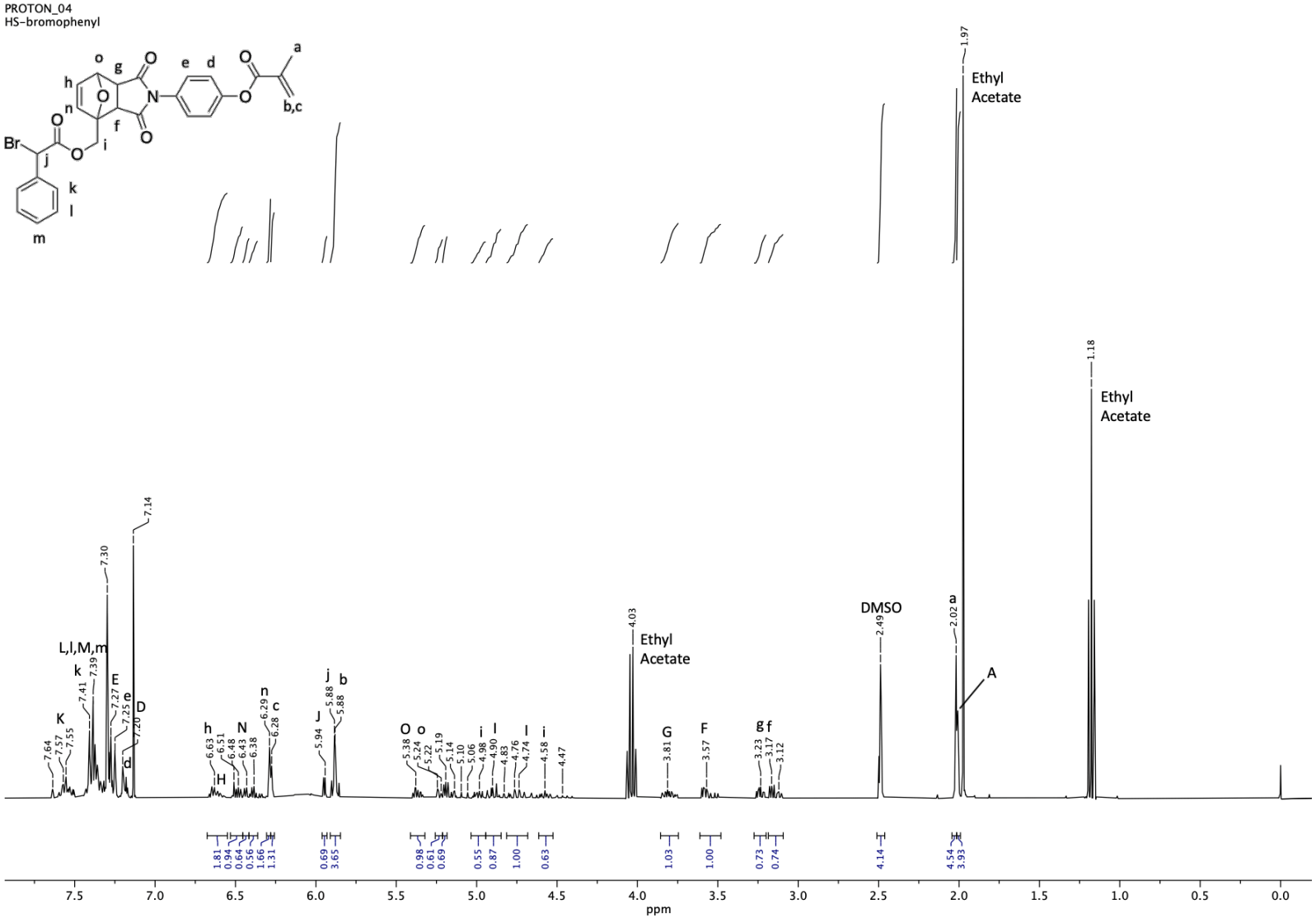

A 39: ATRC-capable monomer variable Temperature ^{1}H NMR - 65 ℃

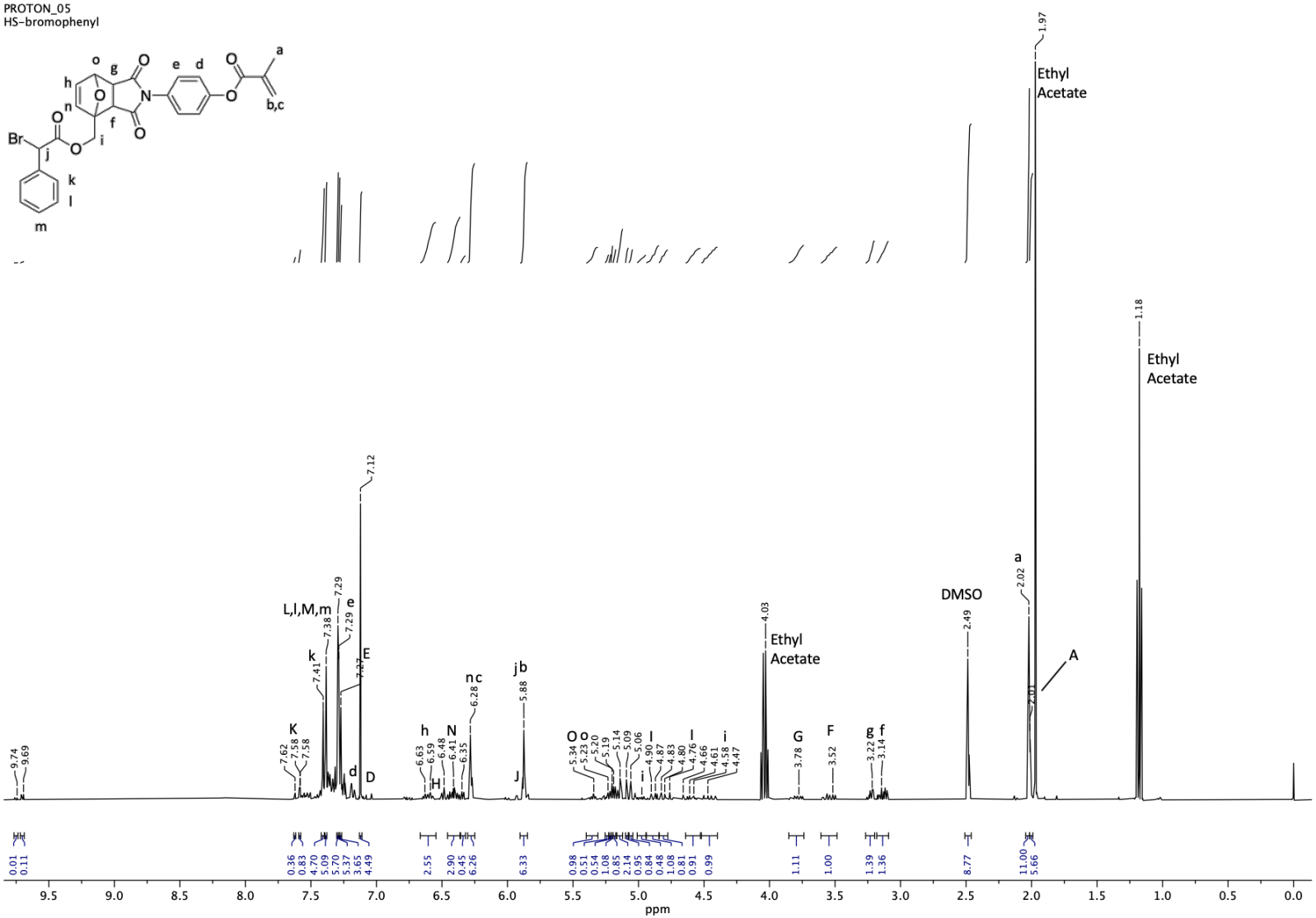

A 40: ATRC-capable monomer variable Temperature ^{1}H NMR - 75 ℃

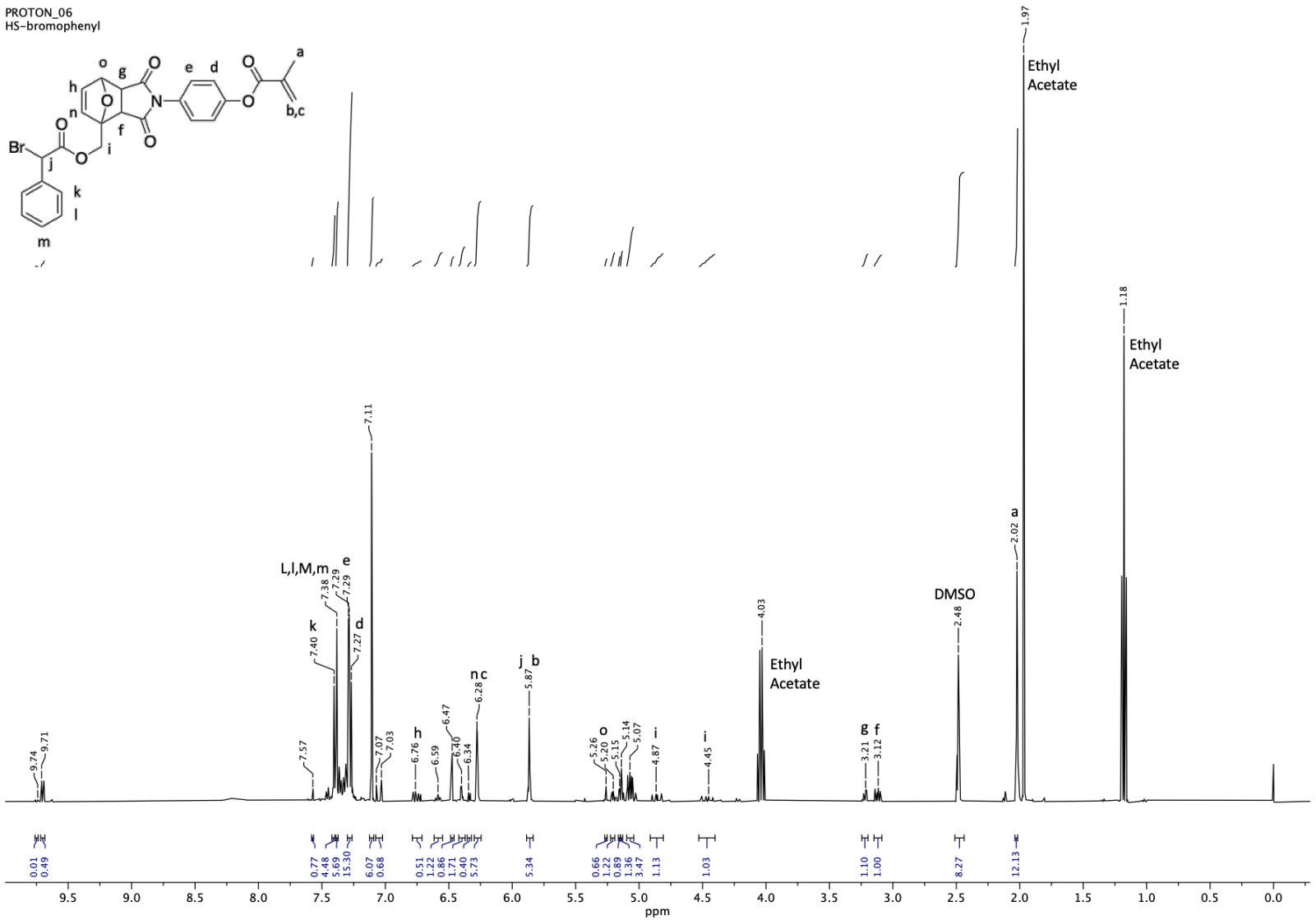

A 41: ATRC-capable monomer variable Temperature ^{1}H NMR - 85℃

HS2-40.1.10.fid
PROTON DMSO /opt/topspin4.0.6 nmrsu 15

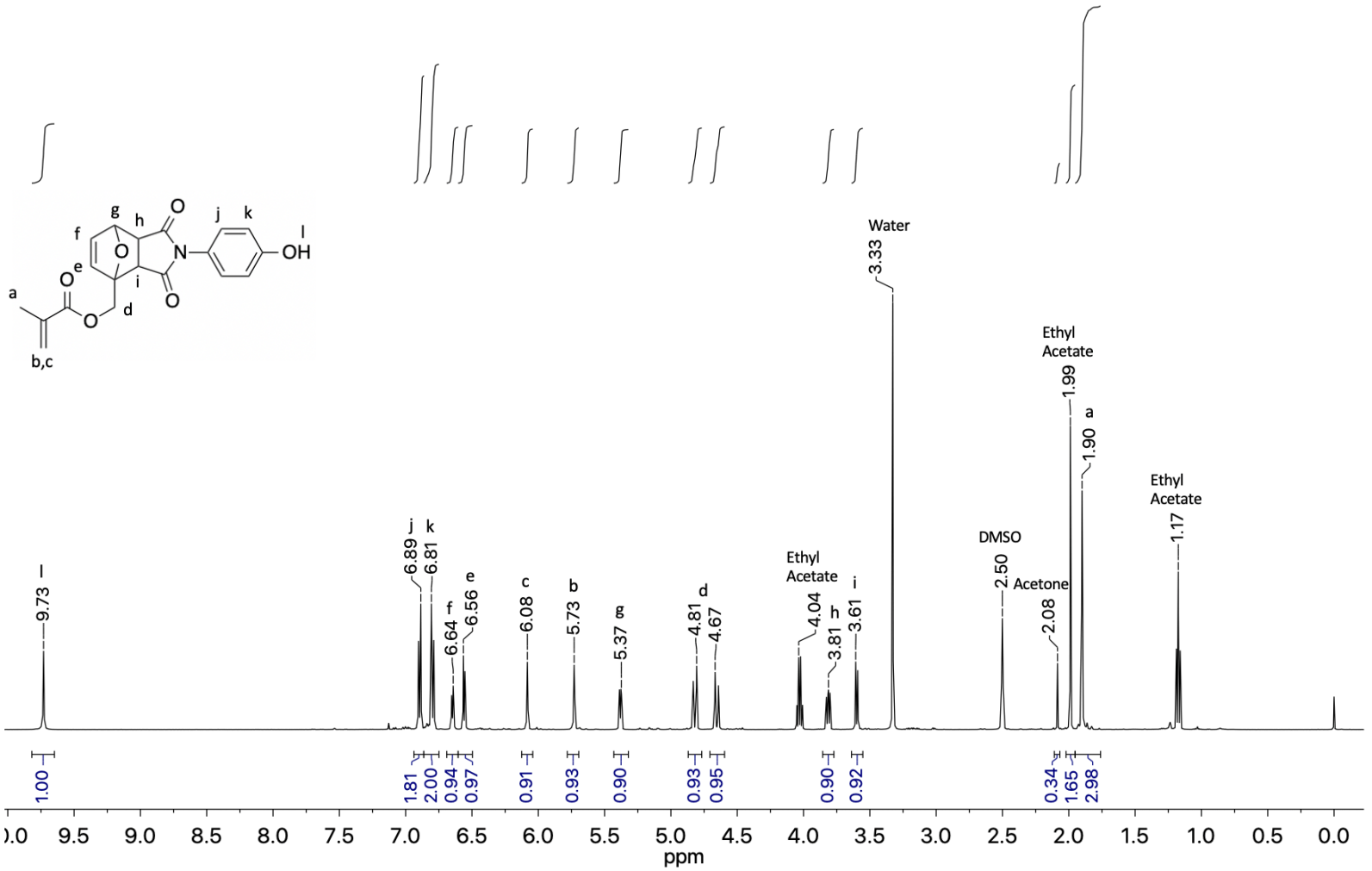

A 42: Endo-Diels-Alder functionalized crosslinker precursor ^{1}H NMR

HS2-40.1.11.fid
C13CPD DMSO /opt/topspin4.0.6 nmrsu 15

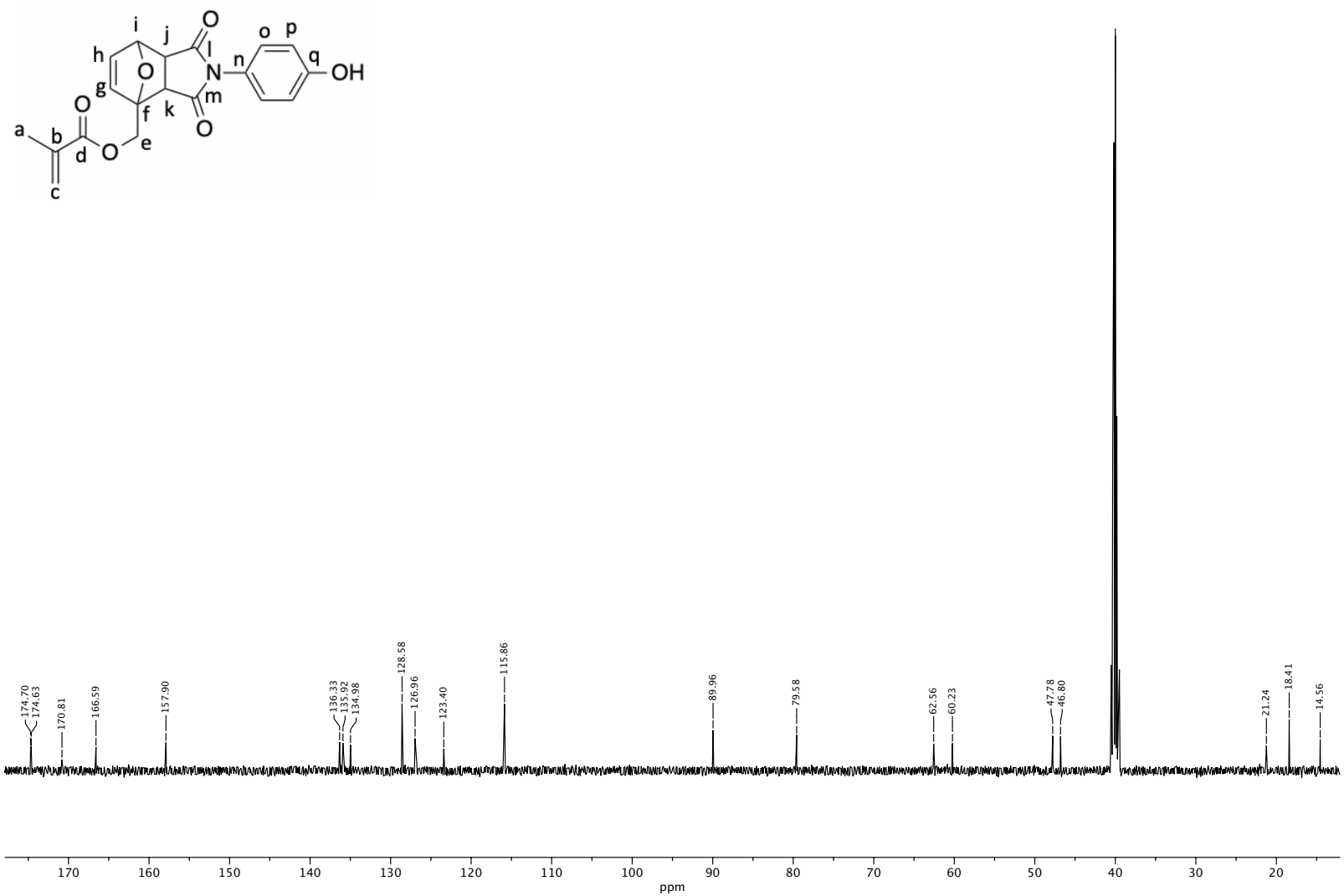

A 43: Endo-Diels-Alder functionalized crosslinker precursor ^{13}C NMR

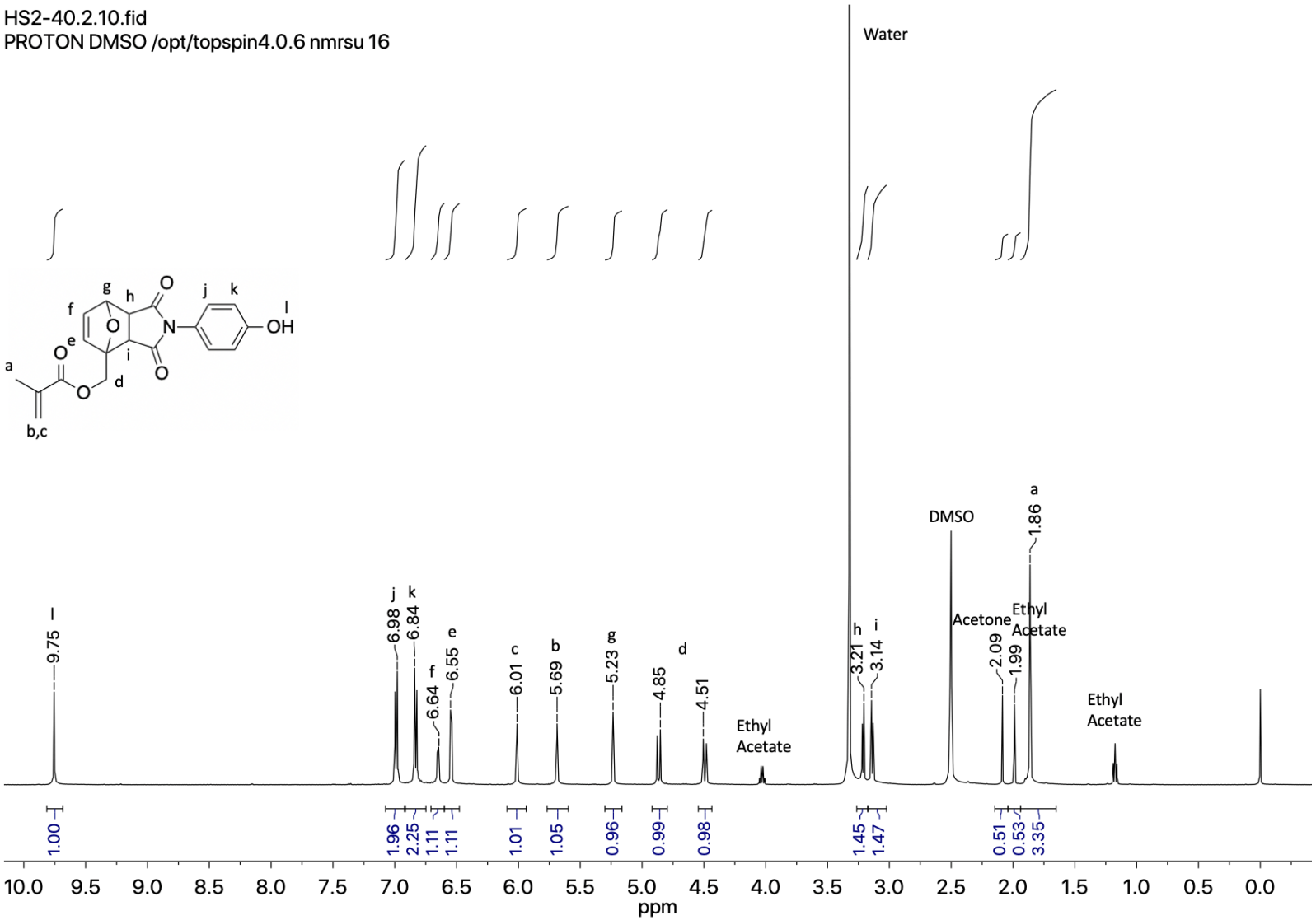

A 44: Exo-Diels-Alder functionalized crosslinker precursor ^{1}H NMR

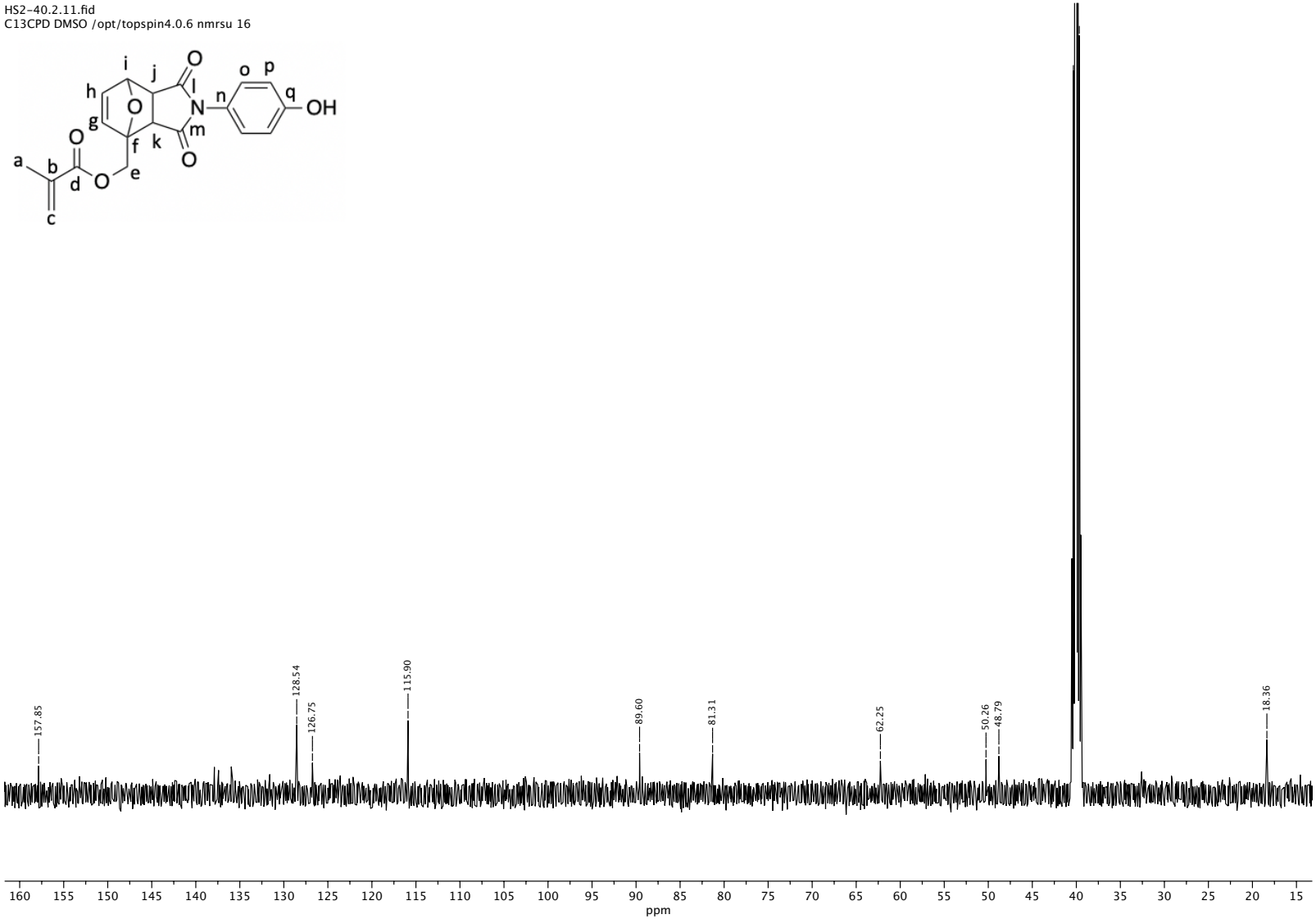

A 45: Exo-Diels-Alder functionalized crosslinker precursor ^{13}C NMR

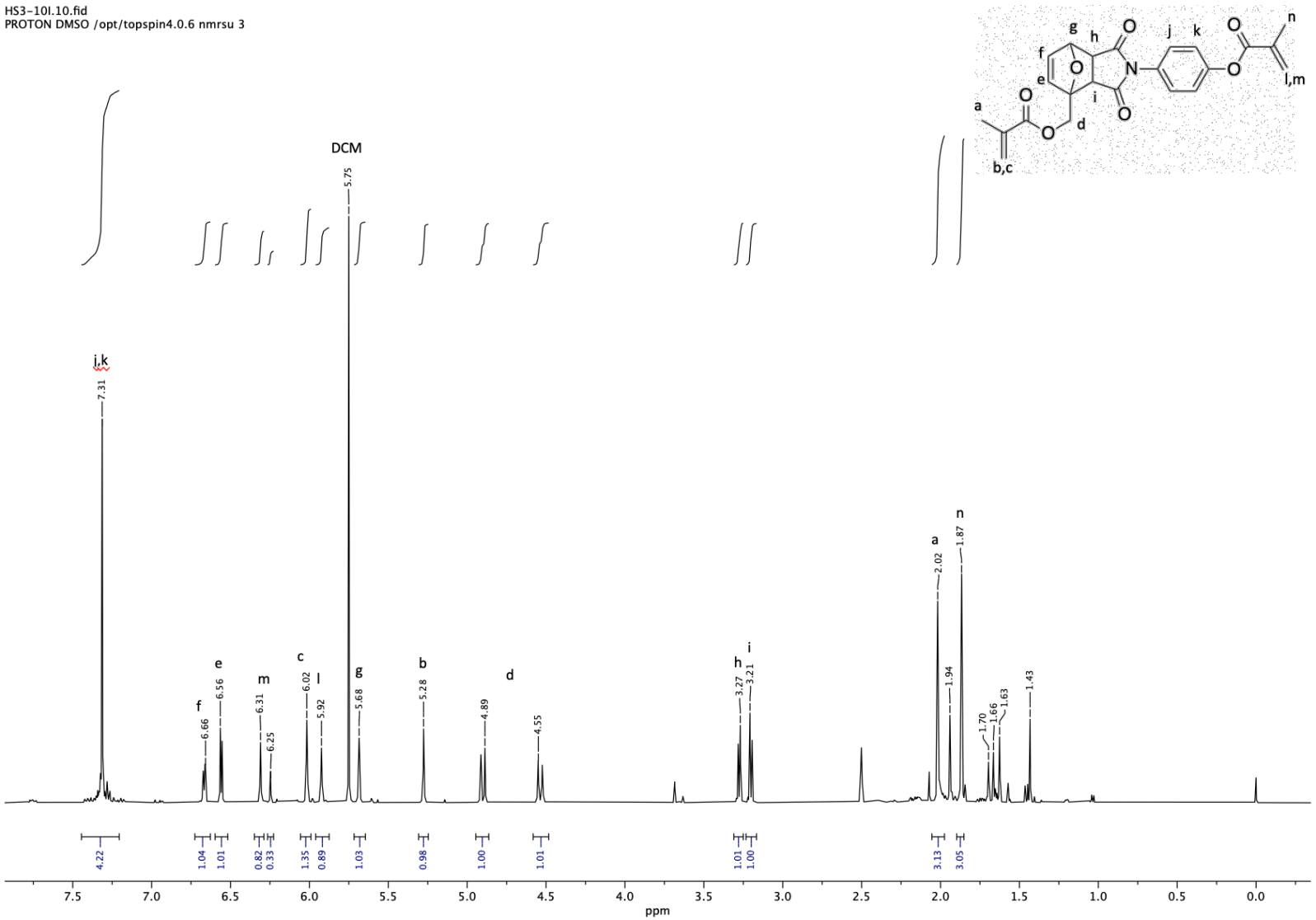

A 46: Exo-Diels-Alder Functionalized Monomer ^{1}H NMR

HS3-10l.11.fid
C13CPD DMSO /opt/topspin4.0.6 nmrsu 3

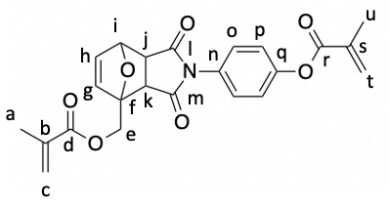

A 47: Exo-Diels-Alder Functionalized Monomer ^{13}C NMR

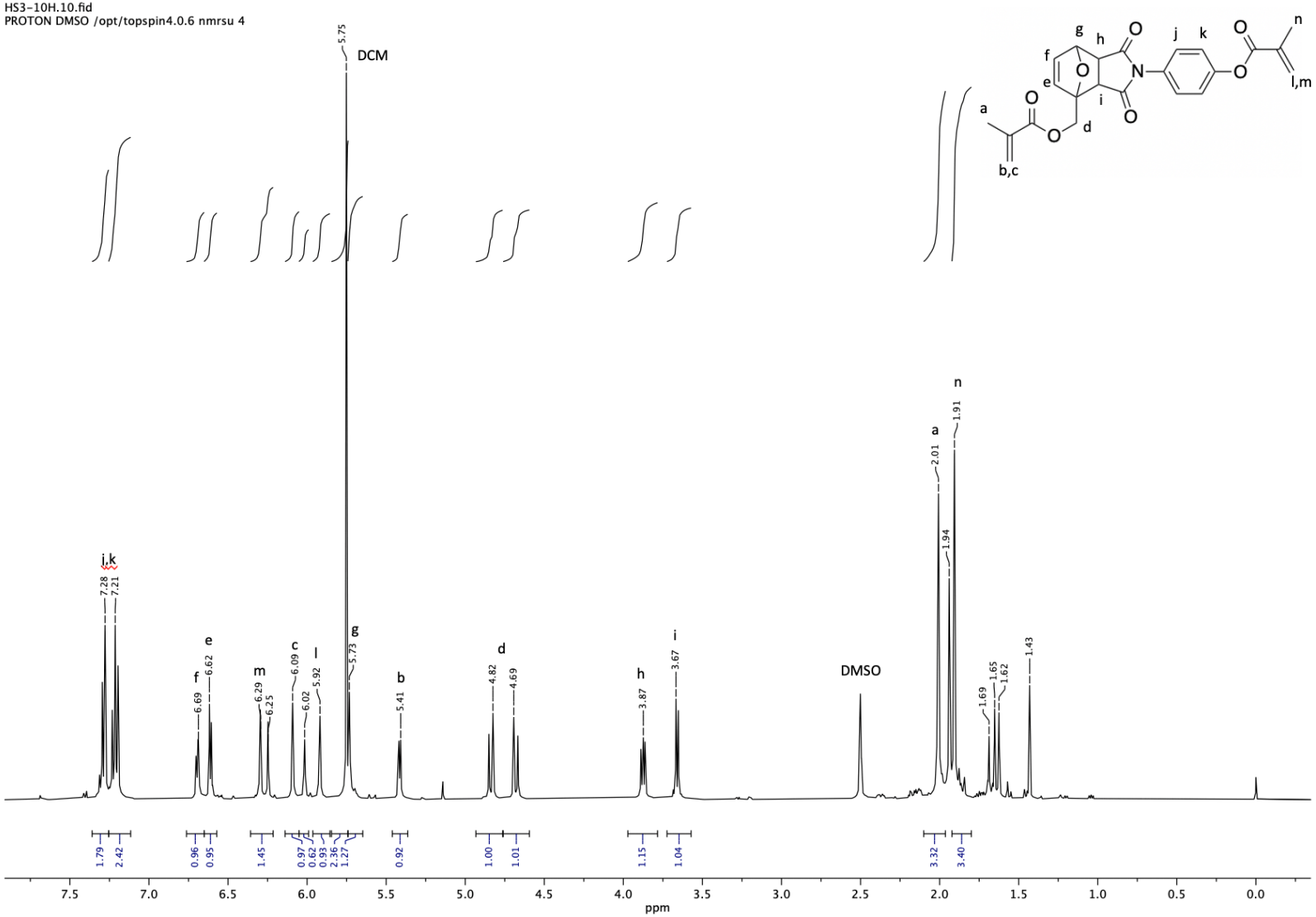

A 48: Endo-Diels-Alder Functionalized Monomer ^{1}H NMR

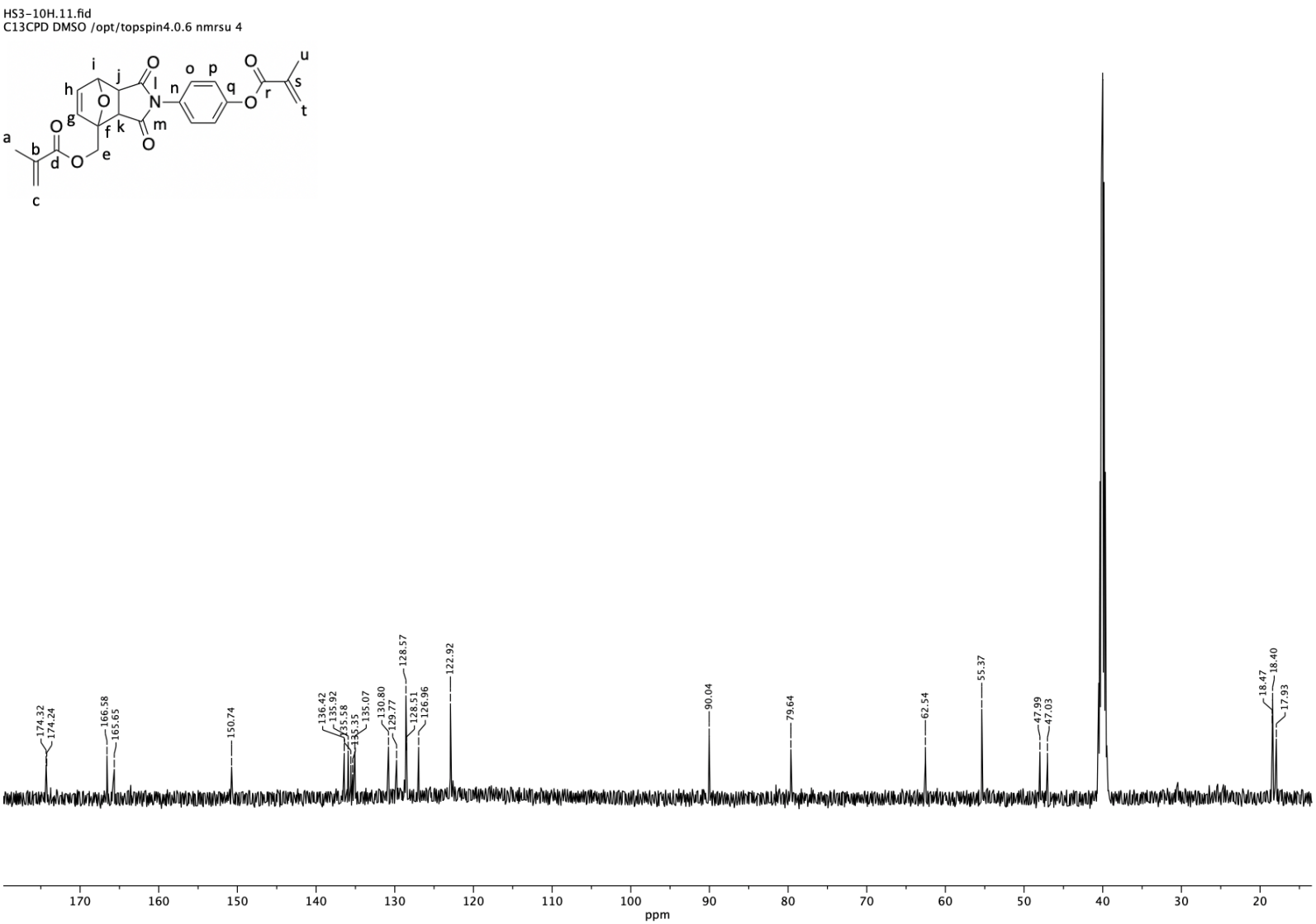

A 49: Endo-Diels-Alder Functionalized Monomer ^{13}C NMR

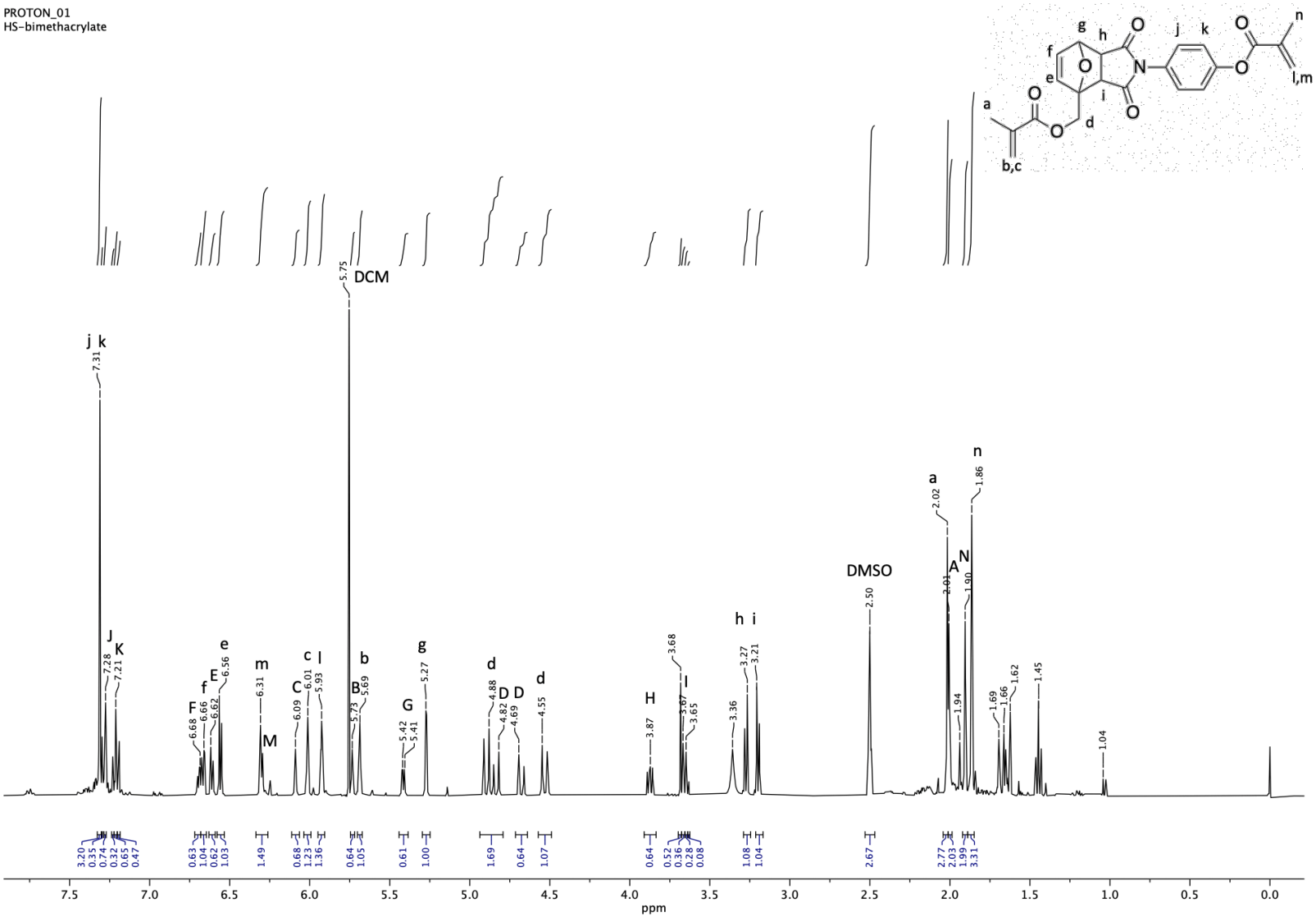

A 50 – Diels-Alder functionalized crosslinker variable Temperature NMR – Room Temperature (21.8℃)

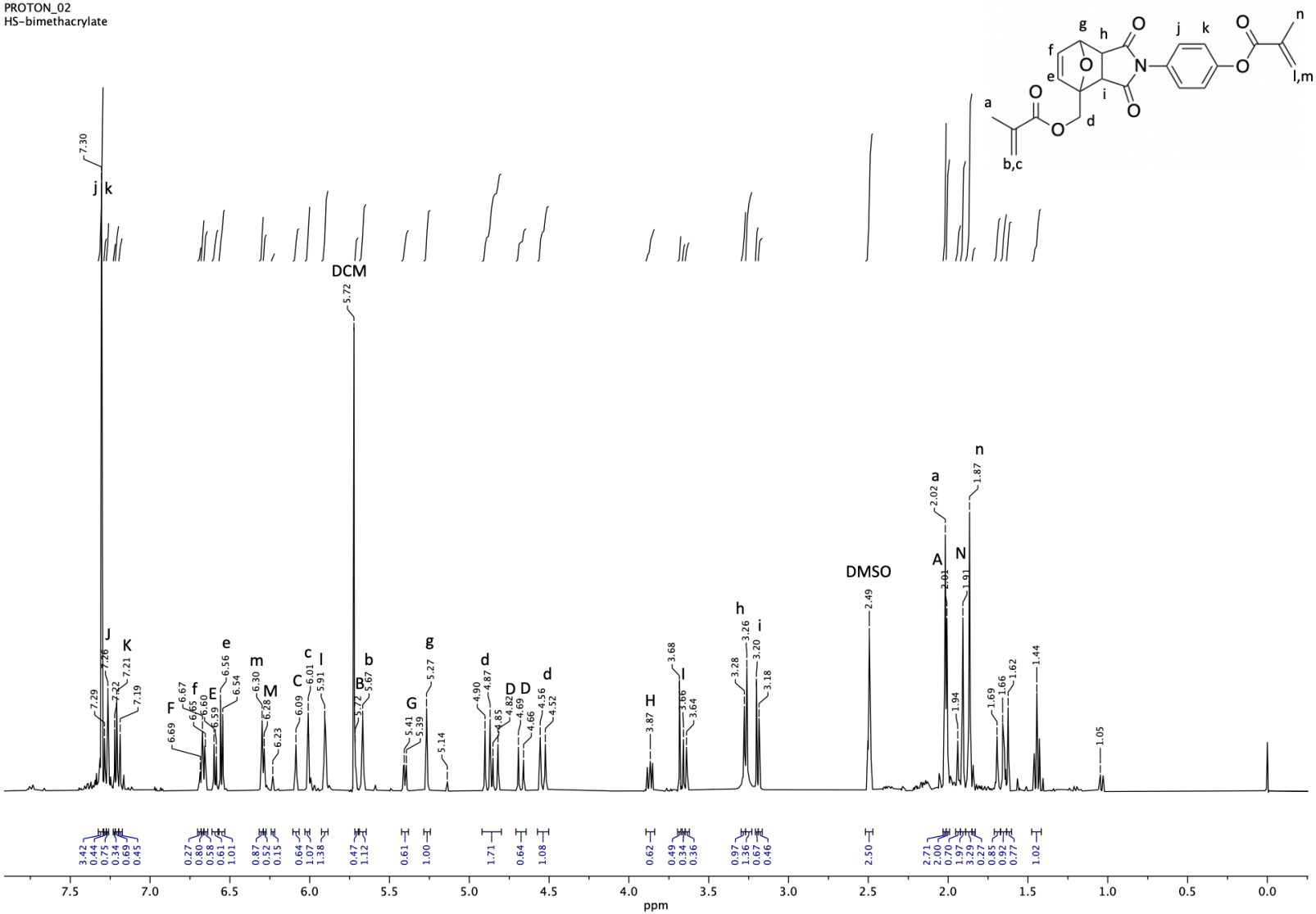

A 51: Diels-Alder functionalized crosslinker variable Temperature ^{1}H NMR - 45 ℃

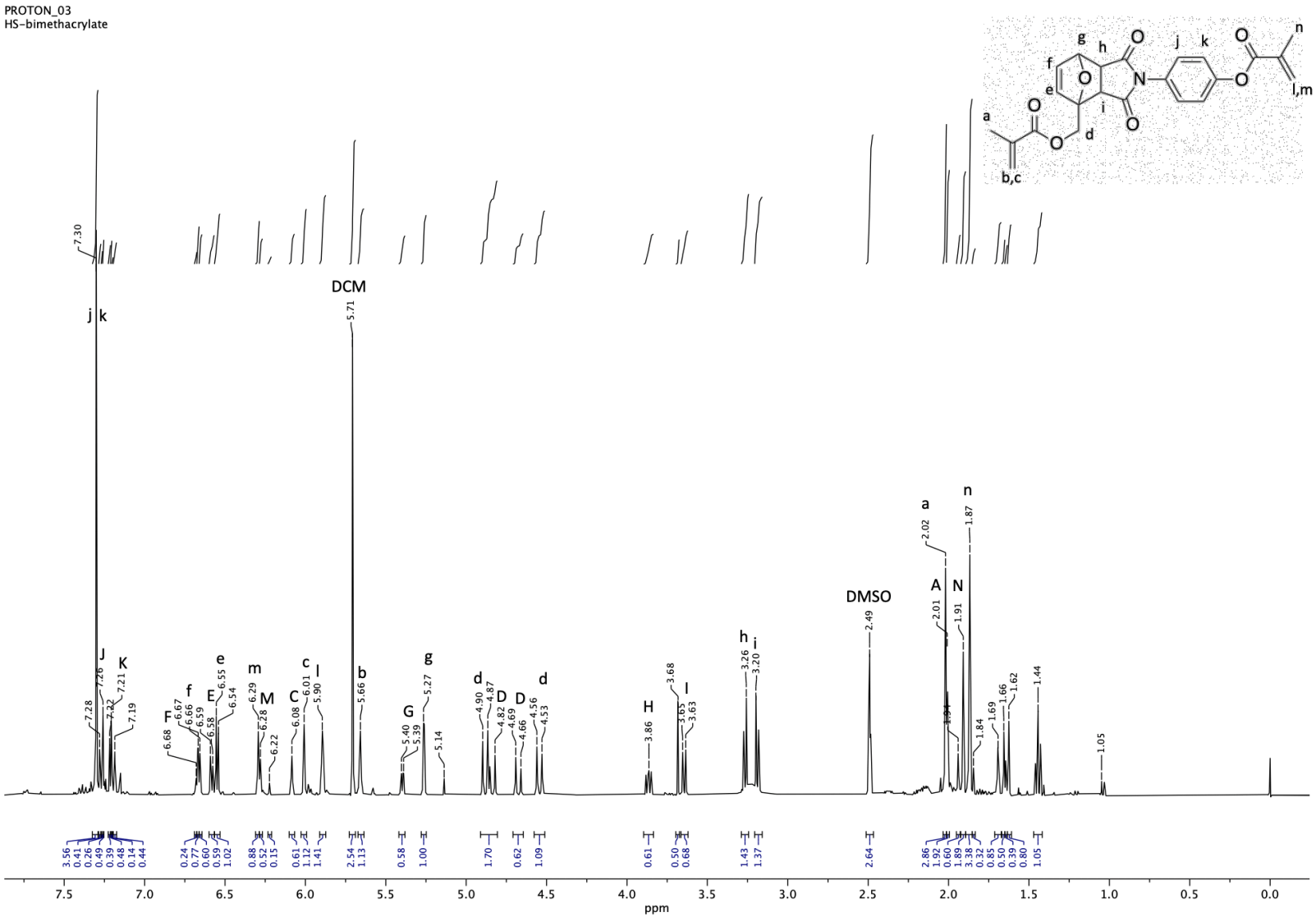

A 52: Diels-Alder functionalized crosslinker variable Temperature ^{1}H NMR - 55 ℃

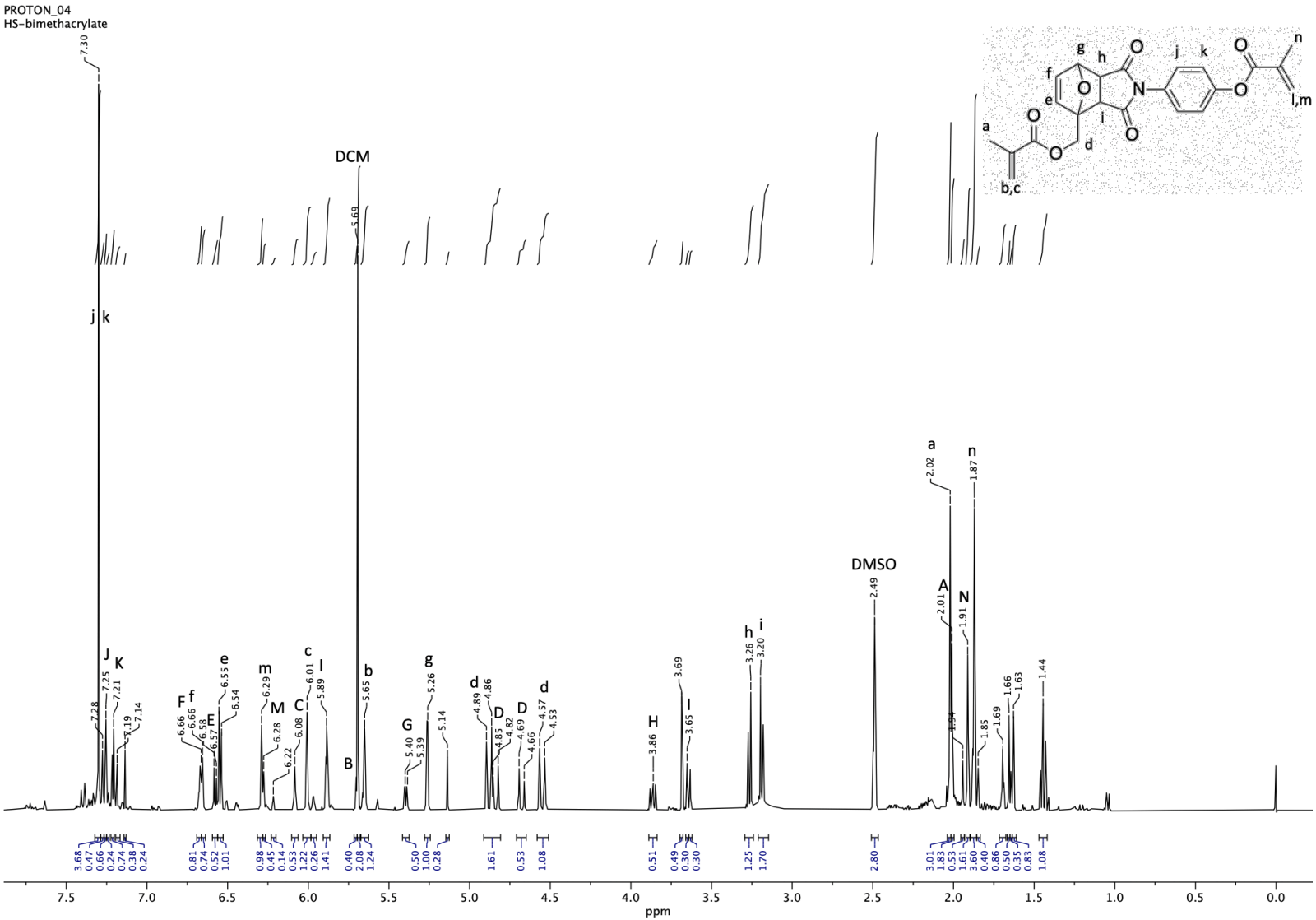

A 53: Diels-Alder functionalized crosslinker variable Temperature ^{1}H NMR - 65 °C

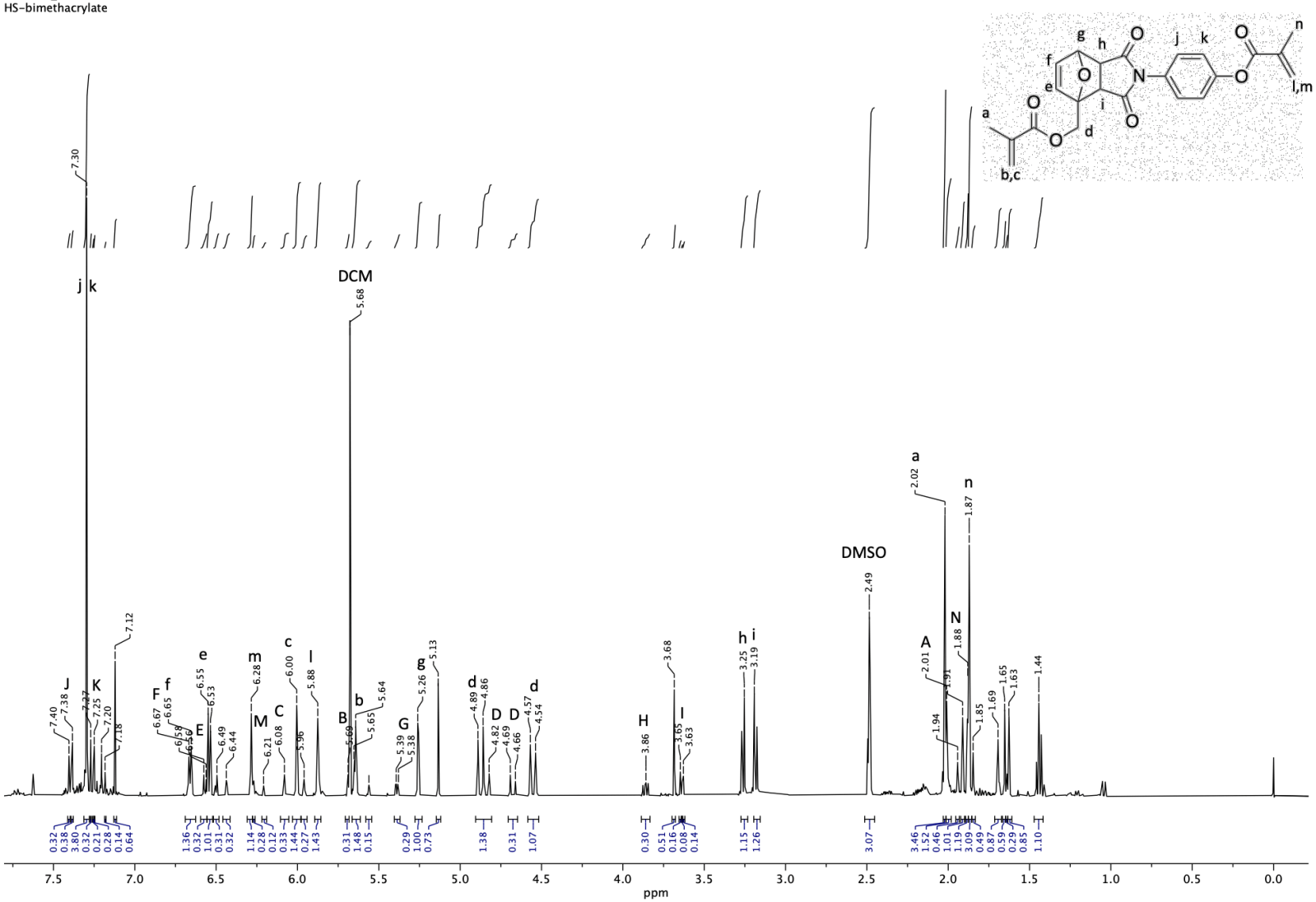

A 54: Diels-Alder functionalized crosslinker variable Temperature ^{1}H NMR - 75 ℃

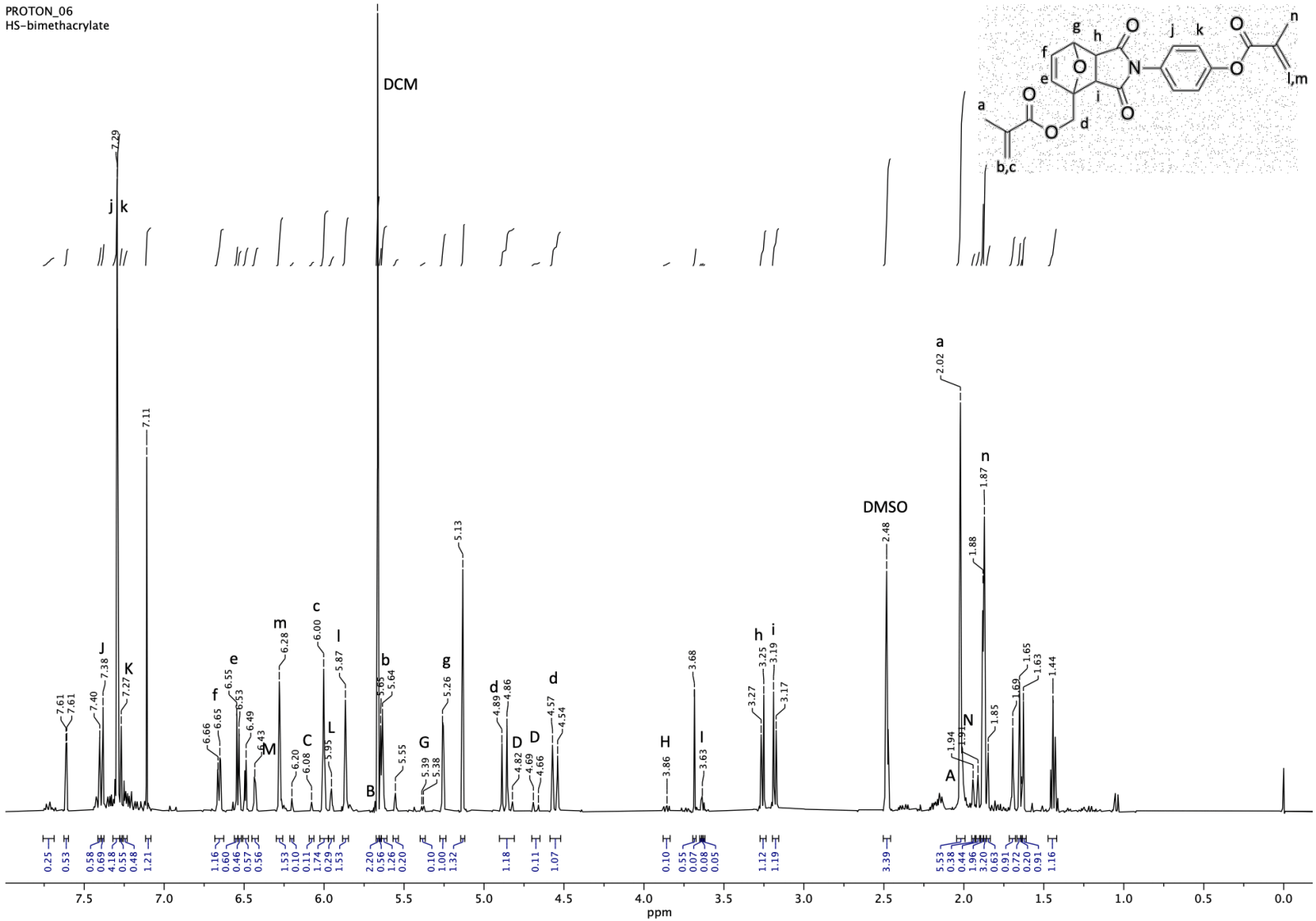

A 55: Diels-Alder functionalized crosslinker variable Temperature ^{1}H NMR - 85 ℃

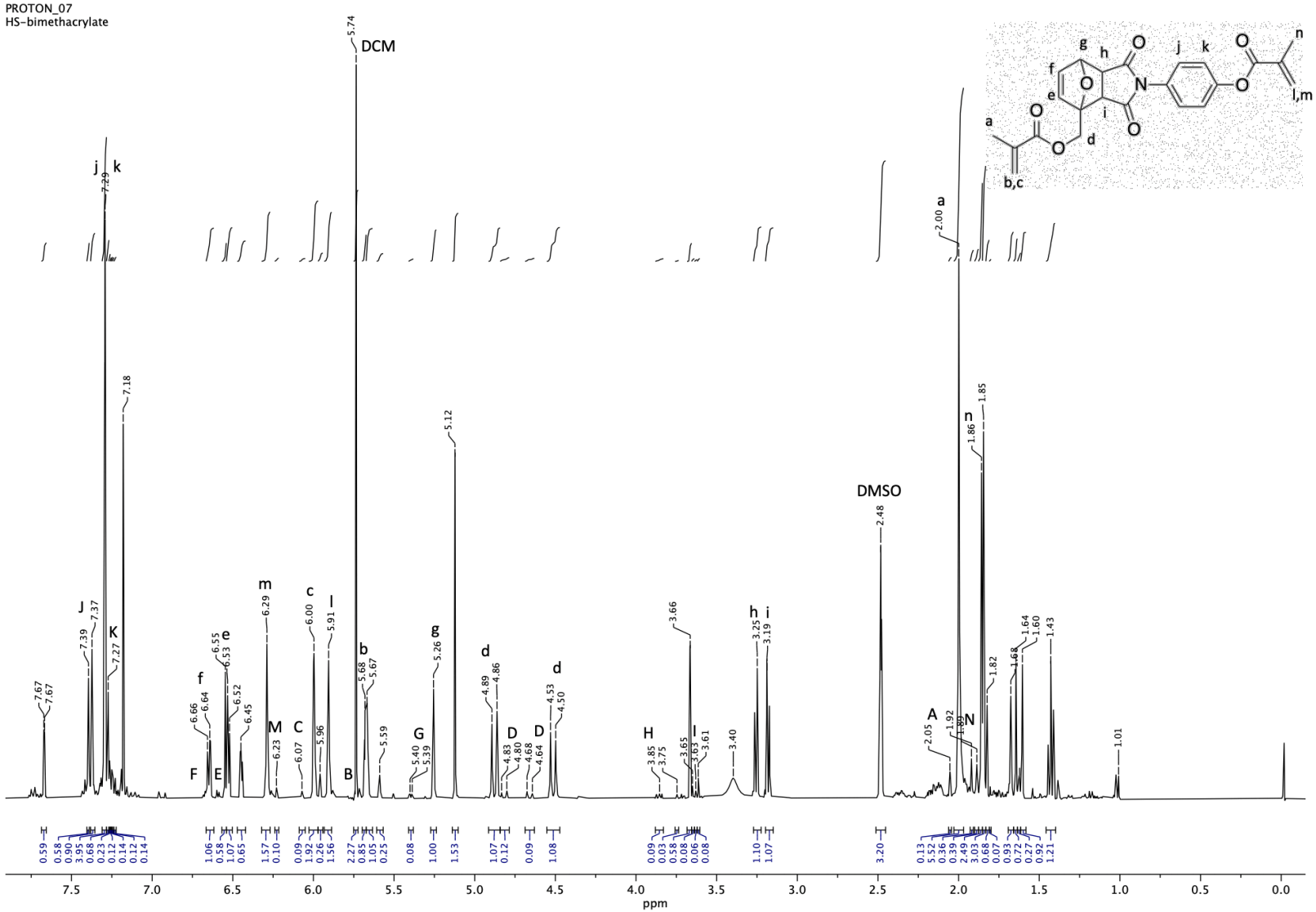

A 56: Diels-Alder functionalized crosslinker variable Temperature ^{1}H NMR - Room Temperature After Cooling

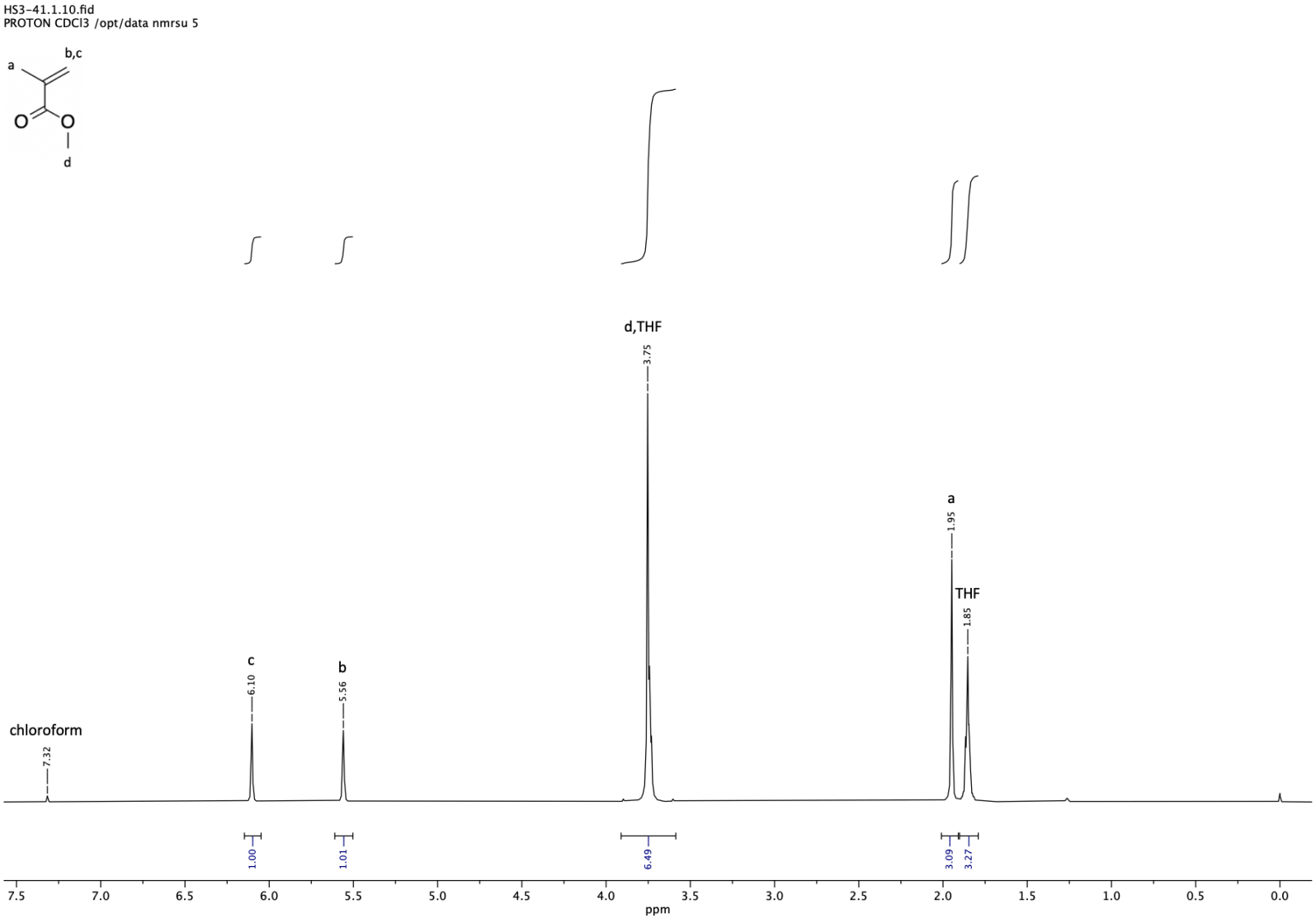

A 57:RAFT - homopolymerization of methyl methacrylate employing initiator V-70 (35 ℃)

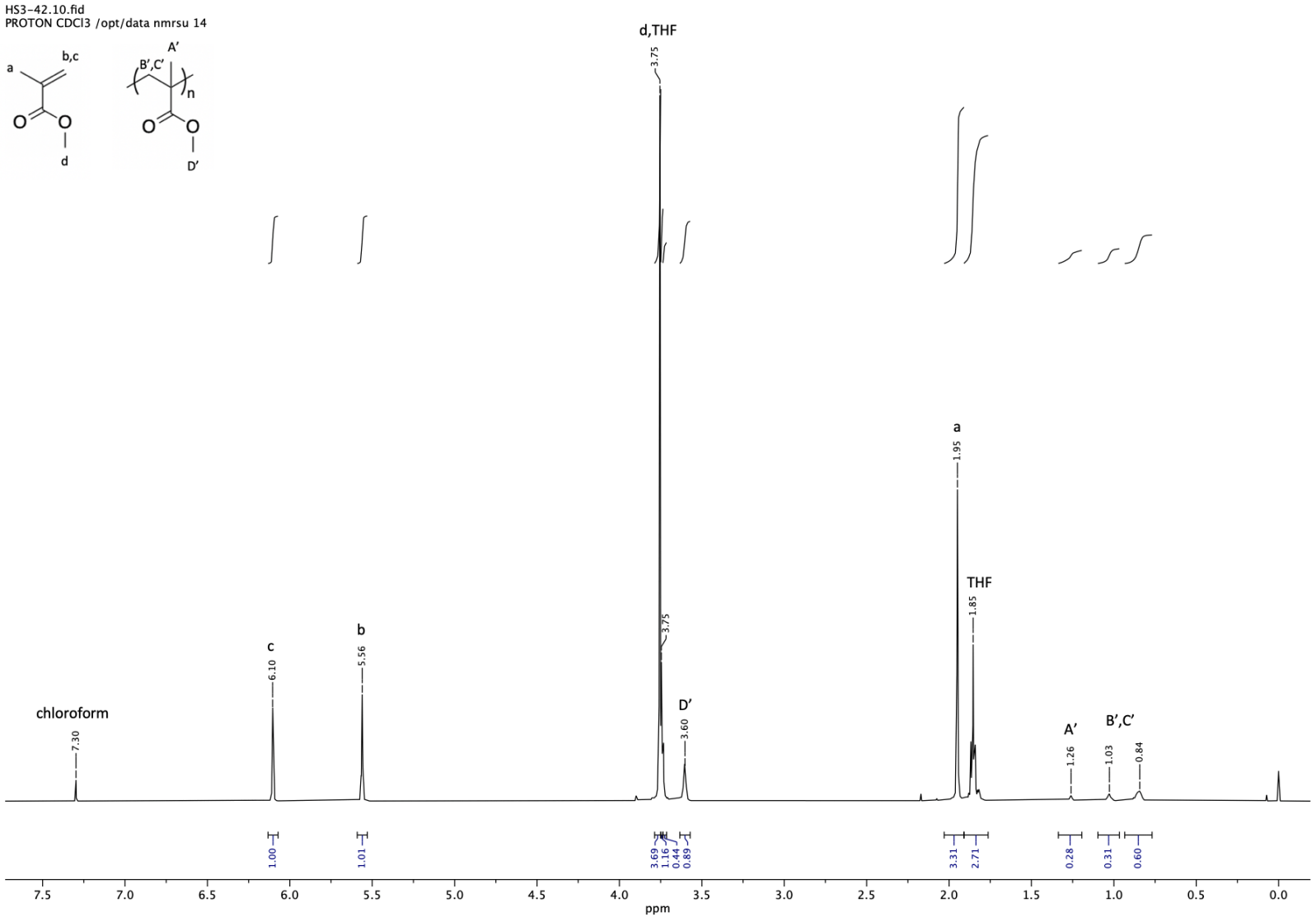

A 58: RAFT - homopolymerization of methyl methacrylate employing initiator V-70 (50 °C)

References

(1) Melchels, F. P. W.; Feijen, J.; Grijpma, D. W. A Review on Stereolithography and Its Applications in Biomedical Engineering. *Biomaterials* **2010**, *31* (24), 6121–6130. https://doi.org/10.1016/j.biomaterials.2010.04.050.

(2) Mohamed, O. A.; Masood, S. H.; Bhowmik, J. L. Optimization of Fused Deposition Modeling Process Parameters: A Review of Current Research and Future Prospects. *Adv. Manuf.* **2015**, *3* (1), 42–53. https://doi.org/10.1007/s40436-014-0097-7.

(3) Lee, H.; Lim, C. H. J.; Low, M. J.; Tham, N.; Murukeshan, V. M.; Kim, Y. J. Lasers in Additive Manufacturing: A Review. *Int. J. Precis. Eng. Manuf. - Green Technol.* **2017**, *4* (3), 307–322. https://doi.org/10.1007/s40684-017-0037-7.

(4) Dou, R.; Wang, T.; Guo, Y.; Derby, B. Ink-Jet Printing of Zirconia: Coffee Staining and Line Stability. *J. Am. Ceram. Soc.* **2011**, *94* (11), 3787–3792. https://doi.org/10.1111/j.1551-2916.2011.04697.x.

(5) Gibson, I.; Rosen, D.; Stucker, B. Additive Manufacturing Technologies: 3D Printing, Rapid Prototyping, and Direct Digital Manufacturing, Second Edition. *Addit. Manuf. Technol. 3D Printing, Rapid Prototyping, Direct Digit. Manuf. Second Ed.* **2015**, No. Dmd, 1–498. https://doi.org/10.1007/978-1-4939-2113-3.

(6) Ngo, T. D.; Kashani, A.; Imbalzano, G.; Nguyen, K. T. Q.; Hui, D. Additive Manufacturing (3D Printing): A Review of Materials, Methods, Applications and Challenges. *Compos. Part B Eng.* **2018**, *143* (February), 172–196. https://doi.org/10.1016/j.compositesb.2018.02.012.

(7) Lee, J.-Y.; An, J.; Chua, C. K. Fundamentals and Applications of 3D Printing for Novel Materials. *Appl. Mater. Today* **2017**, *7*, 120–133. https://doi.org/10.1016/J.APMT.2017.02.004.

(8) Zou, R.; Xia, Y.; Liu, S.; Hu, P.; Hou, W.; Hu, Q.; Shan, C. Isotropic and Anisotropic Elasticity and Yielding of 3D Printed Material. *Compos. Part B Eng.* **2016**, *99*, 506–513. https://doi.org/10.1016/j.compositesb.2016.06.009.

(9) Shafranek, R. T.; Millik, S. C.; Smith, P. T.; Lee, C. U.; Boydston, A. J.; Nelson, A. Stimuli-Responsive Materials in Additive Manufacturing. *Prog. Polym. Sci.* **2019**, *93*, 36–67. https://doi.org/10.1016/j.progpolymsci.2019.03.002.

(10) Davidson, J. R.; Appuhamillage, G. A.; Thompson, C. M.; Voit, W.; Smaldone, R. A. Design Paradigm Utilizing Reversible Diels-Alder Reactions to Enhance the Mechanical Properties of 3D Printed Materials. *ACS Appl. Mater. Interfaces* **2016**, *8* (26), 16961–16966. https://doi.org/10.1021/acsami.6b05118.

(11) Appuhamillage, G. A.; Reagan, J. C.; Khorsandi, S.; Davidson, J. R.; Voit, W.; Smaldone, R.

A. 3D Printed Remendable Polylactic Acid Blends with Uniform Mechanical Strength Enabled by a Dynamic Diels-Alder Reaction. *Polym. Chem.* **2017**, *8* (13), 2087–2092. https://doi.org/10.1039/c7py00310b.

(12) Manufacturing, A. Additive Manufacturing in Materials Innovation. **2013**, No. Lmd, 377–420.

(13) Bergman, S. D.; Wudl, F. Mendable Polymers. *J. Mater. Chem.* **2008**, *18* (1), 41–62. https://doi.org/10.1039/b713953p.

(14) Burattini, S.; Greenland, B. W.; Chappell, D.; Colquhoun, H. M.; Hayes, W. Healable Polymeric Materials: A Tutorial Review. *Chem. Soc. Rev.* **2010**, *39* (6), 1973–1985. https://doi.org/10.1039/b904502n.

(15) Amato, D. N.; Strange, G. A.; Swanson, J. P.; Chavez, A. D.; Roy, S. E.; Varney, K. L.; MacHado, C. A.; Amato, D. V.; Costanzo, P. J. Synthesis and Evaluation of Thermally-Responsive Coatings Based upon Diels-Alder Chemistry and Renewable Materials. *Polym. Chem.* **2014**, *5* (1), 69–76. https://doi.org/10.1039/c3py01024d.

(16) C. Oliver Kappe, S. Shaun Murphree, A. P. Syntheric Applications of Furan Diels-Alder Chemistry. *Tetrahedron* **1997**, *53* (42), 14179–14233.

(17) Nicolaou, K. C.; Snyder, S. A.; Montagnon, T.; Vassilikogiannakis, G. The Diels Alder Reaction in Action. https://doi.org/10.1002/1521-3773(20020517)41:10<1668::AID-ANIE1668>3.0.CO;2-Z.

(18) Chem, P.; Tasdelen, M. A. Polymer Chemistry Diels – Alder ‘“ Click ”’ Reactions : Recent Applications in Polymer and Material. **2011**, No. i, 2133–2145. https://doi.org/10.1039/c1py00041a.

(19) Boutelle, R. C.; Northrop, B. H. Substituent Effects on the Reversibility of Furan - Maleimide Cycloadditions. *J. Org. Chem.* **2011**, *76* (19), 7994–8002. https://doi.org/10.1021/jo201606z.

(20) Oppolzer, W. *Intermolecular Diels-Alder Reactions*; 1991; Vol. 5.

(21) Froidevaux, V.; Borne, M.; Laborbe, E.; Auvergne, R.; Gandini, A.; Boutevin, B. Study of the Diels-Alder and Retro-Diels-Alder Reaction between Furan Derivatives and Maleimide for the Creation of New Materials. *RSC Adv.* **2015**, *5* (47), 37742–37754. https://doi.org/10.1039/c5ra01185j.

(22) Sauer, J.; Sustmann, R. Mechanistic Aspects of Diels-Alder Reactions: A Critical Survey. *Angew. Chemie Int. Ed. English* **1980**, *19* (10), 779–807. https://doi.org/10.1002/anie.198007791.

(23) Keddie, D. J. A Guide to the Synthesis of Block Copolymers Using Reversible-Addition

Fragmentation Chain Transfer (RAFT) Polymerization. *Chem. Soc. Rev.* **2014**, *43* (2), 496–505. https://doi.org/10.1039/c3cs60290g.

(24) Chiefari, J.; Chong, Y. K.; Ercole, F.; Krstina, J.; Jeffery, J.; Le, T. P. T.; Mayadunne, R. T. A.; Meijs, G. F.; Moad, C. L.; Moad, G.; Rizzardo, E.; Thang, S. H. Living Free-Radical Polymerization by Reversible Addition - Fragmentation Chain Transfer: The RAFT Process. *Macromolecules* **1998**, *31* (16), 5559–5562. https://doi.org/10.1021/ma9804951.

(25) Perrier, S. 50th Anniversary Perspective: RAFT Polymerization - A User Guide. *Macromolecules* **2017**, *50* (19), 7433–7447. https://doi.org/10.1021/acs.macromol.7b00767.

(26) Wang, J. S.; Matyjaszewski, K. Controlled/"Living" Radical Polymerization. Atom Transfer Radical Polymerization in the Presence of Transition-Metal Complexes. *J. Am. Chem. Soc.* **1995**, *117* (20), 5614–5615. https://doi.org/10.1021/ja00125a035.

(27) Wang, J. S.; Matyjaszewski, K. "Living"/Controlled Radical Polymerization. Transition-Metal-Catalyzed Atom Transfer Radical Polymerization in the Presence of a Conventional Radical Initiator. *Macromolecules* **1995**, *28* (22), 7572–7573. https://doi.org/10.1021/ma00126a041.

(28) Wang, J. S.; Matyjaszewski, K. Controlled/"Living" Radical Polymerization. Halogen Atom Transfer Radical Polymerization Promoted by a Cu(I)/Cu(II) Redox Process. *Macromolecules* **1995**, *28* (23), 7901–7910. https://doi.org/10.1021/ma00127a042.

(29) Ribelli, T. G.; Lorandi, F.; Fantin, M.; Matyjaszewski, K. Atom Transfer Radical Polymerization: Billion Times More Active Catalysts and New Initiation Systems. *Macromol. Rapid Commun.* **2019**, *40* (1), 1–44. https://doi.org/10.1002/marc.201800616.

(30) Matyjaszewski, K.; Coca, S.; Gaynor, S. G.; Wei, M.; Woodworth, B. E. Zerovalent Metals in Controlled/"living" Radical Polymerization. *Macromolecules* **1997**, *30* (23), 7348–7350. https://doi.org/10.1021/ma971258l.

(31) Debuigne, A.; Hurtgen, M.; Detrembleur, C.; Jérôme, C.; Barner-Kowollik, C.; Junkers, T. Interpolymer Radical Coupling: A Toolbox Complementary to Controlled Radical Polymerization. *Prog. Polym. Sci.* **2012**, *37* (7), 1004–1030. https://doi.org/10.1016/j.progpolymsci.2012.01.003.

(32) Yoshikawa, C.; Goto, A.; Fukuda, T. Reactions of Polystyrene Radicals in a Monomer-Free Atom Transfer Radical Polymerization System. *E-Polymers* **2002**, *2* (1), 1–12. https://doi.org/10.1515/epoly.2002.2.1.172.

(33) Sarbu, T.; Lin, K. Y.; Spanswick, J.; Gil, R. R.; Siegwart, D. J.; Matyjaszewski, K. Synthesis of Hydroxy-Telechelic Poly(Methyl Acrylate) and Polystyrene by Atom Transfer Radical Coupling. *Macromolecules* **2004**, *37* (26), 9694–9700.

https://doi.org/10.1021/ma0484375.

(34) Otazaghine, B.; David, G.; Boutevin, B.; Robin, J. J.; Matyjaszewski, K. Synthesis of Telechelic Oligomers via Atom Transfer Radical Polymerization, 1: Study of Styrene. *Macromol. Chem. Phys.* **2004**, *205* (2), 154–164. https://doi.org/10.1002/macp.200300031.

(35) Nagelsdiek, R.; Keul, H.; Höcker, H. A New Approach to Multiblock Copolymers Using Atom Transfer Radical Coupling. *E-Polymers* **2005**, No. 049, 1–11. https://doi.org/10.1515/epoly.2005.5.1.510.

(36) Voter, A. F.; Tillman, E. S.; Findeis, P. M.; Radzinski, S. C. Synthesis of Macrocyclic Polymers Formed via Intramolecular Radical Trap-Assisted Atom Transfer Radical Coupling. *ACS Macro Lett.* **2012**, *1* (8), 1066–1070. https://doi.org/10.1021/mz300311p.

(37) Voter, A. F.; Tillman, E. S. An Easy and Efficient Route to Macrocyclic Polymers via Intramolecular Radical-Radical Coupling of Chain Ends. *Macromolecules* **2010**, *43* (24), 10304–10310. https://doi.org/10.1021/ma102319r.

(38) Delafresnaye, L.; Schmitt, C. W.; Barner, L.; Barner-Kowollik, C. A Photochemical Ligation System Enabling Solid-Phase Chemiluminescence Read-Out. *Chem. - A Eur. J.* **2019**, *25* (54), 12538–12544. https://doi.org/10.1002/chem.201901858.

(39) Sinner, F.; Buchmeiser, M. R. A New Class of Continuous Polymer Supports Prepared by Ring-Opening Metathesis Polymerization: A Straightforward Route to Functionalized Monoliths. *Macromolecules* **2000**, *33* (16), 5777–5786. https://doi.org/10.1021/ma000322n.

(40) Matuszak, N.; Muccioli, G. G.; Labar, G.; Lambert, D. M. Synthesis and in Vitro Evaluation of N-Substituted Maleimide Derivatives as Selective Monoglyceride Lipase Inhibitors. *J. Med. Chem.* **2009**, *52* (23), 7410–7420. https://doi.org/10.1021/jm900461w.

(41) Pitchaimari, G.; Vijayakumar, C. T. Functionalized Monomers Based on N-(4-Hydroxy Phenyl)Maleimide: Thermal Polymerization and Degradation. *J. Therm. Anal. Calorim.* **2013**, *114* (3), 1351–1361. https://doi.org/10.1007/s10973-013-3174-4.

(42) Pitchaimari, G.; Vijayakumar, C. T. Functionalized N-(4-Hydroxy Phenyl) Maleimide Monomers: Kinetics of Thermal Polymerization and Degradation Using Model-Free Approach. *J. Appl. Polym. Sci.* **2014**, *131* (4), 1–11. https://doi.org/10.1002/app.39935.

(43) Wu, T.; Jiang, P.; Zhang, X.; Guo, Y.; Ji, Z.; Jia, X.; Wang, X.; Zhou, F.; Liu, W. Additively Manufacturing High-Performance Bismaleimide Architectures with Ultraviolet-Assisted Direct Ink Writing. *Mater. Des.* **2019**, *180*, 107947. https://doi.org/10.1016/j.matdes.2019.107947.

(44) Gandini, A. The Furan/Maleimide Diels-Alder Reaction: A Versatile Click-Unclick Tool in

Macromolecular Synthesis. *Progress in Polymer Science*. 2013. https://doi.org/10.1016/j.progpolymsci.2012.04.002.

(45) Wilborn, E. G.; Gregory, C. M.; Machado, C. A.; Page, T. M.; Ramos, W.; Hunter, M. A.; Smith, K. M.; Gosting, S. E.; Tran, R.; Varney, K. L.; Savin, D. A.; Costanzo, P. J. Unraveling Polymer Structures with RAFT Polymerization and Diels–Alder Chemistry. *Macromolecules* **2019**, *52*, 1308–1316. https://doi.org/10.1021/acs.macromol.8b01967.

(46) Kwart, H.; Burchuk, I. Isomerism and Adduct Stability in the Diels-Alder Reaction.1a I. The Adducts of Furan and Maleimide. *J. Am. Chem. Soc.* **1952**, *74* (12), 3094–3097. https://doi.org/10.1021/ja01132a042.

(47) Yates, P.; Eaton, P. Acceleration of the Diels-Alder Reaction by Aluminum Chloride. *J. Am. Chem. Soc.* **1960**, *82* (16), 4436–4437. https://doi.org/10.1021/ja01501a085.